

Magma storage at Ocean Islands: insights from Cape Verde

Abigail Barker¹, Elin Rydeblad¹, and Sónia Silva²

¹Uppsala University

²University of Cabo Verde

November 24, 2022

Abstract

The Cape Verde archipelago is a group of Ocean Islands in the Central Atlantic that forms two chains of islands trending Northwest and Southwest. Several of the islands are considered to be volcanically active, with frequent eruptions on Fogo. We examine the mineral chemistry and thermobarometry of the southern islands; Santiago, Fogo and Brava together with the Cadamosto Seamount. Our objective is to explore the magmatic storage system and implications for volcanic eruptions and associated hazards at Cape Verde. The volcanic rocks at Cape Verde are alkaline and dominantly mafic, whereas the island of Brava and the Cadamosto Seamount are unusually felsic. Clinopyroxene compositions range from 60 to 90 Mg# at Santiago and Fogo. In contrast, at Brava and the Cadamosto Seamount the clinopyroxene compositions are 5 to 75 Mg#. Mineral chemistry and zonation records fractional crystallization, recharge, aggregation of crystals, magma mixing and variations in thermal conditions of the magma at temperatures from 925 to 1250C. Magma storage depths at Santiago, Fogo, Brava and the Cadamosto Seamount are between 12 and 40 km, forming deep sub-Moho magma storage zones. Transient magma storage in the crust is suggested by fluid inclusion re-equilibration and pre-eruption seismicity. A global compilation of magma storage at Ocean Islands suggests deep magma storage is a common feature and volcanic eruptions are often associated with rapid magma ascent through the crust. Shallow magma storage is more variable and likely reflects local variations in crustal structure, sediment supply and tectonics. Petrological constraints on the magma plumbing system at Cape Verde and elsewhere are vital to integrate with deformation models and seismicity in order to improve understanding and mitigation of the volcanic hazards.

Magma storage at Ocean Islands: insights from Cape Verde

Barker AK^{1,2}, Rydeblad E^{1,3}, Silva SMDM⁴

1 Mineralogy, Petrology, Tectonics, Department of Earth Sciences, Uppsala University, Villavägen 16, Uppsala SE-752 36, Sweden

2 Centre of Natural Hazards and Disaster Sciences (CNDS), Villavägen 16, Uppsala SE-752 36, Sweden

3 Department of Earth Science and Engineering, South Kensington Campus, Imperial College London, SW7 2AZ, UK

4 Faculty of Science and Technology, University of Cabo Verde, CP 279, Praia, Santiago, Cabo Verde

Abstract

The Cape Verde archipelago is a group of Ocean Islands in the Central Atlantic that forms two chains of islands trending Northwest and Southwest. Several of the islands are considered to be volcanically active, with frequent eruptions on Fogo. We examine the mineral chemistry and thermobarometry of the southern islands; Santiago, Fogo and Brava together with the Cadamosto Seamount. Our objective is to explore the magmatic storage system and implications for volcanic eruptions and associated hazards at Cape Verde. The volcanic rocks at Cape Verde are alkaline and dominantly mafic, whereas the island of Brava and the Cadamosto Seamount are unusually felsic. Clinopyroxene compositions range from 60 to 90 Mg# at Santiago and Fogo. In contrast, at Brava and the Cadamosto Seamount the clinopyroxene compositions are 5 to 75 Mg#. Mineral chemistry and zonation records fractional crystallization, recharge, aggregation of crystals, magma mixing and variations in thermal conditions of the magma at temperatures from 925 to 1250°C. Magma storage depths at Santiago, Fogo, Brava and the Cadamosto Seamount are between 12 and 40 km, forming deep sub-Moho magma storage zones. Transient magma storage in the crust is suggested by fluid inclusion re-equilibration and pre-eruption seismicity. A global compilation of magma storage at Ocean Islands suggests deep magma storage is a common feature and volcanic eruptions are often associated with rapid magma ascent through the crust. Shallow magma storage is more variable and likely reflects local variations in crustal structure, sediment supply and tectonics. Petrological constraints on the magma plumbing system at Cape Verde and elsewhere are vital to integrate with deformation models and seismicity in order to improve understanding and mitigation of the volcanic hazards.

31 *Introduction*

32 Ocean Islands occur in all of the world's oceans and are formed by intraplate volcanism. Several
33 Ocean Islands are volcanically active with eruptions at Reunion, Canary Islands, Cape Verde and Hawaii
34 between 2007 and 2018 (e.g. Di Muro et al., 2014; Longpré et al., 2014; Worsley, 2015; Liu et al., 2018).
35 Many of the Ocean Islands are inhabited and have lucrative tourist industries, which put people directly at
36 risk from the volcanic hazards associated with eruptions. Additionally, submarine and subaerial eruptions
37 can also be hazardous for the shipping and aviation industries respectively (O'Mangain et al., 2007; Di
38 Muro et al., 2014). Consequently, understanding the magma plumbing systems from the magma storage
39 zones to the volcanic centers is imperative for assessing and monitoring the volcanic hazards. We present
40 insights into the magma storage at Cape Verde, to explore the nature of the volcanically active parts of the
41 archipelago which is motivated by the recent eruptions at Fogo (Ribeiro, 1960; Worsley et al., 2015).

42 The Cape Verde archipelago is an Ocean Island group built upon the Cape Verde Rise (Ramalho et al.,
43 2010a,b). The older and now heavily eroded islands of Maio, Sal and Boa Vista are found in the East,
44 from where two volcanic chains emerge. The northern chain consists of São Nicolau, Santa Luzia, São
45 Vicente and Santa Antão. The islands of Santiago, Fogo, and Brava as well as the Cadamosto Seamount
46 form the southern island chain (Figure 1). The island of Fogo displays the iconic Pico do Fogo, peaking at
47 2829 m above sea level, located inside the Bordiera, on the Chã das Caldeiras, where the historic eruption
48 sites are found; the latest eruption was November 2014 to February 2015 (Silva et al., 2015; Fernandes &
49 Faria, 2015; González et al., 2015; Worsley 2015; Richter et al., 2016; Jenkins et al., 2017). Prior to that
50 nine eruptions occurred at Fogo between 1760 and 1995, with a total of 28 eruptions since settlement in
51 the 15th century (Ribeiro, 1960; Nascimento, 2015). Brava and the Cadamosto Seamount have no
52 historical record of volcanic activity. However, Holocene volcanic activity is documented at Brava and
53 the Cadamosto Seamount records eruption ages of 21 ka (Madeira et al., 2010; Faria & Fonseca, 2014;
54 Samrock et al., 2019). Additionally, seismicity extends from Fogo to the Cadamosto Seamount suggesting
55 that Brava and the Cadamosto Seamount are also underlain by active magmatic systems (Heleno et al.,
56 2006; Grevemeyer et al., 2010).

57 The volcanic hazards on Fogo are in the form of ash and lapilli associated with strombolian
58 activity and lava flows as well as occasional sub-plinian to plinian eruptions (Torres et al., 1997; Eilese et
59 al., 2015). The residents of Fogo are vulnerable to the direct volcanic hazards associated with an eruption,
60 especially the approximately one thousand who live and work inside the Bordeira close to Pico do Fogo,
61 followed by the 11,000 residents of the East coast of Fogo (Faria & Fonseca, 2014). The eruptions in
62 1995 and 2014/2015 led to large-scale evacuation as well as significant damage to property, agricultural
63 land and buildings (Silva et al., 2015; Worsley 2015; Jenkins et al., 2017). Potential volcanic hazards at

64 Brava are connected to pyroclastic and phreatomagmatic eruptions and endanger the 6,000 inhabitants
65 (Faria & Fonseca, 2014).

66 In addition, the onshore and offshore geological record of the Cape Verde archipelago shows
67 evidence for flank collapses and landslide deposits (Masson et al., 2002, 2008; Paris et al., 2018; Barrett
68 et al., 2020). The Bordeira cliffs of Fogo were potentially exposed by a huge landslide (Day et al., 1999;
69 Foeken et al., 2009; Ramalho et al., 2015; Martínez-Moreno et al., 2018). Tsunami deposits have been
70 used to constrain the associated flank collapse and landslide to approximately 73 ka (Ramalho et al.,
71 2015). Furthermore tsunami deposits associated with local flank collapses are found, among other
72 locations, on Santiago and Maio (Paris et al., 2011, 2018; Ramalho et al., 2015; Madeira et al., 2019).
73 Therefore the Cape Verde Islands are associated with multiple natural hazards that may pose a threat to
74 the population both locally and farther afield.

75 Monitoring of the volcanism is the responsibility of the National Institute for Metrology and
76 Geophysics. In addition the University of Cape Verde has been conducting geochemical monitoring in
77 partnership with national and international institutions (Fonseca et al., 2003; Barrancos et al., 2015; Pérez
78 et al., 2015; Dionis et al., 2015a, b). Seismicity and deformation is monitored throughout Cape Verde
79 with 15 seismometers and a geodetic network (Faria & Fonseca, 2014). The Fogo-Brava seismic network
80 consists of seven seismometers on Fogo and two on Brava and Fogo hosts three geodetic stations.
81 Additional monitoring targets volcanic gas emissions with semi-frequent measurements of CO₂ and SO₂
82 emissions and fumerole temperatures (Faria & Fonseca, 2014; Worsley 2015). The National Institute for
83 Metrology and Geophysics work with the National Civil Protection service to provide risk
84 communication (Faria & Fonseca, 2014).

85 The magmatic system can be investigated through minerals in the erupted products. The minerals
86 capture the compositional signature of the host magma during growth, therefore they respond to
87 variations in magma composition. Consequently minerals provide a chronological record of magma
88 evolution (Davidson et al., 2007). On this basis mineral thermobarometry offers a petrological method to
89 estimate the crystallization conditions of magma chambers, including the temperature and pressure of
90 crystal growth (e.g. Putirka, 2008). Igneous thermobarometers have been widely applied in many settings
91 such as volcanic arcs (e.g. Till, 2017; Lai et al., 2018) and to investigate continental magmatism (Putirka
92 et al., 2003; Putirka & Condit, 2003). Clinopyroxene-melt thermobarometers have also been applied in
93 Ocean Islands settings to explore tholeiitic to alkaline systems e.g. Hawaii, Cape Verde, Canary Islands
94 (e.g. Putirka, 1997; Klügel et al., 2000, 2005, Nikogosian et al., 2002; Aulinas et al., 2010; Hildner et al.,
95 2011, 2012; Longpré et al., 2014; Mata et al., 2017). Despite large uncertainties associated with

96 crystallization pressure estimates, thermobarometry offers several advantages that complement
97 geophysical methods for determining magma chamber depth location (Magee et al., 2018). Firstly a
98 magma pocket requires significant dimensions to be detected by seismic arrays, even at dense seismic
99 station distribution (e.g. Gudmundsson, 2012). Secondly seismicity picks up differences in seismic
100 velocities, and thereby requires magma pockets to be melt rich, if they are mush zones with a significant
101 proportion of crystals then the melt:solid ratio may not be high enough to observe variations in seismic
102 wave velocities (e.g. Gudmundsson, 2012). Additionally, studies of deformation often employ
103 petrological data as inputs to estimate the shape, size and depth of the point source, to model the inflation
104 of a magma chamber (e.g. Amelung & Day, 2002; González et al., 2015). Petrological techniques can
105 thus provide crucial information on magma storage for integration with geophysical models (Magee et al.
106 2018). Whereas geophysical methods are not only useful for investigating the magma storage system but
107 also have distinct advantages in real-time monitoring of magma movement prior to eruptions (Magee et
108 al., 2018).

109 Furthermore, thermobarometry determines pressure and temperature of mineral growth and is
110 often sensitive to crystals growing in small magma pockets (e.g. Geiger et al., 2016; Stock et al., 2018). In
111 many cases these magma pockets are not detected until earthquakes trace magma ascent prior to an
112 eruption. Several cases have shown that other methods confirm the models for magma plumbing systems
113 developed from thermobarometry (e.g. Longpré et al., 2014; Barker et al., 2019). However
114 thermobarometry is not without limitations, restricted by the minerals present as well as magma
115 compositions and experimental conditions of calibrations (e.g. Putirka, 2008). For instance, although
116 clinopyroxene crystallizes over wide temperature, pressure and compositional ranges the felsic magmas in
117 many settings evolve beyond clinopyroxene crystallization (e.g. Weidendorfer et al., 2016). Therefore
118 other minerals or features such as fluid inclusions and volatile solubility in glass are required to trace the
119 more evolved parts of the magmatic system (e.g. Schwarz & Klügel 2004; Jeffery et al., 2016).

120 All volcanic activity is fed from the magma plumbing system, therefore it is important to
121 understand the magma storage, magmatic processes and where they occur as well as the processes that
122 lead to magma ascent (Cooper, 2017; Putirka, 2017; Sparks & Cashman, 2017). To address the
123 connection between the magmatic system and volcanic hazards at Cape Verde we will discuss magmatic
124 processes recorded by mineral chemistry and the magma plumbing system derived from
125 thermobarometric modelling for the southern Cape Verde archipelago. Mineral chemistry from the islands
126 of Santiago, Fogo, Brava and the Cadamosto seamount will be examined to provide insights into the
127 magmatic processes. These examples have been selected based on availability of mineral chemistry and
128 geophysical data as well as relevance from a volcanic hazard perspective. Mineral-melt equilibrium

129 thermobarometry for Santiago, Fogo, Brava and the Cadamosto Seamount will be integrated into a model
130 for the magmatic plumbing systems in southern Cape Verde. Evidence for the shallower parts of the
131 magma plumbing systems and the volcanic hazards at Fogo will be reviewed. Finally, the magma
132 plumbing system for Cape Verde will be compared with other Ocean Islands globally.

133

134 *The Cape Verde Archipelago*

135 The Cape Verde Rise is situated 2000 km East of the Mid-Atlantic Ridge in the Central Atlantic,
136 between 15 and 17°N and approximately 500 km West of Dakar, Senegal (Figure 1). The Cape Verde
137 Rise forms a gigantic bathymetric swell reaching circa 2 km above the surrounding ocean crust and
138 covers an area of more than 0.3 million km² (Crough, 1982; McNutt, 1988; Jørgensen & Holm, 2002;
139 Lodge and Helffrich, 2006; Holm et al., 2008; Masson et al., 2008; Brown et al., 2009). The Cape Verde
140 islands and seamounts are located in the Southwest of the Cape Verde Rise (Figure 1; Rona, 1971; Egloff,
141 1972; Dash et al., 1976). The islands are arranged in a semi-circle opening to the West, with older heavily
142 eroded islands occurring in the East and two subparallel chains of islands in the North and South, which
143 extend westwards (Figure 1; Gerlach et al., 1988).

144 The northern and southern island chains are subparallel to the fracture zones found to the West of
145 the Cape Verde archipelago (Figure 3; Jacobi and Hayes, 1982). Therefore fracture zones may influence
146 the orientation of the island chains (Klerkx et al., 1974; Le Pichon and Fox, 1971; Doucelance et al.,
147 2003). Evidence for fracture zone offsets is documented by magnetic lineations and gravity anomalies
148 (Figure 3; Hayes and Rabinowitz, 1975; Dash et al., 1976; Williams et al. 1990; Verhoef et al. 1991;
149 Roest et al. 1992; Ali et al., 2003). Additionally brittle deformation through normal, reverse and
150 transverse faults has formed horst and graben structures on the Cape Verde Rise (Figure 3b; Efimov &
151 Skolotnev, 2006; Skolotnev et al., 2007; 2009).

152 The Cretaceous ocean crust, formed at the Mid Atlantic Ridge, is overlain by a several kilometer
153 thick sequence of hemipelagic sediments (Figure 2; Dash et al. 1976; Courtney & White, 1986; Williams
154 et al., 1990; Ali et al., 2003; Müller et al., 2008; Pim et al., 2008). The oceanic lithosphere is
155 approximately 85 km thick, confirmed by elevated seismic velocities extending to ca. 80 km and a Lower
156 Velocity Zone that appears at 90±6 km depth (Cazenave et al., 1988; Lodge and Helffrich, 2006).
157 Although the ocean crust beneath Cape Verde has normal thicknesses of 7 to 8 km, the islands are
158 underlain by thickened crust (Pim et al., 2008; Wilson et al., 2010, 2013). The Moho beneath individual
159 islands decreases westwards from >20 km beneath Maio, to 17 to 18 km beneath Santiago and to 12 to 14

160 km beneath Fogo (Lodge and Helffrich, 2006; Pim et al., 2008; Wilson et al., 2010, 2013). The
161 sedimentary stratigraphy observed at Deep Sea Drilling Project (DSDP) Site 368 is composed of marl and
162 nanofossil ooze, underlain by clay, claystone and minor chert associated with turbidites, plus black shale
163 interbedded with dikes below (Lancelot et al., 1978; Faugères et al., 1989).

164 The Cape Verde islands display core complexes composed of intrusive carbonatite to alkaline
165 assemblages as well as submarine pillow basalts (Serralheiro, 1970; De Paepe et al., 1974; Serralheiro,
166 1976; Stillman et al., 1982; Gerlach et al., 1988; Davies et al., 1989; Madeira et al., 2010; Ramalho et al.,
167 2010b). The extrusives are dominantly mafic as exemplified by nephelinites and basanites at Santiago and
168 Fogo (Gerlach et al., 1988; Davies et al., 1989; Barker et al., 2009; Hildner et al., 2011, 2012). However
169 several volcanic centers such as the island of Brava and the Cadamosto Seamount exhibit largely felsic
170 assemblages (Assunção et al. 1965; Machado et al. 1968; Madeira et al., 2008, 2010; Barker et al., 2012;
171 Weidendorfer et al., 2016; Samrock et al., 2019). Cape Verde is one of the few Ocean Island groups
172 hosting carbonatites, which are widespread on Brava with minor exposures on Fogo, Santiago and São
173 Vicente (e.g., Assunção et al., 1965; Silva et al., 1981; Turbeville et al., 1987; Hoernle et al., 2002;
174 Jørgensen and Holm, 2002; Mata et al., 2010; Mourão et al., 2010).

175

176 **Geochronology of the Cape Verde archipelago**

177 The Cape Verde islands exhibit a general age progression from the early Miocene, for the oldest
178 exposures, which decrease westwards to the presently volcanically active parts of the archipelago (Figure
179 4; Bernard-Griffiths et al. 1975; Stillman et al., 1982; Mitchell et al. 1983; Torres et al. 2002; Plesner et
180 al. 2003; Jørgensen and Holm 2002; Duprat et al., 2007; Holm et al. 2008; Foeken et al. 2009; Dyhr and
181 Holm 2010; Madeira et al. 2010; Samrock et al., 2019). The older islands in the East are highly eroded
182 displaying relatively flat and low topography in contrast to the shield volcanoes that occur further West.
183 The earliest age of the eastern islands is recorded by submarine pillow basalts from the island of Sal at 26
184 Ma (Torres et al., 2002). The volcano-magmatic activity continues until approximately 1 Ma at Sal
185 (Figure 4; Mitchell et al., 1983; Torres et al., 1997; Holm et al., 2008; Dyhr & Holm, 2010). The northern
186 islands show volcanic activity from approximately 8 to 10 Ma to between 100,000 and 300,000 years ago
187 at São Nicolau to Santa Antão (Figure 4; Plesner et al. 2003; Duprat et al., 2007; Holm et al. 2008).
188 Seismic activity beneath Santa Antão suggests this region continues to be volcanically active (Faria &
189 Fonseca, 2014).

190 There is evidence that volcanism in the southern islands commenced at Santiago approximately
191 11 Ma ago (Figure 4; Stillman et al., 1982; Mitchell et al., 1983; Torres et al., 2002; Ali et al, 2003). The
192 majority of the volcano-magmatic activity on the southern islands emerges from 5.5 Ma at Santiago, 4.5
193 Ma at Fogo and 2.3 Ma at Brava (Holm et al., 2008; Foeken et al. 2009; Madeira et al., 2010; Ramalho et

194 al., 2010). The most recent volcanic eruptions from Santiago are dated to 740,000 years ago and 300,000
195 years ago at Brava (Holm et al., 2008; Madeira et al., 2010). The islands typically show multiple stages of
196 volcanism interrupted by periods of quiescence (Figure 4; Holm et al., 2008; Foeken et al., 2009; Madeira
197 et al., 2010; Ramalho et al., 2010a, 2010b, 2010c). Volcanic activity at the Cadamosto Seamount appears
198 to occur in the last 20,000 to 100,000 years (Samrock et al., 2019). The island of Fogo displays historical
199 volcanism with around 30 eruptions since discovery and settlement in 1460 including recent eruptions in
200 1995 and 2014 to 2015 (Ribeiro, 1960; Da Silva et al., 1999; Hildner et al., 2011, 2012; Silva et al., 2015;
201 Fernandes & Faria, 2015; Worsley 2015). Additionally Fogo, Brava and the Cadamosto Seamount display
202 ongoing seismic activity (Heleno et al., 2006; Grevemeyer et al., 2010; Faria & Fonseca, 2014).

203

204 **The geology of Santiago**

205 The island of Santiago is composed of an intrusive complex, followed by submarine and subaerial
206 volcanics (Figures 5 & 6; Bebiano, 1932; Serralheiro et al., 1976; Ramalho, 2011). The Complexo Antigo
207 consists of alkaline silicate intrusives and carbonatites. The submarine stage is represented by the
208 Flamengos Formation and exhibits pillow lavas embedded in hyaloclastite with eruption ages of 4.0 to 5.5
209 Ma (Figures 4, 5 & 6; Serralheiro, 1976; Holm et al., 2008; Barker et al., 2009; Ramalho et al., 2020c;
210 Ramalho, 2011). The shield stage is formed by subaerial lavas of the Pico da Antonía Formation between
211 1.5 and 3.2 Ma (Figures 4, 5 & 6; Serralheiro, 1976; Holm et al., 2008; Barker et al., 2010; Ramalho et
212 al., 2020c). Occasional carbonatite lava flows belong to the Pico da Antonía Formation (Jørgensen and
213 Holm, 2002). The Assomada and Monte das Vacas formations erupted post-erosional lavas and scoria
214 cones between 0.7 and 1.1 Ma (Figures 4 & 6; Serralheiro, 1976; Holm et al., 2008; Barker et al., 2010;
215 Ramalho et al., 2020c). Additionally, a sliver of the Jurassic ocean crust has been uplifted and emplaced
216 at Baía de Angra, plus uplifted sediments are found at Tarrafal (Serralheiro, 1976; Gerlach et al., 1988;
217 Ogg et al., 1995; Ramalho, 2011).

218

219 **The geology of Fogo**

220 The geology of Fogo can be divided into four units. The stratigraphy begins with the submarine stage
221 composed of carbonatites and alkaline basalts from approximately 4.5 Ma (Figure 4; Day et al., 1999;
222 Madeira et al., 2010). The emergence of Fogo as an island is recorded by the subaerial lavas of the Monte
223 Barro Group (Day et al., 1999). Subsequently a large stratovolcano known as Monte Amarelo developed
224 during the Quaternary, reaching up to 3 km above sea level (Figure 7; Day et al., 1999). A giant landslide

225 occurred at approximately 73 ka, leaving the Bordiera cliffs as a remnant of the caldera wall or flank
226 collapse scarp (Figure 1; Elsworth & Day, 1999; Masson et al., 2008; Foeken et al., 2009; Paris et al.,
227 2011, 2018; Ramalho et al., 2015; Madeira et al., 2019). The associated structure is filled with volcanic
228 materials to form a plateau known as the Chã das Caldeiras, which hosts the majority of the volcanic
229 activity from 62 ka to present (Figures 4 & 7; Ribeiro, 1960; Torres et al., 1997; Day et al., 1999; Foeken
230 et al., 2009). The spectacular Pico do Fogo, rising 2829 m above sea level formed by Hawaiian and
231 Strombolian activity that produced basanite to tephrite lapilli and lava (Figures 5 & 7; Torres et al., 1997).
232 Historic eruptions emanated from the base of Pico do Fogo, the eastern flank of Pico do Fogo or from
233 vents on the Chã das Caldeiras plain. The eruptions have typical durations of 2 months, and the last
234 eruption was 23rd November 2014 to 7th February 2015 (Figure 5; Silva et al., 2015; Fernandes & Faria,
235 2015; Worsley 2015). The eight previous eruptions occurred in 1785, 1799, 1816, 1847, 1852, 1857, 1951
236 and 1995 (Figure 4; Ribeiro, 1960; Torres et al., 1997; Day et al., 1999).

237

238 **The geology of Brava**

239 Brava is smaller than Fogo and Santiago with an area of 64 km², located 18 km from Fogo on the
240 Brava-Fogo platform, which is only 1400 mbsl (Figure 1; Da Silva et al., 1999; Madeira et al., 2010). The
241 geology was first investigated by Bebiano (1932) and later by Machado et al. (1968). Recent work by
242 Madeira et al. (2010) has divided the stratigraphy into three units. The submarine volcanism consists of
243 hyaloclastite and pillow basalt breccias and flows that radiate from the centre of the island (Figure 8;
244 Madeira et al., 2010). They are intruded by N-S and E-W oriented dikes. Subsequently the intrusive
245 complex was emplaced in the submarine volcanics. The alkaline-carbonatite intrusives are represented by
246 pyroxenites, ijolite-melteigites-urites and nepheline syenites plus carbonatites (Figure 8; Madeira et al.,
247 2010; Mourão et al., 2010). Post-erosional volcanism is dominantly phonolitic and ranges from
248 ignimbrites and tephra deposits due to phreatomagmatic eruptions, to phonolite lava flows and domes
249 (Figures 5 & 8). Mafic volcanism is rare in the post-erosional sections, however carbonatites in the form
250 of ignimbrites and lava flows are not uncommon (Figure 8; Madeira et al., 2010). Seismicity, particularly
251 NE and SE of Brava associated with volcanic cones on the Brava-Fogo platform, indicate that Brava is
252 magmatically active. Seismic swarms at depths of 2 to 10 km, along with seismic tremor suggest volcano-
253 tectonic events related to submarine intrusions (Faria & Fonseca, 2014).

254

255 **The Cadamosto Seamount**

256 The Cadamosto Seamount is a large circular submarine volcano, with a diameter of approximately 15 km,
257 and a height of 3 km, reaching water depths of up to 1380 mbsl (Figure 1; Hansteen et al., 2014). The
258 seamount has three main craters in the summit area, where pillow and sheet flows have been observed
259 (Figure 5). The samples are mainly phononphelinites to phonolites, with occasional basaltic samples
260 (Barker et al., 2012; Hansteen et al., 2014; Samrock et al., 2019). New ^{40}Ar - ^{39}Ar geochronology gives
261 eruption ages of 20 to 97 ka confirming the young nature of the seamount (Samrock et al., 2019).
262 Additionally the Cadamosto Seamount is seismically active with notable earthquakes of magnitudes 4.9
263 and 4.3 recorded in 1998 and 2004 respectively (Grevemeyer et al., 2010). The seismicity is interpreted to
264 be formed by brittle rock failure resulting from submarine intrusion (Grevemeyer et al., 2010).

265

266 **Volcanic eruptions and hazards at Fogo**

267 The natural hazards faced by the population of Fogo are weather related, such as droughts that lead to
268 famine, as well as flash floods and related landslides that destroy roads and buildings. Less common and
269 therefore considered less of a risk are volcanic eruptions and associated earthquakes. The volcanic
270 eruptions pose hazard to the communities living in the Chã das Caldeiras area (964 people) plus
271 potentially the towns on the East Coast of Fogo (11,000 people). Lava flows are the greatest hazard,
272 however volcanic gases and tephra also contribute to the volcanic hazards (Texier-Teixeira et al., 2014;
273 Nascimento, 2015; Silva et al., 2015, 2017; Richter et al., 2016).

274 There have been 28 eruptions on Fogo since discovery of the island by Portuguese sailors in 1460
275 (Ribeiro, 1960). The most recent eruption commenced on 22nd November 2014 and continued for 77 days,
276 finally ceasing on 7th February 2015. The eruption consisted of a 6 km high eruption cloud causing tephra
277 deposits in eight villages and towns, as well as other islands such as Brava to the West and São Vicente to
278 the North (Nascimento, 2015). The lava flows rapidly cut off the road access to Chã das Caldeiras and
279 went on to destroy the villages of Portela and Bandaeira including 75% of the buildings in the Chã das
280 Caldeiras area and 25% of the agricultural land and water storage facilities (Jenkins et al., 2017).

281 The volcano monitoring activities carried out by the Institute of National Meteorology and Geophysics
282 and the University of Cape Verde are essential to volcanic crisis management. Regular automated
283 monitoring covers seismicity and deformation of the volcano (Fonseca et al., 2003; Faria & Fonesca,
284 2014; Dionis et al., 2015a, b; Fernandes & Faria, 2015). During the eruption in 1995, volcanic tremor and
285 seismic swarms occurred between 1 and 5 km depths (Da Silva et al., 1999). Approximately seven weeks
286 prior to the eruption in 2014-2015, earthquakes were detected originating at depths of >15 km (Fernandes
287 & Faria, 2015). Additional geochemical monitoring of the volcanic gases is manual and therefore

288 sampling is conducted during specific campaigns and does not provide a continuous record of volcano
289 degassing (Dionis et al., 2015a,b; Pérez et al., 2015). For instance, air quality was monitored during the
290 2014-2015 eruption by the deployment of an instrument at one station in São Filipe on the West coast of
291 Fogo (Nascimento, 2015).

292

293 *Magmatic processes*

294 We use mineral chemistry from Cape Verde to explore the magmatic processes recorded by
295 clinopyroxene (Davidson et al., 2007). Advantages of focusing on clinopyroxene include crystallization
296 over a wide temperature range and during a large extent of magmatic differentiation. The volcanic rocks
297 from Santiago and Fogo classify as basanite, tephrite, alkali basalt, nephelinite and melanepehinite, with
298 minor tephriphonolite occurring at Fogo. Whereas those from Brava and the Cadamosto Seamount are
299 dominantly phonolite and phonotephrite combined with the presence of intrusive syenite at Brava (Figure
300 9; Barker et al., 2009, 2012; Hildner et al., 2011, 2012; Weidendorfer et al., 2016; Mata et al., 2017;
301 Samrock et al., 2019).

302 Clinopyroxene from Santiago and Fogo classifies as diopside-augite, whereas Brava and the
303 Cadamosto Seamount host both diopside-augite and green aegirine-augite (Barker et al., 2009, 2012;
304 Hildner et al., 2011, 2012; Weidendorfer et al., 2016; Rydeblad, 2018). Clinopyroxene from Santiago and
305 Fogo display compositions of dominantly 60 to 90 Mg# and 60 to 85 Mg# respectively (Figure 10; Mg#
306 $\text{mol\%} = (\text{Mg}/\text{Mg} + \text{Fe}^{\text{total}})$). The samples from Fogo also show minor abundances of clinopyroxene at 10 to
307 20 Mg# and 45 to 60 Mg#. Analysed clinopyroxene from Brava are dominantly aegirine-augite that
308 display a much wider range of compositions from 5 to 65 Mg# (Figure 10). The nephelinites and ijolites
309 host clinopyroxene with the highest frequency between 35 and 55 Mg#, whereas the syenites host
310 clinopyroxene with 10 to 35 Mg# (Figure 10). The seven diopside-augite analyses have 45 to 65 Mg#.
311 Clinopyroxene from the Cadamosto Seamount shows a skewed distribution with a range of 40 to 75 Mg#
312 and mode at 40 to 55 Mg# (Figure 10). When the diopside-augite and aegirine-augite are distinguished,
313 they range from 41 to 74 Mg# and 42 to 72 Mg# respectively (Figure 10). High $\text{Fe}^{3+}/\text{Fe}^{\text{total}}$ observed for
314 volcanic rocks from Cape Verde indicates crystallization under oxidizing conditions with high oxygen
315 fugacity (Holm et al., 2006; Duprat et al., 2007; Mata et al., 2017). This may increase the Mg# of the
316 clinopyroxene and would likely have a more significant effect as the iron content increases, thereby
317 having the greatest influence on the clinopyroxene compositions from Brava and the Cadamosto
318 Seamount (Freise et al., 2003). Additionally, the presence of h auyne and high sulphur contents in the
319 Brava and Cadamosto Seamount samples would further contribute to higher Mg# contents in

320 clinopyroxene (Andújar et al., 2008; Barker et al., 2012; Weidendorfer et al., 2016). The clinopyroxene
321 compositions reflect the overall composition of the volcanic centers with a restricted range of mafic
322 volcanic rocks found at Santiago and Fogo with high clinopyroxene Mg#, therefore differentiation has
323 played a limited role in these locations. At Brava and the Cadamosto Seamount the volcanic centers
324 become more felsic with wider compositional ranges and lower clinopyroxene Mg#. Consequently, the
325 clinopyroxene compositions exhibit wider ranges or skewed distributions recording the influence of
326 extensive fractional crystallization.

327 More detailed examination of the mineral chemistry shows that clinopyroxene from Santiago and
328 Fogo display increasing Al₂O₃, TiO₂ and low but increasing Na₂O and MnO with decreasing Mg# (Figure
329 11). In contrast, the clinopyroxene crystals from Brava and the Cadamosto Seamount form a different
330 trend at low and decreasing Al₂O₃, TiO₂ with decreasing Mg#. The clinopyroxene crystals from Brava
331 exhibit high Na₂O of 2.1 to 6.2 wt% compared to 0.3 to 1.3 wt% Na₂O in the clinopyroxene from
332 Santiago and Fogo. At the Cadamosto Seamount Na₂O contents increase from diopside-augite with 0.8 to
333 2.7 wt% to the aegirine-augite population with Na₂O of 2.7 to 4.5 wt% (Figure 11). The MnO contents
334 increase from 0.2 to 1.3 wt% in clinopyroxene with Mg# between 35 and 75 including all crystals from
335 the Cadamosto Seamount (Figure 11). Clinopyroxene crystals with Mg# ≤35 from Brava show a decrease
336 in MnO contents from 1.0 to 0.1 wt% as Mg# decreases (Figure 11).

337 The majority of the clinopyroxene crystals from Santiago and Fogo display strong correlations,
338 with only a relatively small proportion of clinopyroxene from Fogo plotting at lower Mg# for given Al₂O₃
339 and TiO₂ contents (Figure 11). This suggests dominantly equilibrium growth during fractional
340 crystallization of the magma and phenocryst formation (Mollo et al., 2013, 2018; Welsch et al., 2016).
341 The extensive differentiation trends in the clinopyroxene chemistry and the liquid lines of descent
342 observed in the whole rock geochemistry (Barker et al., 2009; Mata et al., 2017), suggest that equilibrium
343 crystallization occurred during melt evolution (e.g. Mollo et al., 2018). Thus, much of the crystal
344 population is in disequilibrium with the final host melt, and this disequilibrium is not homogenized by
345 diffusion or mixing of magmas. Consequently, the erupted products host antecrysts crystallized under
346 different conditions compared to the final melt compositions (e.g. Davidson et al., 2007; Barker et al.,
347 2009; Mollo et al., 2013, 2018; Welsch et al., 2016). At Brava and the Cadamosto Seamount the
348 clinopyroxene populations are more scattered illustrating greater compositional diversity. The equilibrium
349 mineral-melt pairs indicate that the diopside-augite population grew in equilibrium with low Na₂O melts
350 (<8 wt% Na₂O), whereas the host rocks have much higher Na₂O contents (8 to 14 wt% Na₂O; Barker et
351 al., 2012; Weidendorfer et al., 2016). Therefore despite their similar compositions, the diopside-augite
352 and aegirine-augite populations were likely aggregated from different melts (Figure 11).

353 Whole rock geochemistry for Santiago, Fogo and Brava confirms significant fractional
354 crystallization. At Santiago the full range of compositions indicate a total of 24% fractional crystallization
355 of predominantly clinopyroxene (Barker et al., 2009). The Fogo lavas record significant fractional
356 crystallization to produce the basanites and tephrites, which requires crystallization of up to 21%
357 clinopyroxene and minor olivine, Fe-Ti-oxides and apatite (Magnusson, 2016; Mata et al., 2017).
358 Likewise, the magmatic system at Brava shows 15% olivine and 35% clinopyroxene crystallization, with
359 subordinate Fe-Ti-oxides and apatite, which explains the ijolite and nephelinite compositions
360 (Weidendorfer et al., 2016). Furthermore, a total of 90% fractional crystallization is required to produce
361 the entire range of whole rock compositions (Weidendorfer et al., 2016). The lavas at Santiago and a few
362 of those from Fogo display high MgO contents implying a role for aggregation of crystals (Barker et al.,
363 2009; Magnusson, 2016; Mata et al., 2017). These accumulated crystals must have grown in very similar
364 magmas following the liquid line of descent for clinopyroxene crystallization shown by their Mg# and
365 Al₂O₃ content (Figure 11).

366 Now we consider zoning patterns in clinopyroxene crystals and the processes they reveal.
367 Petrographically at Santiago we frequently observe patchy cores that are rounded by resorption. Apparent
368 in this example the resorbed, patchy core passes into an area of concentric zonation, where oscillatory
369 zoning emphasizes the different growth rates for different sectors of the crystal (Figure 12). The
370 associated chemistry for the zoned clinopyroxene crystal from Santiago exhibits a plateau over the patchy
371 core with only small variations. The outer oscillatory zonation displays trends of fractional crystallization
372 with decreasing Mg# and MnO content simultaneous with increasing TiO₂ content (Figure 12; Streck,
373 2008). Additionally, at Santiago the oscillatory zonation records recharge events with increasing Mg# and
374 MnO associated with a decrease in TiO₂ content. The behaviour of Mg# and MnO are also observed to be
375 decoupled, which indicates the occurrence of magma mixing. The selected clinopyroxene crystal from
376 Fogo also reveals a patchy core followed by two outer zones. The fractures highlight differences in
377 resorption of the core. The zone surrounding the core shows oscillatory zoning and then passes into a
378 relatively homogeneous rim (Figure 12). The patchy core shows small variations in Mg#, whereas the
379 oscillatory zone exhibits large variations in Mg# and the rim shows homogeneously high Mg# (Figure
380 12). The variations in TiO₂ and MnO contents are not consistent with the variations in Mg#, therefore
381 much of the variation cannot be attributed to fractional crystallization or recharge events. Instead the
382 zonation records magma chamber dynamics associated with temperature and compositional differences
383 causing convection and mixing (Figure 12; Streck, 2008; Rydeblad, 2018). The clinopyroxene crystal
384 from the Cadmosto Seamount shows a resorbed core surrounded two concentric outer zones (Figure 12).
385 The concentric zones are homogeneous and incongruent with curved boundaries. In the associated

386 chemical variations, we observe a decrease in both Mg# and TiO₂ in the outer zones of the crystal,
387 reflecting differentiation in this felsic system (Figure 11, 12). The variation in MnO content in the outer
388 zones, despite the decrease in Mg# suggests that MnO behaves differently in felsic alkali magmas than
389 their mafic counterparts (Streck, 2008). However the offset in composition of Mg# and TiO₂ in the two
390 outer zones and the change in MnO also points towards magma mixing or variations in thermal conditions
391 of the magma (>32 μm; Figure 12). The small variations in the inner part of the crystal (<27 μm), reflect
392 variations in magma chamber compositional and thermal conditions. The zonation and textures of
393 clinopyroxene crystals from southern Cape Verde indicate that the host magmas were not homogeneous
394 in composition or temperature. This is traced by significant differences in behaviour between the major
395 cation species in the mineral structure such as MgO, FeO and CaO and the trace elements TiO₂, MnO and
396 Al₂O₃. The latter record the chemical and thermal disequilibrium of the magma chamber (Mollo et al.,
397 2013, 2018; Welsch et al., 2016).

398

399 *Magma storage in southern Cape Verde*

400 The volcanics at Cape Verde are highly alkaline, in contrast most thermobarometers for igneous
401 minerals are calibrated for subalkaline tholeiitic and calc-alkaline systems (e.g. Nimis, 1995; Putirka,
402 2008, Neave & Putirka, 2017). The clinopyroxene thermobarometers that are appropriate for alkaline
403 systems often target mafic and ultramafic compositions (Ashchepkov et al., 2011), and are thereby not
404 suited to the range of differentiated compositions observed at Cape Verde. The only available
405 clinopyroxene-melt thermobarometer that has been developed for evolved alkaline systems is calibrated
406 for relatively high K/Na (Masotta et al., 2013). Unfortunately, the lavas from Cape Verde are highly
407 enriched in Na, giving a low K/Na ratio and thus this formulation is not ideal for clinopyroxene from
408 Cape Verde (Barker et al., 2012, 2019). The only thermobarometer that has been calibrated for a range of
409 alkaline compositions, providing a method for intercomparison between all samples, is the clinopyroxene-
410 melt equilibrium thermobarometer of Putirka (Putirka et al., 1996, 2003; Putirka 2008). The Putirka
411 clinopyroxene-melt thermobarometer has been widely applied in many alkaline settings (e.g. Klügel et al.,
412 2000, 2005, Nikogosian et al., 2002). It has also been shown to be consistent with independent depth
413 estimates such as seismic tomography, seismic reflection profiles or earthquakes patterns (e.g. Longpré et
414 al., 2014; Barker et al., 2019). Unfortunately the data used by Putirka (2008) for calibration of evolved
415 alkali compositions is sparse and therefore also not ideal (Putirka et al., 1996, 2003; Putirka 2008).
416 Hence, we compare the results from the models of Masotta with those of Putirka (Putirka et al., 1996,
417 2003; Putirka 2008; Masotta et al., 2013). Therefore, we employ models A and B for pressure and

418 temperature respectively from Putirka et al. (2003) for consistency with Hildner et al. (2011, 2012) and
419 additionally for the evolved compositions equations P-alk and T-alk from Masotta et al. (2013).

420 The clinopyroxene-melt thermobarometer is based upon jadeite (NaAl) and diopside-
421 hedenbergite (CaMgFe) exchange between clinopyroxene and melt for determination of temperature. The
422 corresponding pressure is estimated from the distribution of the jadeite component (NaAl) between
423 clinopyroxene and the equilibrium melt (Putirka, 2008). Employment of the clinopyroxene-melt
424 equilibrium thermobarometer thus requires demonstration of equilibrium between the clinopyroxene and
425 melt. There are two commonly used approaches to test for equilibrium. Firstly, testing for equilibrium
426 from Fe-Mg partitioning utilizing a Rhodes diagram, with $K_d(\text{Fe-Mg})$ of 0.275 ± 0.067 (Putirka, 2008;
427 Barker et al., 2009, 2012). A second approach is to employ the variations between clinopyroxene
428 components as observed from the mineral chemistry and calculated from the melt composition (Putirka,
429 2008; Mollo et al., 2013). Typically, equilibrium is considered to be within ± 0.06 DiHd, ± 0.07 EnFs and
430 ± 0.02 Jd of unity (Putirka, 1999). Mollo et al. (2013) proposed an additional multicomponent equilibrium
431 test, expressed as the difference between the DiHd component and tested on the alkaline compositions
432 characteristic of Mt. Etna. The multicomponent equilibrium test derives from a comparison between the
433 clinopyroxene components calculated from the equilibrium with the melt and directly from the
434 clinopyroxene composition.

435 Ideal mineral-melt pairs are considered to be analysis of groundmass glass and proximal crystal
436 rims. However it is rare to have much glass in lavas from Cape Verde, which tend to display a
437 microcrystalline groundmass (Barker et al., 2009, 2012; Hildner et al., 2011, 2012). Glassy melt
438 inclusions are typically modified during cooling of volcanic rocks and are therefore not suitable (Baker,
439 2008). Glass or groundmass separates would provide equilibrium melt compositions for crystal rims,
440 representing the final growth from the melt. Consequently, whole rock compositions that include minerals
441 and groundmass are more likely to represent core compositions (Barker et al., 2009). Employing the
442 whole rock composition of a sample as nominal melts for testing clinopyroxene-melt equilibrium is
443 therefore not only suitable but also necessary to understand the crystallization conditions of the entire
444 crystal population. Equilibrium between clinopyroxene and melt can be further optimized, by subtracting
445 the compositions of the modal mineral content from the whole rock composition (Barker et al., 2009).
446 Another approach to find an optimal equilibrium match between clinopyroxene and melt is to select
447 equilibrium melt compositions from a related suite of volcanic rocks (Barker et al., 2015; Neave &
448 Putirka, 2017). The minimum ΔDiHd for data from Santiago, Fogo, Brava and the Cadamosto Seamount
449 occurs at a temperature difference of 20°C (Figure 13). The ΔDiHd ranges from $+0.02$ to $+0.15$,
450 meanwhile the temperature decreases to $+0.4^\circ\text{C}$ at ΔDiHd of $+0.03$ and increases up to 75°C as the ΔDiHd

451 increases to a maximum of +0.15. The multicomponent equilibrium appears to be equally good for
452 evolved compositions such as at the Cadamosto Seamount as for the more mafic systems, for example
453 Fogo.

454 Evaluation of the oxygen fugacity for the most recent eruptions at Fogo suggests fO_2 of +0.9 to
455 +2.3 log ΔNNO with Fe^{3+}/Fe^{total} of 0.21 (Mata et al., 2017). These relatively oxidized conditions are
456 confirmed by ultramafic xenoliths with fO_2 of up to +2.2 log ΔQFM (Ryabchikov et al., 1995). Other
457 approaches have determined the Fe^{3+}/Fe^{total} to 0.19 to 0.26 at Santo Antão and São Nicolau (Holm et al.,
458 2006; Duprat et al., 2007). Cape Verde like many Ocean Island Basalts is apparently relatively oxidized
459 compare to Mid Ocean Ridge Basalts. Herzberg and Asimow (2008) calculate primary magma
460 compositions for Ocean Island Basalts globally and find a range in Fe^{3+}/Fe^{total} of 0.15 to 0.25. Their
461 findings are consistent with estimates of oxygen fugacity and Fe^{3+}/Fe^{total} at Cape Verde that represent
462 relatively oxidized conditions. The influence of oxidation on the clinopyroxene compositions may impact
463 the equilibrium especially that based on Mg# and clinopyroxene components that contain iron (Freise et
464 al., 2003; Andújar et al., 2008). It is possible to vary Fe^{3+}/Fe^{total} in the thermobarometric modeling, and
465 therefore we have adopted a Fe^{3+}/Fe^{total} of 0.21. However, the potential implications on the resulting
466 crystallization conditions are unclear and the applicability of the calibration data to such oxidized
467 conditions is also uncertain.

468 Conversion of pressure to depth has been performed with a crustal density of 2800 kg/m³ for the
469 mafic ocean crust (Barker et al., 2009, 2012; Hildner et al., 2011, 2012). Uncertainties associated with the
470 experimental calibration data are $\pm 33^\circ C$ and ± 0.17 GPa (SEE; Putirka, 2008), which equates to depths of
471 ± 6 km. Hence, much of the range in pressure estimates described below are within error of the method
472 (Figure 14).

473 Now turning to southern Cape Verde, the equilibrium clinopyroxene crystals from Santiago
474 display compositions of 75 to 90 Mg#. These clinopyroxene crystals belong to alkaline basalts, basanites,
475 tephrites and melanephelinites and are in equilibrium, $\Delta DiHd$ of 0.01 to 0.08, with compositions in the
476 range of 52 to 65 Mg# (Figure 9, 13; Barker et al., 2009). The corresponding crystallization conditions are
477 temperatures of 1165 to 1255°C and pressures of 0.40 to 1.15 GPa (Figure 14; Barker et al., 2009).

478 From Fogo the clinopyroxene mineral chemistry shows the highest frequency compositions
479 between 60 and 85 Mg# (Figure 10). The host rocks are tephrite, basanite, foidite and tephriphonolite and
480 equilibrium, $\Delta DiHd$ of <0.12 and corresponding melt compositions for the main clinopyroxene
481 population range between 30 and 54 Mg# (Figures 9 & 13; Hildner et al., 2011, 2012; Rydeblad, 2018).
482 The resulting crystallization conditions are 1010 to 1255°C and 0.45 to 1.35 GPa, which compare well

483 with existing data of 1010 to 1150°C and 0.42 to 0.90 GPa for pre-eruptive magma storage conditions
484 (Hildner et al., 2011, 2012; Mata et al., 2017). Mata et al. (2017) further divide the crystallization
485 conditions for the 2014-2015 eruption at Fogo by host magma into 1045 to 1065°C and 0.56 to 0.78 GPa
486 for phonotephrites and 1100 to 1145°C at 0.70 to 0.90 GPa for tephrites. This study extends the range of
487 crystallization conditions to higher temperatures and pressures, thereby also characterizing the deeper part
488 of the magma storage system (Figure 14; Hildner et al., 2011, 2012; Mata et al., 2017).

489 There are only a few analyses of diopside-augite from Brava that are hosted by nephelinite with
490 Mg# 47 to 62 (Weidendorfer et al., 2016). They show equilibrium, ΔDiHd of 0.02 to 0.13, with low Na
491 melt compositions of Mg# 20 to 32 (Figures 10 & 13). The Putirka et al. (2003) models estimate
492 crystallization at 1170 to 1300°C and 0.2 to 1.0 GPa (Figure 14). In comparison the Masotta et al. (2013)
493 model indicates crystallization at lower temperatures of 930 to 980°C and 0.29 to 0.67 GPa and shows
494 less scatter than the estimate from Putirka et al. (2003).

495 Diopside-augite from the Cadamosto Seamount have 40 to 75 Mg# (Figure 10; Barker et al.,
496 2012). The corresponding whole rocks are phonolite to phononephelinite and equilibrium melt
497 compositions are 29 to 37 Mg# with ΔDiHd of 0.01 to 0.16 (Figures 9 & 13; Barker et al., 2012). The
498 Putirka et al. (2003) model gives crystallization conditions of 970 to 1025°C and 0.45 to 1.35 GPa,
499 whereas the Masotta et al. (2013) model indicates 925 to 980°C and 0.26 to 0.70 GPa (Figure 14). Hence
500 the results from the Masotta et al (2013) model overlap with those estimated by the model of Putirka et al.
501 (2003) and extend to lower temperature and pressure. These evolved magmas from Brava and the
502 Cadamosto Seamount crystallized at lower temperatures compared to the clinopyroxene from Santiago
503 and Fogo (Figure 14; Barker et al., 2012).

504 The clinopyroxene crystals feature significant zonation through which we track the magma
505 chamber dynamics for samples from Fogo. Rapid decreases in clinopyroxene Mg# occur under several
506 scenarios, sometimes with no discernable temperature or pressure changes, suggesting mixing processes
507 (Figure 15a). A second scenario observed in the zonation is a rapid decrease in clinopyroxene Mg# with a
508 decrease in temperature on the order of 30°C and simultaneous decrease in pressure suggesting
509 convection and ascent within the magma reservoir (Figure 15b). In contrast, rapid increase in
510 clinopyroxene Mg# occurs with large variations in temperature (Figure 15b). This implies that the thermal
511 and compositional gradients are not perfectly contemporaneous and that thermal and chemical mixing
512 occur at different rates. Whereas there are also examples of gradual increase in clinopyroxene Mg#
513 corresponding with slight increases in temperature and pressure (Figure 15c). In some places the outer

514 rims record a decrease in clinopyroxene Mg#, with simultaneous decreases in temperature and pressure
515 (Figure 15d), indicating magma evolution during ascent within the magma reservoir.

516 Integrating the thermobarometry from the different locations, we find that crystallization was in
517 the range of 12 to 40 km (Figure 14 & 16). Therefore, the magma storage beneath southern Cape Verde
518 occurs below the Moho in the oceanic lithospheric mantle. At Santiago and Fogo the highest frequency of
519 crystallization is at 30 to 40 km (Figure 16; Barker et al., 2009; Hildner et al., 2011, 2012; Rydeblad,
520 2018). We also observe in the samples from Fogo that the rims crystallize with highest frequency between
521 20 and 30 km and extend to lower pressures approaching the Moho (Figure 14). This suggests that the
522 more mafic magmas begin to crystallize clinopyroxene deep in the system and move upwards towards the
523 Moho as crystallization continues and zonation and final rim compositions progressively form (Figure
524 15d). Evolution of magma storage depths with differentiation is consistent with the increase in Al₂O₃
525 contents up to 13 wt% as MgO content decreases signaling magmatic differentiation and associated with
526 lower pressures of crystallization (Figure 11; Marianelli et al. 1999; Morgan et al., 2004). Hildner et al.
527 (2012) proposed that the pre-eruptive magma storage conditions become shallower with time in the
528 historic eruptions. However, no trends with time appear when we investigate the crystallization conditions
529 of the whole range of clinopyroxene compositions. The absence of systematic temporal variations is
530 confirmed by clinopyroxene from the 2014-2015 eruption recording pressures of 0.56 to 0.9 GPa, which
531 are deeper than for the 1995 and 1951 eruptions (Mata et al., 2017).

532 The dominance of the deep magma storage zone indicates that the magmatic processes of
533 differentiation, recharge, mixing and potentially convection recorded by the crystal populations take place
534 in this deep magma storage zone (Figures 12, 14 & 15). The accumulation of antecrysts and aggregation
535 of crystal populations is likely to also occur in this deep magma storage zone before magmas ascend and
536 erupt. Thus, the resorbed kaersutite crystals frequently found in lavas from Fogo probably crystallized in
537 the oceanic lithospheric mantle, consistent with amphibole thermobarometry yielding pressures of
538 approximately 0.6 GPa (Mata et al., 2017). Subsequently they would have been incorporated into magmas
539 with starkly different compositions leading to their break down (Hildner et al., 2011, 2012).

540

541 *Controls on the depth of magma storage*

542 The location of the magma storage is controlled by the crustal structure beneath the South of the
543 Cape Verde archipelago. The islands and seamounts stand several kilometers above the seafloor at
544 approximately 4000 mbsl and beneath them is 1 to 2 km of sediments (Figure 2; Lancelot et al., 1978;

545 [Pim et al., 2008](#)). The sediments overlie relatively old 130-135 Ma Central Atlantic ocean crust which
546 extends down to the Moho at depths of 12 to 18 km, that decrease from East to West ([Ali et al., 2003](#);
547 [Lodge & Helffrich, 2006](#); [Pim et al., 2008](#)). Hence the deep mantle plume source generates magmas
548 which ascend in to the oceanic lithospheric mantle where they stagnant below the mantle-crust boundary
549 ([Figure 16](#); [Barker et al., 2009](#)).

550 The density of the ocean islands and seamounts, as well as the ocean crust extending down to the
551 crust mantle boundary at 12 to 18 km beneath Cape Verde is estimated to be 2.75 to 2.80 g/cm³ ([Ali et al.,](#)
552 [2003](#); [Lodge & Helffrich, 2006](#); [Pim et al., 2008](#)). The sediments would be expected to provide a low
553 density layer between the mafic ocean crust and the Cape Verde islands and seamounts ([Pim et al., 2008](#)).
554 The expected upper mantle density is 3.1 g/cm³ ([Tenzer et al., 2013](#)). The density contrast between the
555 upper mantle and the oceanic crust evidently controls the depth and pressures of magma storage ([Figure](#)
556 [14 & 16](#)). The basanite, tephrite and melanephelinite at Fogo and Santiago have calculated densities of
557 2.65 to 2.80 g/cm³ ([Bottinga & Weill, 1970](#); [Bottinga et al., 1982](#)). This range is similar to the mafic
558 ocean crust and extends to slightly lower densities, therefore the mafic magmas would be expected to
559 pool at the Moho or slowly ascend. However the actual density of magma is a function of both the melt
560 density and the crystal cargo. Many of the erupted basanitic lavas have crystal contents of 5 to 20% and
561 even more in ankaramite samples ([Barker et al., 2009](#)). Such crystal cargoes of dominantly clinopyroxene
562 and olivine would increase the density of the magma, leading to a decrease in buoyancy and stagnation of
563 the magma below the crust-mantle boundary.

564 Common magma storage depths, irrespective of magma composition and age are likely associated
565 with significant magma intrusion, solidification and formation of crystal mush zones. This would serve to
566 underplate the oceanic crust with mafic materials, building a magma storage zone of lower density than
567 the surrounding upper mantle lithologies ([Klügel et al., 2015](#)). Evidence for this comes from Fogo lavas
568 that host several cumulate nodules, containing olivine, clinopyroxene, kaersutite, spinel and phlogopite
569 ([Hildner et al., 2012](#)). The spinel, kaersutite and phlogopite are consistent with crystallization in the
570 oceanic lithospheric mantle. Therefore, these nodules are likely sampling cumulates formed in the deep
571 magma storage zone. Furthermore, crustal thickening associated with underplating and potentially
572 shallower intrusions contributes to localized uplift on individual islands, such as observed on Santiago
573 and Brava ([Madeira et al., 2010](#); [Ramalho et al., 2010a, 2010b](#)).

574 The phonolites and syenites at Brava and the Cadamosto Seamount have calculated densities of
575 2.35 to 2.48 g/cm³ and even the clinopyroxene-equilibrium melts show densities of 2.45 to 2.48 g/cm³,
576 consistent with recent experimental constraints ([Bottinga & Weill, 1970](#); [Bottinga et al., 1982](#); [Seifert et](#)

577 al., 2013). Such densities for phonolitic magma carrying relatively low density minerals should promote
578 magma buoyancy and ascent through the ocean crust. Although the viscosity of magma would also
579 change during differentiation and influence the magma dynamics. The resulting increase in viscosity of
580 the magma plus the entrained crystal population potentially inhibit magma ascent. Crystal contents of 40
581 to 50% cause the magma to behave as a rigid crystal network, trapping it in the magma storage zone
582 (Cooper, 2017). The crystal content ranges from 10 to 50% for the Cadamosto Seamount, thus the crystal
583 assemblages along with the magma evolution controls the viscosity and thereby promote continued
584 magma storage in the upper oceanic lithospheric mantle (Barker et al., 2012).

585 The equilibrium clinopyroxene compositions at Brava and the Cadamosto Seamount are 45 to 75
586 Mg# with equilibrium melt densities of 2.45 to 2.48 g/cm³ (Figure 10). However, it is likely that the host
587 magma carrying the existing crystal cargo, would have continued to evolve with a corresponding density
588 change to 2.35 g/cm³. Such a change in density provides a larger density contrast between the mafic
589 ocean crust and the most evolved phonolitic compositions that may have promoted magma ascent.

590

591 *Insights into the shallower magmatic system*

592 Evidence of magmatic processes occurring shallower in the crust at Cape Verde is limited. At the
593 Cadamosto Seamount, the majority of the diopside-augite crystallization occurs below the Moho in the
594 deep magma storage zone (Figure 16). However the magma differentiation and aegirine-augite
595 crystallization is unaccounted for by this crystallization model. Furthermore, at the Cadamosto Seamount
596 the $\delta^{18}\text{O}$ for clinopyroxene (diopside-augite) have mantle derived values of +5.3‰, whereas the
597 feldspathoids show $\delta^{18}\text{O}$ of +6.3 to +7.1‰, elevated over the mantle equilibrium value of +6.25‰ ($\delta^{18}\text{O}$
598 SMOW; Zhao and Zheng 2003; Barker et al., 2012). Additionally the sulfur isotopes for whole rock
599 powders gave $\delta^{34}\text{S}$ of +4.7 to +5.9‰, highly enriched compared to mantle values with $\delta^{34}\text{S}$ of $+0.8 \pm$
600 0.2‰ (Sakai et al. 1984; Barker et al., 2012). Barker et al. (2012) interpreted these feldspathoid and
601 whole rock isotope signatures to be caused by assimilation of a few percent of oceanic sediments and
602 anhydrite. Hence the magmas associated with the Cadamosto Seamount interact with the sediment crustal
603 layer, which is likely located at 4 to 6 km below sea level (Figures 2 & 16; Lancelot et al., 1978; Pim et
604 al., 2008). This evidence suggests that less differentiated magmas ascend from the deep magma storage
605 zone and evolve to phonolitic compositions through assimilation during storage in the upper crust.
606 Seismicity in the vicinity of the Cadamosto Seamount also records crustal magmatic activity at depths of
607 0.5 to 15 km, which is likely associated with shallow hydrothermal processes and slightly deeper volcano-
608 tectonic events such as magma intrusion in the ocean crust (Figure 16; Grevenmeyer et al., 2010). The

609 volcano-tectonics events provide evidence for crustal magma storage, consistent with assimilation of
610 sedimentary components by the magmas.

611 Brava hosts a carbonatite-silicate intrusive complex, where the silicate rock types are represented
612 by ijolite, nephelinite and nepheline syenite (Weidendorfer et al., 2016). Extreme fractional crystallization
613 takes place, up to 90%, which is reflected in the large range of clinopyroxene compositions of 5 to 65
614 Mg# (Figure 10). The presence of clinopyroxene from 3 to 90% fractional crystallization is consistent
615 with the wide range in clinopyroxene compositions (Figure 10). Significant crystallization may have
616 occurred in the deep magma storage zone (<30%; Weidendorfer et al., 2016), in the presence of olivine,
617 perovskite and magnetite as illustrated by the crystallization of clinopyroxene with Mg# 47 to 62 at and
618 below the Moho in the nephelinites from Brava (Figure 13). Given the challenges of mobilizing magmas
619 containing more than 40 to 50% crystals (Cooper, 2017), deep crystallization is likely followed by magma
620 ascent and intrusion into the upper crust beneath the volcanic edifice, where *in situ* differentiation and
621 crystallization continue. Thereby crystallizing the majority of the aegirine-augite and other phases of the
622 syenite in the ocean crust. Persistent and relatively shallow magma storage is required to provide the heat
623 source for the active geothermal system on Brava that contains a mixture of magmatic and biogenic gases
624 (Dionis et al., 2015a). Additionally, Brava is seismically active recording volcano-tectonic events at
625 depths of 2 to 10 km in the ocean crust and volcanic edifice (Figure 16; Faria & Fonseca, 2014). The
626 seismicity is consistent with continued magma differentiation in the volcanic edifice.

627 There is evidence for temporary magma storage at Fogo, associated with magma ascent and
628 eruption. Olivine and clinopyroxene hosted fluid inclusions from the eruptions in 1995 and 1951 re-
629 equilibrated at depths of 8 to 13 km (Figure 16; Hildner et al., 2011; 2012). Hildner et al. (2011, 2012)
630 report relatively rapid re-equilibration during stagnation at these lower crustal depths over timescales of
631 hours to days. Hence eruption related temporary magma pooling occurs in the lower ocean crust.
632 Seismicity associated with the 1995 eruption at Fogo locates depths of magma storage between 1 and 5
633 km in the volcanic edifice and oceanic crust (Figure 16; Da Silva et al., 1999). Additionally, the surface
634 deformation signals from the 1995 eruption have been explained by a 2 km deep magma source, fed from
635 a conduit that extends to depths of more than 16 km (Figure 16; Amelung and Day, 2002). Precursory
636 seismicity to the 2014 eruption commenced in early October before the eruption on 23rd November 2014
637 (Fernandes & Faria, 2015). The initial earthquakes were recorded at depths exceeding 15 km, associated
638 with the sub-Moho magma storage zone. On 22nd November the seismicity was dominated by high
639 frequency and magnitude long-period earthquakes at depths of 2 to 4 km (Fernandes & Faria, 2015;
640 Jenkins et al., 2017). The 2014/2015 surface deformation is consistent with a dike propagating vertically
641 from sub-Moho depths and arriving below Pico do Fogo where the magma flowed laterally towards the

642 Southwest before erupting (González et al., 2015). Therefore, the transient eruption related magma
643 pathways can be traced from the sub-Moho magma storage zone, through the lower ocean crust to the
644 magma pockets in the volcanic edifice feeding the magma to the eruption fissure.

645 Long-term magma storage in the crust is suggested by shallow seismicity and the sustained
646 geothermal system. Fogo hosts a geothermal system with typical temperatures of 90-100°C recorded at
647 degassing fumeroles and values up to 130 to 190°C reported in the months leading up to the 2014
648 eruption (Risby & Sandback 2014; Dionis et al., 2015b). The active degassing is composed of a mixture
649 between magmatic and biogenic-atmospheric gases (Dionis et al., 2015b). Shallow seismicity at depths of
650 300 to 400 m below the Chã das Caldeiras plateau are confirmed by drilling to correspond to the
651 geothermal system (Faria & Fonseca, 2014). This requires a relatively shallow long-term heat source to
652 sustain the geothermal activity, although it has not yet been detected by geophysical methods (Caranova
653 & Silva, 2012). The heat source may be associated with the volcano-tectonic earthquakes at depths of up
654 to 7 km, this would imply that these earthquakes are caused by magma intrusion (Faria & Fonseca, 2014).

655 This information of magma storage depths and magma ascent timescales provides vital
656 information to scientists at the Institute of National Meteorology and Geophysics and the University of
657 Cape Verde attempting to interpret seismicity, deformation and volcanic gas geochemistry. Thereby
658 contributing to the decision making and communication with the National Civil Protection of Cape Verde
659 in times of impending volcanic crisis (Faria & Foneses, 2014; Dionis et al., 2015a, b). Additional
660 information on the volcanic hazards offered by Earth science comes in the form of volcanic hazard maps.
661 Richter et al. (2016) have examined the probable pathways of lava flows following the 2014-2015
662 eruption. Their results suggest that the locations of Portela and Bandaeira continue to be a risk of future
663 lava flows.

664

665 *Ocean Islands globally*

666 The southern chain of the Cape Verde hotspot therefore exhibits a predominantly deep magma
667 storage zone at depths of between 12 and 40 km traced by clinopyroxene thermobarometry, seismicity
668 and deformation (Figure 17). Magma ascent through the ocean crust is documented by fluid inclusions
669 and seismicity. Additionally, shallow crustal magma storage is found by seismicity and deformation in
670 the upper 5 km of the oceanic crust and volcanic edifice. Prior to the eruption in 2014/2015 seismicity
671 traced the magma ascent from below the Moho, through the crust to the upper crust in the months leading
672 up to the eruption (Fernandes & Faria, 2015; González et al., 2015; Jenkins et al., 2017).

673 A comparison with the Canary Islands, suggests that the clinopyroxene equilibrium
674 thermobarometry and seismicity also display similarly deep magma storage relative to a Moho depth of
675 13 to 15 km (Figure 17; Ranero et al., 1995). Gran Canaria records magma storage at 15 to 36 km below
676 the Moho with a subsidiary zone at 3 to 4 km (Table 1; Aulinas et al., 2010). The island of Tenerife also
677 shows deep magma storage at 20 to 45 km (Longpré et al., 2008). Estimates for magma storage at La
678 Palma also range from 12 to 45 km placing the magma storage within the oceanic lithospheric mantle
679 (Klügel et al., 2000; 2005; Nikogosian et al., 2002; Galipp et al., 2006; Barker et al., 2015). Magma
680 storage for the 2011 eruption at El Hierro has been reported to occur at depths of 17 to 24 km consistent
681 with seismic activity (Longpré et al., 2014 and references therein). Fluid inclusions and deformation
682 suggest magma storage in the lower crust (Longpré et al., 2014). Additionally investigation of the
683 deformation places a magma storage zone in the upper crust (Figure 17). In the 2011 eruption offshore el
684 Hierro the seismicity migrated upwards and laterally tracking the movement of magma supplied from
685 sub-Moho magma storage through the crust to eruption at the seafloor (González et al., 2013).

686 At Madeira, magma storage from clinopyroxene equilibrium thermobarometry has been shown to
687 occur at depths of 15 to 35 km and therefore deep relative to Moho depths of 14 to 15 km (Figure 17;
688 Schwarz & Klügel 2004; Klügel and Klein, 2006). Furthermore, fluid inclusions record temporary
689 stagnation in the lower and upper crust (Schwarz & Klügel 2004; Klügel and Klein, 2006).

690 The Azores also record deep crystallization of clinopyroxene, olivine and plagioclase as well as
691 entrapment of primary fluid inclusions (Figure 17; Renzulli & Santi 2000; Beier et al., 2006; Dias et al.,
692 2007; Madureira et al., 2011; Zanon et al., 2013; Zanon & Pimentel 2015). In the lower crust magma
693 storage is recorded by continued crystallization of clinopyroxene, along with fluid inclusion equilibration
694 and the appearance of seismicity (Renzulli & Santi 2000; Beier et al., 2006; Dias et al., 2007; Silva et al
695 2012; Madureira et al., 2011; Zanon et al., 2013; Zanon & Pimentel 2015). A shallow crustal magma
696 pocket is picked out by seismicity, water solubility and plagioclase-olivine experimental phase petrology
697 (Renzulli & Santi 2000; Silva et al 2012; Jeffery et al., 2016).

698 Clinopyroxene crystallization in basanites traces magma storage at Tristan da Cunha to the
699 oceanic mantle lithosphere and for more evolved trachyandesite to the middle of the ocean crust (Figure
700 17; Weit et al., 2017). Earthquakes were felt on Tristan da Cunha commencing several months prior to the
701 eruption in 1961 and again associated with the nearby submarine eruption in 2004 (O'Mangain et al.,
702 2007). These earthquakes showed high signal to noise ratios on the nearest seismometers, thus the
703 earthquakes were deemed to have shallow epicenters and the seismicity was employed to locate the
704 eruption to 40 to 50 km South of Tristan da Cunha (O'Mangain et al., 2007).

705 Information for the magma storage system at Ascension is derived from melt inclusions, placing
706 stagnation in the lower crust (Figure 17; Chamberlain et al., 2016). Additionally, seismic data suggests
707 volcano-tectonic events some of which occur in the shallow crust of the Ascension rift zone (Hanson et
708 al., 1996).

709 In the Pacific Ocean, the two hotspots with records of magma plumbing systematics are Hawaii
710 and the Galapagos. Investigations at Hawaii record clinopyroxene crystallization in the oceanic
711 lithosphere and through to the lower crust (Figure 17; Putirka et al. 1996; Putirka 1997; Chatterjee et al.,
712 2005; Hammer et al., 2016). Whereas seismicity occurs in the upper crust beneath the central volcanoes
713 and extends into the middle crust at rift zones (Poland et al., 2015). Wolf island in the Galapagos shows
714 clinopyroxene crystallization in the lower crust (Stock et al., 2018). Lower crustal magma storage is
715 confirmed by deformation, which places magma storage at 6 to 9 km depth as well as in the volcanic
716 edifice at approximately 1 km (Stock et al., 2018).

717 Reunion hotspot in the Indian Ocean hosts Piton de la Fournaise volcano, which frequently
718 displays volcanic activity, including an eruption in 2007. Magma storage at the Moho and below is traced
719 by seismicity, as well as melt inclusions and volatile solubility which extend to much greater depths
720 (Figure 17; Bureau et al., 1998; Peltier et al. 2009; Di Muro et al., 2014). Mid-crustal magma stagnation
721 is indicated by melt inclusions and seismicity (Bureau et al., 1998; Peltier et al. 2009), whereas shallow
722 magma storage below the volcanic edifice is shown by fluid inclusions, volatile solubility and seismicity
723 above a deformation center (Figure 17; Famin et al., 2009; Peltier et al. 2009; Di Muro et al., 2014;
724 Fontaine et al., 2014). Notably for the 2007 eruption at Piton de la Fournaise volcano, the seismicity
725 started shallow and penetrated downwards with time, as the eruption was fed from progressively deeper
726 (Massin et al., 2011).

727 Studies of the magma plumbing system associated with the volcanic islands of the Kerguelen
728 archipelago are scarce. Partly due to their inaccessibility and relatively evolved character often hosting
729 phonolites (e.g. Quilty & Wheller, 2000; Freise et al., 2003). However several islands seem to be
730 volcanically active, as observed by passing vessels on long Ocean voyages (Quilty & Wheller, 2000).
731 Volcanic eruptions have been reported from Heard Island in 1910, 1948 to 1954, 1985 to 1987 and 1996,
732 whilst a submarine eruption likely occurred in 1992. An eruption was reported from McDonald Island in
733 1997 and satellite images show evidence for an eruption in 2001 (Quilty & Wheller, 2000; Wunderman,
734 2003; Stephenson et al., 2005). The only constraints on the magma storage suggest mid-crustal magma
735 evolution of phonolitic magmas based on experimental petrology (Figure 17; Freise et al., 2003). Given
736 the recent history of eruptions in the Kerguelen archipelago and potential hazard for shipping, we

737 recommend detailed investigation into the magma storage system. Sample material exists from several of
738 the islands that can be used for petrological investigation (Barling et al., 1994; Freise et al., 2003) and
739 InSAR would provide useful insights into the shallow magma storage system without the need for an
740 expedition or deployment of equipment.

741 This comparison shows that deep magma storage is common to Ocean Islands, however the
742 shallow crustal magma storage systems vary considerably and are therefore likely controlled by local
743 factors opposed to the tectonic setting (Figure 17). Magma storage in the crust may be controlled by
744 density differences such as the transition between the ocean crust and sediments, the presence of which
745 will vary depending on the supply of sedimentary materials to the Ocean Islands. Sedimentary layers
746 provide a low density zone between the mafic ocean crust and the base of the volcano, hence creating an
747 opportunity for magmas to stall. Evidence for magma-sediment interaction is observed in lavas from Cape
748 Verde and seismicity, plus intrusions at this level likely contribute to local uplift at Santiago and Brava
749 (Da Silva et al., 1999; Ramalho et al., 2010a, 2010b; Barker et al., 2012; Fernandes & Faria, 2015).
750 Magmas stalling deeper in ocean crust may be influenced by the gabbro-dike or lava-dike transitions,
751 where porosity and permeability change. Additionally at these contacts, the ocean crust changes from
752 massive gabbro to vertically aligned dikes and then to horizontal lava flows and random orientations of
753 pillow lavas in the volcanic pile. Such changes potentially modifying the relationship between the magma
754 and crust, leading to readjustment of magma flow. The characteristics of magmatic conduits will also
755 influence magma ascent, with high permeability associated with fractures or faults aiding direct magma
756 ascent, whereas sealing of previous pathways may enforce stalling of magma. Some Ocean Islands, such
757 as Tenerife, Canary Islands have well developed rift zones, which may promote magma ascent (Carracedo
758 et al., 2007). The regional fracture zones that potentially control the alignment of volcanic islands in Cape
759 Verde likely provide effective pathways for magma ascent (Klerkx et al., 1974; Le Pichon and Fox, 1971;
760 Jacobi and Hayes, 1982). Furthermore, magmatic properties may also influence magma dynamics on
761 ascent through the crust, with magma buoyancy affected by density contrasts with the wall rock as well as
762 viscosity associated with the crystal cargo and magma composition (Bottinga & Weill, 1970; Bottinga et
763 al., 1982; Seifert et al., 2013; Cooper, 2017). This may explain storage of mafic magmas in the lower
764 crust, as the magma density may have changed just enough for magma to ascend above the Moho and
765 then stall in the lower crust where a similar density is encountered.

766

767

768

769 **Conclusions and recommendations**

770 Globally at Ocean Islands, we observe that clinopyroxene crystallization tends to occur deep in
771 the magmatic system; in the oceanic lithosphere and sometimes up into the lower crust. Therefore,
772 clinopyroxene captures the magmatic processes and magma storage that occur deep in these relatively
773 mafic volcanic islands. Recent, well monitored eruptions of Fogo, Cape Verde (2014-2015) and el Hierro,
774 Canary Islands (2011) have been fed from deep magma storage zones and seismicity traced the ascent of
775 magma through the crust to the eruption site (González et al., 2013, 2015). In contrast the eruption at
776 Piton de la Fournaise, Reunion (2007) appears to have started with fracturing of the shallow magma
777 storage zone followed by magma ascent from progressively deeper to feed the ongoing eruption (Massin
778 et al., 2011).

779 Therefore, knowledge of the deep magma storage system from clinopyroxene crystallization is
780 appropriate for volcanoes where eruptions are fed from deep magma chambers, allowing monitoring
781 teams to interpret enhanced deep seismicity. However for others such as Piton de la Fournaise it is
782 essential to understand the shallow magma storage system. The presence of such long-lived shallow
783 magmatic systems may influence the eruption style, therefore the presence or absence of protracted
784 shallow magma storage may be a useful indicator of likely eruptive behaviour. To investigate the
785 temporary as well as long-term shallow magma storage zones a combination of methods is recommended.
786 Petrological methods that lend themselves to investigating the shallower magmatic system are water
787 solubility, experimental studies, glassy melt inclusions and to some extent fluid inclusions depending on
788 the timescales available for re-equilibration (Renzulli & Santi 2000; Freise et al., 2003; Famin et al.,
789 2009; Zanon et al., 2013; Di Muro et al., 2014; Jeffery et al., 2016). Ideally seismicity and deformation
790 data are used both for developing models of the magma storage system as well as real-time monitoring
791 (Magee et al., 2018).

792 Investigation of timescales of magmatic processes that provide indications of typical timescales
793 for magma ascent from a magma storage zone to eruption are also important. Such indications may be
794 assessed on a case by case basis from the extent of re-equilibration of fluid inclusions (Hildner et al.,
795 2011, 2012). Further information about magmatic timescales that may give insights into the magma
796 ascent processes involved in volcanic eruptions may be gleaned by exploring diffusion between
797 compositional zones within crystals. An example of olivine diffusion chronometry from Fogo, Cape
798 Verde suggests rapid ascent of magmas and corresponding eruption on the order of 3 to 12 hours (Hildner
799 et al., 2011). We recommend integration of all types of petrological data to provide indications of
800 magmatic processes and their location and timescales with geophysical methods such as seismicity to

801 track magma storage and transport as well as InSAR and geodetics to reveal deformation patterns and
802 assess source location and geometry (Magee et al., 2018).

803

804 **Acknowledgements**

805 We are particularly grateful to the editors Matteo Massotta, Silvio Mollo and Christoph Beier, for the
806 invitation to contribute to this volume and their professional editorial handling. We are grateful to
807 Andreas Klügel, David Neave and Ricardo Ramalho for constructive reviews that helped improve this
808 contribution.

809

810 **References:**

811 Ali, M.Y., Watts, A.B. and Hill, I., 2003. Structure of Mesozoic oceanic crust in the vicinity of the Cape Verde
812 Islands from seismic reflection profiles. *Marine Geophysical Researches*, 24(3-4): 329-343.

813 Ali, M.Y., and Watts, A.B., (2003). A seismic reflection profile study of lithospheric flexure in the vicinity of the
814 Cape Verde Islands. *Journal of Geophysical Research* **108(B5)**: 2239-2263.

815 Amelung, F., & Day, S. (2002). InSAR observations of the 1995 Fogo, Cape Verde, eruption: Implications for the
816 effects of collapse events upon island volcanoes. *Geophysical Research Letters*, 29(12), 47-1.

817

818 Andújar, J., Costa, F., Martí, J., Wolff, J.A. and Carroll, M.R., (2008). Experimental constraints on pre-eruptive
819 conditions of phonolitic magma from the caldera-forming El Abrigo eruption, Tenerife (Canary Islands). *Chemical*
820 *Geology*, 257(3-4), pp.173-191.

821

822 Ashchepkov, I.V.; André, L.; Downes, H.; Belyatsky, B.A. (2011) Pyroxenites and megacrysts from Vitim

823 picrite-basalts (Russia): Polybaric fractionation of rising melts in the mantle? *J. Asian Earth Sci.* 42, 14–37.

824 Assunção CFT, Machado F, Gomes RAD (1965) On the occurrence of carbonatites in the Cape Verde Islands.

825 *Boletim da Sociedade Geológica de Portugal* 16:179–188

826 Aulinas M, Gimeno D, Fernandez-Turiel JL, Pérez-Torrado FJ, Rodriguez- González A, Gasperini D (2010) The

827 Plio-Quaternary magmatic feeding system beneath Gran Canaria (Canary Islands, Spain): constraints from

828 thermobarometric studies. *Journal of the Geological Society* 167:785-801.

829 Baker, D.R. (2008) The fidelity of melt inclusions as records of melt composition. *Contrib. Mineral. Petrol.* 156,

830 377–395.

- 831 Barker, A.K., Nilsson, D., Hansteen, T., (2019). Unravelling the crustal architecture of Cape Verde; the xenolith
832 record. Submitted to Special Issue: Mineral Textural and Compositional Variations as a Tool for Understanding
833 Magmatic Processes editor: Silvio Mollo Minerals, 9(2), 90.
- 834 Barker, A.K., Troll, V.R., Carracedo, J.C., Nicholls, P., (2015). The magma plumbing system for the 1971 Tengüfa
835 eruption, La Palma, Canary Islands. *Contrib Mineral Petrol* 170(5) doi: 10.1007/s00410-015-1207-7
- 836 Barker, A.K., Troll, V.R., Ellam, R.M., Hansteen, T.H., Harris, C., Stillman, C.J., Andersson, A., (2012), Magmatic
837 evolution of the Cadamosto Seamount, Cape Verde: Beyond the spatial extent of EM1. *Contributions to Mineralogy
838 and Petrology* 163, 949-965. doi: 10.1007/s00410-011-0708-2.
- 839 Barker, A.K., Holm, P.M., Peate, D.W., & Baker, J.A., (2010), A five million year record of compositional
840 variations in mantle sources to magmatism on Santiago, southern Cape Verde archipelago. *Contributions to
841 Mineralogy and Petrology* doi: 10.1007/s00410-009-0470-x
- 842 Barker, A., Holm, P., Peate, D. & Baker, J., (2009). A 5 million year record of compositional variations in mantle
843 sources to magmatism on Santiago, southern Cape Verde archipelago. *Mineralogy & Petrology*, 160: 33-154.
- 844 Barling, J., Goldstein, S. L., & Nucholls, I. A. (1994). Geochemistry of Heard Island (southern Indian Ocean):
845 characterization of an enriched mantle component and implications for enrichment of the sub-Indian Ocean mantle.
846 *Journal of Petrology*, 35(4), 1017-1053.
- 847 Barrancos, J., Dionis, S., Quevedo, R., Fernandes, P., Rodríguez, F., Pérez, N., Silva, S., Cardoso, N., Hernández,
848 P., Melián, G., Padrón, E., Padilla, G., Asensio-Ramos, M., Calvo, D., Semedo, H. & Alfama, V., (2015). Sulphur
849 dioxide (SO₂) emissions during the 2014-15 Fogo eruption, Cape Verde. *Geophysical Research Abstracts* Vol. 17,
850 2015. EGU General Assembly 2015.
- 851 Bebiano, J., (1932). A geologia do Arquipélago de Cabo Verde, *Comunicações dos Serviços Geológicos de
852 Portugal*, (18), 167–187.
- 853 Beier, C., Haase, K.M. and Hansteen, T.H., (2006). Magma evolution of the Sete Cidades volcano, São Miguel,
854 Azores. *Journal of Petrology*, 47(7), pp.1375-1411.
855
- 856 Bernard-Griffiths, J., Cantagrel, J.-M., Alves, C., Mendes, F., Serralheiro, A., & Macedo, J., (1975).
857 Geochronologie: Données radiométriques potassium-argon sur quelques formations magmatiques des îles de
858 l'archipel du Cap Vert, *C. R. Seances Acad. Sci. Ser. D.*, 280, 2429–2432.
- 859 Bottinga, Y., & Weill, D. F. (1970). Densities of liquid silicate systems calculated from partial molar volumes of
860 oxide components. *American Journal of Science*, 269(2), 169-182.
861
- 862 Bottinga, Y., Weill, D., & Richet, P. (1982). Density calculations for silicate liquids. I. Revised method for
863 aluminosilicate compositions. *Geochimica et Cosmochimica Acta*, 46(6), 909-919.
864

865 Brown, M. C., Singer, B. S., Knudsen, M. F., Jicha, B. R., Finnes, E., & Feinberg, J. M. (2009). No evidence for
866 brunhes age excursions, santo antão, cape verde. *Earth and Planetary Science Letters*, 287(1-2), 100-115.

867 Bureau, H., Pineau, F., Me α trich, N., Semet, M. P. & Javoy, M. (1998). A melt and fluid inclusion study of the gas
868 phase at Piton de la Fournaise volcano (Reunion Island). *Chemical Geology* 147, 115-130.

869 Caranova, R., & Silva, R. P. (2012) Geothermal resource assessment in volcanic islands-Fogo Island, Cape Verde.

870 Carracedo, J-C., Perez-Torrado, F., Rodriguez- Gonzalez, A., Paris, R., Troll, V.R., Barker, A.K. (2015) Volcanic
871 and structural evolution of Pico do Fogo, Cape Verde. *Geology Today* 31 (4), 146-152. 10.1111/gto.12101

872 Carracedo, J.C., Rodríguez Badiola, E., Guillou, H., Paterne, M., Scaillet, S., Pérez Torrado, F.J., Paris, R., Fra-
873 Paleo, U., Hansen, A., (2007). Eruptive and structural history of Teide volcano and rift zones of Tenerife, Canary
874 Islands. *Geological Society of America Bulletin* 19, 1027–1051. <http://dx.doi.org/10.1130/B26087.1>.

875 Cazenave, A., Dominh, K., Rabinowicz, M., & Ceuleneer, G. (1988). Geoid and depth anomalies over ocean swells
876 and troughs: evidence of an increasing trend of the geoid to depth ratio with age of plate. *Journal of Geophysical*
877 *Research: Solid Earth*, 93(B7), 8064-8077.

878 Chamberlain, K.J., Barclay, J., Preece, K., Brown, R.J. and Davidson, J.P., (2016). Origin and evolution of silicic
879 magmas at ocean islands: Perspectives from a zoned fall deposit on Ascension Island, South Atlantic. *Journal of*
880 *Volcanology and Geothermal Research*, 327, pp.349-360.

881 Chatterjee, N., Bhattacharji, S. and Fein, C., (2005). Depth of alkalic magma reservoirs below Kolekole cinder cone,
882 Southwest rift zone, East Maui, Hawaii. *Journal of Volcanology and Geothermal Research*, 145(1-2), pp.1-22.

883 Cooper, K. M. (2017). What does a magma reservoir look like? The “crystal's-eye” view. *Elements*, 13(1), 23-28.

884 Courtney, R. C. & White, R.S. (1986). Anomalous heatflow and geoid across the Cape Verde Rise: Evidence for
885 dynamic support from a thermal plume in the mantle. *Geophysical Journal of the Royal Astronomical Society*. **87**:
886 815-867.

887 Crough, S. (1982). Geoid height anomalies over the Cape Verde Rise. *Marine Geophysical Researches*, 5, 263–271.

888 Da Silva, S.H., Day, S.J. and Fonseca, J.F.B.D., (1999). Fogo Volcano, Cape Verde Islands: seismicity-derived
889 constraints on the mechanism of the 1995 eruption. *Journal of volcanology and geothermal research*, 94(1-4),
890 pp.219-231.

891 Dash, P., Ball, M.M., King G.A., Butler, L.W. and Rona, P.A. (1976). Geophysical investigation of the Cape Verde
892 Archipelago. *Journal of Geophysical Research* **81(29)**: 5249-5259.

893 Davidson, J. P., Morgan, D. J., & Charlier, B. L. (2007). Isotopic microsampling of magmatic rocks. *Elements*, 3(4),
894 253-259.

895 Davies, G., Norry, M., Gerlach, D. & Cliff, R., (1989). A combined chemical and Pb.Sr.Nd isotope study of the
896 Azores and Cape Verde hot spots, the geodynamic implications. In: Saunders, A.D. & Norry, M.J. (eds) Magmatism
897 in the Ocean Basins. Geological Society, Special Publications, London 42, pp. 231-255.

898 Day, S., Heleno, S. & Fonseca, J., (1999). A past giant lateral collapse and present day flank instability of Fogo,
899 Cape Verde Islands. *Journal of Volcanology and Geothermal Research*, 94: pp. 191-218.

900 De Paepe, P.D., Klerkx, J., Hertogen, J. & Plinke, P., (1974). Oceanic tholeiites on Cape Verde Islands -
901 petrochemical and geochemical evidence. *Earth and Planetary Science Letters*, 22(4): 347-354.

902 Di Muro, A., Métrich, N., Vergani, D., Rosi, M., Armienti, P., Fougereux, T., Deloule, E., Arienzo, I., & Civetta, L.
903 (2014). The shallow plumbing system of Piton de la Fournaise Volcano (La Reunion Island, Indian Ocean) revealed
904 by the major 2007 caldera-forming eruption. *Journal of Petrology*, 55(7), 1287-1315.

905
906 Dias, N.A., Matias, L., Lourenço, N., Madeira, J., Carrilho, F. and Gaspar, J.L., (2007). Crustal seismic velocity
907 structure near Faial and Pico Islands (AZORES), from local earthquake tomography. *Tectonophysics*, 445(3-4),
908 pp.301-317.

909

910 Dionis, D., Melián, G., Rodríguez, R., Hernández, P., Padrón, E., Pérez, N., Barrancos, B., Padilla, G., Sumino, H.,
911 Fernandes, P., Bandomo, Z., Victória, S., Pereira, J. & Semedo, H., (2015b). Diffuse volcanic gas emission and
912 thermal energy release from the summit crater of Pico do Fogo, Cape Verde. *Bulletin of Volcanology*. Bull
913 *Volcanol.* 77:10.

914 Dionis, S., Pérez, N., Hernández, P., Melián, G., Rodríguez, F., Padrón, E., Sumino, H., Barrancos, J., Padilla, G.,
915 Fernandes, P., Bandomo, Z., Silva, S., Pereira, J. & Semedo, H. (2015a) Diffuse CO₂ degassing and volcanic activity
916 at Cape Verde islands, West Africa. *Earth, Planets and Space* 67:48.

917 Doucelance, R., Escrig, S., Moreira, M., Gariépy, C. and Kurz, M. D., (2003). Pb-Sr-He isotope and trace element
918 geochemistry of the Cape Verde Archipelago. *Geochimica et Cosmochimica Acta*, 67(19), 3717-3733.

919 Duprat, H., Friis, J., Holm, P., Grandvuiet, T., & Sørensen, R., (2007). The volcanic and geochemical development
920 of São Nicolau, Cape Verde Islands: Constraints from field and ⁴⁰Ar/³⁹Ar evidence, *Journal of Volcanology and*
921 *Geothermal Research*, 162(1-2), 1 – 19.

922 Dyhr CT, Holm PM (2010) A volcanological and geochemical investigation of Boa Vista, Cape Verde Islands;
923 ⁴⁰Ar/³⁹Ar geochronology and field constraints. *J Volcanol Geotherm Res* 189:19–32

924 Efimov, V. N., & Skolotnev, S. G. (2006). New data on the structure of sedimentary cover at the Cape Verde
925 Seamount and the Cape Verde Basin (central Atlantic) based on continuous seismic profiling data. In *Doklady earth*
926 *sciences* (Vol. 407, No. 2, pp. 376-380). MAIK Nauka/Interperiodica.

927 Egloff, J. (1972). Morphology of ocean basin seaward of northwest Africa: Canary Islands to Monrovia, Liberia.
928 *AAPG Bulletin*, 56(4), 694-706.

- 929 Eisele, S., Reißig, S., Freundt, A., Kutterolf, S., Nürnberg, D., Wang, K. L., & Kwasnitschka, T. (2015). Pleistocene
930 to Holocene offshore tephrostratigraphy of highly explosive eruptions from the southwestern Cape Verde
931 Archipelago. *Marine Geology*, 369, 233-250.
- 932 Elsworth, D., & Day, S. J. (1999). Flank collapse triggered by intrusion: the Canarian and Cape Verde
933 Archipelagos. *Journal of Volcanology and Geothermal Research*, 94(1-4), 323-340.
- 934 Famin, V., Welsch, B., Okumura, S., Bachèlery, P., & Nakashima, S. (2009). Three differentiation stages of a single
935 magma at Piton de la Fournaise volcano (Reunion hot spot). *Geochemistry, Geophysics, Geosystems*, 10(1).
936
- 937 Faria, B. & Fonseca, J.F.B.D. (2014). Investigating volcanic hazard in Cape Verde Islands through geophysical
938 monitoring: network description and first results. *Natural Hazards and Earth System Sciences*, v.14, pp.485–494.
- 939 Faria, B. (2010) Monitorização Geofísica do Vulcão do Fogo e Níveis de Alerta, Ph.D thesis, Universidade Técnica
940 de Lisboa, (in Portuguese).
- 941 Faugères, J., Legigan, P., Maillet, N., and Latouche, C., (1989), Pelagic, turbiditic, and contouritic sequential
942 deposits on the Cape Verde Plateau (Leg 108, Site 659, Northwest Africa): Sediment record during Neogene time:
943 Proceedings of the Ocean Drilling Program, Scientific Results, v. 108, p. 311–327.
- 944 Fernandes, R., & Faria, B. (2015). FOGO-2014: monitoring the Fogo 2014 eruption, Cape Verde. In EGU General
945 Assembly Conference Abstracts Vol. 17 id.12709
- 946 Foeken, J., Day, S., & Stuart, F., (2009). Cosmogenic ³He exposure dating of the Quaternary basalts from Fogo,
947 Cape Verdes: Implications for rift zone and magmatic reorganisation, *Quaternary Geochronology*, 4(1), 37–49.
- 948 Fonseca, J. F., Faria, B. V., Lima, N. P., Heleno, S. I., Lazaro, C., d’Oreye, N. F., Ferreira, A.M.G, Barros, I.J.M.,
949 Santos, P., Bandomo, Z., Day, S. J., Osorio, J.P., Baio, M., Matis, J.L.G (2003). Multiparameter monitoring of Fogo
950 Island, Cape Verde, for volcanic risk mitigation. *Journal of volcanology and geothermal research*, 125(1-2), 39-56.
- 951 Fontaine, F. R., Roult, G., Michon, L., Barruol, G., & Muro, A. D. (2014). The 2007 eruptions and caldera collapse
952 of the Piton de la Fournaise volcano (La Réunion Island) from tilt analysis at a single very broadband seismic
953 station. *Geophysical Research Letters*, 41(8), 2803-2811.
- 954
- 955 Freise, M., Holtz, F., Koepke, J., Scoates, J. and Leyrit, H., (2003). Experimental constraints on the storage
956 conditions of phonolites from the Kerguelen Archipelago. *Contributions to Mineralogy and Petrology*, 145(6),
957 pp.659-672.
- 958 Galipp K, Klügel A, Hansteen TH (2006) Changing depths of magma fractionation and stagnation during the
959 evolution of an oceanic island volcano: La Palma (Canary Islands). *Journal Volcanol Geotherm Res* 155:285–306
- 960 Geiger, H., Barker, A.K., Troll, V.R., (2016). Locating the depth of magma supply for volcanic eruptions, insights
961 from Mt. Cameroon. *Sci. Rep.* 6, 33629; doi: [10.1038/srep33629](https://doi.org/10.1038/srep33629)
- 962 Geissler, W.H., Jokat, W., Jegen, M., Baba, K., (2016). Thickness of the oceanic crust and the mantle transition zone
963 in the vicinity of the Tristan da Cunha hot spot estimated from ocean-bottom and ocean-island seismometer receiver
964 functions. *Tectophysics this volume*.
- 965 Gerlach, D.C., Cliff, R.A., Davies, G.R., Norry, M. and Hodgson, N., (1988). Magma sources of the Cape-Verdes
966 Archipelago - isotopic and trace-element constraints. *Geochimica Et Cosmochimica Acta*, 52(12): 2979-2992.

- 967 González, P. J., Bagnardi, M., Hooper, A. J., Larsen, Y., Marinkovic, P., Samsonov, S. V., & Wright, T. J. (2015).
968 The 2014–2015 eruption of Fogo volcano: Geodetic modeling of Sentinel- 1 TOPS interferometry. *Geophysical*
969 *research letters*, 42(21), 9239-9246.
- 970 González, P.J., Samsonov, S.V., Pepe, S., Tiampo, K.F., Tizzani, P., Casu, F., Fernández, J., Camacho, A.G. and
971 Sansosti, E., (2013). Magma storage and migration associated with the 2011–2012 El Hierro eruption: implications
972 for crustal magmatic systems at oceanic island volcanoes. *Journal of Geophysical Research: Solid Earth*, 118(8),
973 pp.4361-4377.
- 974 Grevemeyer I, Helffrich G, Faria B, Booth-Rea G, Schnabel M, Weinrebe RW (2010) Seismic activity at Cadamosto
975 seamount near Fogo Island, Cape Verdes—formation of a new ocean island? *Geophys J Int* 180:552–558.
976 doi:10.1111/j.1365-246X. 2009.04440.x
- 977 Gudmundsson, A. (2012). Magma chambers: Formation, local stresses, excess pressures, and compartments. *Journal*
978 *of Volcanology and Geothermal Research*, 237, 19-41.
- 979 Hammer, J., Jacob, S., Welsch, B., Hellebrand, E. and Sinton, J., (2016). Clinopyroxene in postshield Haleakala
980 ankaramite: 1. Efficacy of thermobarometry. *Contributions to Mineralogy and Petrology*, 171(1), p.7.
- 981 Hanson, J. A., Given, H. K., & Berger, J. (1996). Earthquake activity near Ascension Island, South Atlantic Ocean,
982 as seen by a combined seismic/hydrophone array. *Geothermics*, 25(4-5), 507-519.
- 983
- 984 Hansteen, T., Kwasnitschka, T., Klügel, A., (2014). Cape Verde Seamounts - Cruise No. M80/3: December 29, 2009
985 - February 1, 2010 - Dakar (Senegal) - Las Palmas de Gran Canaria (Spain). DFG-Senatskommission für
986 Ozeanographie, Bremen, 1–42. doi:10.2312/cr_m80_3, 42 pp.
- 987 Hayes, D. E. and Rabinowitz, P. D., (1975), Mesozoic Magnetic Lineations and the Magnetic Quiet Zone off
988 Northwest Africa, *Earth Planet. Sci. Lett.* **28**, 105–115.
- 989 Heleno, S.I.N., Faria, B.V.E., Bandomo, Z. & Fonseca, J.F.B.D., (2006). Observations of high-frequency harmonic
990 tremor in Fogo, Cape Verde Islands, *J. Volc. Geotherm. Res.*, **158**, 361–379.
- 991 Herzberg, C.; Asimow, P. D. (2008) Petrology of some oceanic island basalts: PRIMELT2. XLS software for
992 primary magma calculation. *Geochemistry, Geophysics, Geosystems*, 9(9).
- 993 Hildner, E.; Klügel, A.; Hansteen, T. (2012) Barometry of lavas from the 1951 eruption of Fogo, Cape Verde
994 Islands: Implications for historic and prehistoric magma plumbing systems. *Journal of Volcanology and Geothermal*
995 *Research* 217-218 73–90.
- 996 Hildner, E.; Klügel, A.; Hauff F. (2011) Magma storage and ascent during the 1995 eruption of Fogo, Cape Verde
997 archipelago. *Contributions to Mineralogy and Petrology*, 162, 751-772, doi:10.1007/s00410-011-0623-6.
- 998 Hoernle K, Tilton G, Le Bas MJ, Duggen S, Garbe-Schönberg D (2002) Geochemistry of oceanic carbonatites
999 compared with continental carbonatites: mantle recycling of oceanic crustal carbonate. *Contributions to Mineralogy*
1000 *and Petrology*, 142(5), 520-542.
- 1001 Holm, P. M., Grandvuinet, T., Friis, J., Wilson, J. R., Barker, A. K. and Plesner, S., (2008). An $^{40}\text{Ar}/^{39}\text{Ar}$ study of
1002 the Cape Verde hot spot: Temporal evolution in a semistationary plate environment. *Journal of Geophysical*
1003 *Research: Solid Earth* (1978 – 2012), 113 (B8).

- 1004 Holm, P.M.; Wilson, J.R.; Christensen, B.P.; Hansen, L.; Hansen, S.L.; Hein, K.H.; Mortensen, A.K.; Pedersen, R.;
 1005 Plesner, S.; Runge, M.K. (2006) Sampling the Cape Verde mantle plume: Evolution of melt compositions on Santo
 1006 Antão, Cape Verde Islands. *Journal of Petrology*, 47, 145-189.
- 1007 Jacobi, R. D., & Hayes, D. E. (1982). Bathymetry, microphysiography and reflectivity characteristics of the West
 1008 African margin between Sierra Leone and Mauritania. In *Geology of the Northwest African continental margin* (pp.
 1009 182-212). Springer, Berlin, Heidelberg.
- 1010 Jeffery, A. J., Gertisser, R., O'Driscoll, B., Pacheco, J. M., Whitley, S., Pimentel, A., & Self, S. (2016). Temporal
 1011 evolution of a post-caldera, mildly peralkaline magmatic system: Furnas volcano, São Miguel, Azores.
 1012 *Contributions to Mineralogy and Petrology*, 171(5), 42.
- 1013 Jenkins, S. F., Day, S. J., Faria, B. V. E., & Fonseca, J. F. B. D. (2017). Damage from lava flows: insights from the
 1014 2014–2015 eruption of Fogo, Cape Verde. *Journal of Applied Volcanology*, 6(1), 6.
- 1015 Jørgensen, J. & Holm, P. (2002). Temporal variation and carbonatite contamination in primitive ocean island
 1016 volcanic from São Vicente. Cape Verde Islands. *Chemical Geology* (192), pp. 249–267.
- 1017 Klerkx, J., Deutsch, S., and De Paepa, P., (1974). Rubidium, strontium content and strontium isotopic composition
 1018 of strongly alkalic basaltic rocks from the Cape Verde Islands. *Contributions to Mineralogy and Petrology* 45: 107-
 1019 118.
- 1020 Klingelhöfer, F., Minshull, T.A., Blackman, D.K., Harben, P. and Childers, V., (2001). Crustal structure of
 1021 Ascension Island from wide-angle seismic data: implications for the formation of near-ridge volcanic islands. *Earth
 1022 and Planetary Science Letters*, 190(1-2), pp.41-56.
- 1023 Klitgord, K., & Schouten, H. (1987). Plate kinematics of the Central Atlantic: in Tucholke, BE, and Vogt, PR, eds.
 1024 *The Geology of North America: the Western Atlantic Region: Geol. Soc, America, Decade of North American
 1025 Geology*.
- 1026 Klügel, A., Klein, F., (2006). Complex magma storage and ascent at embryonic subma- rine volcanoes from
 1027 Madeira Archipelago. *Geology* 34, 337–340.
- 1028 Klügel, A., Longpré, M. A., García-Cañada, L., & Stix, J. (2015). Deep intrusions, lateral magma transport and
 1029 related uplift at ocean island volcanoes. *Earth and Planetary Science Letters*, 431, 140-149.
- 1030 Klügel A, Galipp K, Hansteen TH (2005) Magma storage and underplating beneath Cumbre Vieja volcano, La
 1031 Palma (Canary Islands). *Earth Planet Sci Lett* 236:211–226
- 1032 Klügel A, Hoernle KA, Schmincke HU, White JDL (2000) The chemically zoned 1949 eruption on La Palma
 1033 (Canary Islands): petrologic evolution and magma supply dynamics of a rift- zone eruption, *J Geophys Res*
 1034 105(B3):5997–6016
- 1035 Kokfelt, T. F., Holm, P.M., Hawkesworth, C.J., Peate, D.W. (1998). A lithospheric mantle source for the Cape
 1036 Verde Island magmatism: Trace element and isotopic evidence from the Island of Fogo. *Mineralogical Magazine*
 1037 62A, 801-802.
- 1038 Lai, Z., Zhao, G., Han, Z., Huang, B., Li, M., Tian, L., Bu, X. (2018). The magma plumbing system in the Mariana
 1039 Trough back-arc basin at 18° N. *Journal of Marine Systems*, 180, 132-139.
- 1040 Lancelot, Y., Seibold, E., Cepek, P., Dean, W., Eremeev, V., Gardner, J., Jansa, L., Johnson, D., Krasheninnikov,
 1041 V., Pflaumann, U., Rankin, J. G., Trabant, P. and Bukry, D., (1978). Site 368: Cape Verde Rise, in Initial Rep. Deep
 1042 Sea Drill. Proj., vol. 41, pp. 233–326, eds Lancelot, Y., Seibold, E., Cepek, P., Dean, W., Eremeev, V., Gardner, J.,
 1043 Jansa, L., Johnson, D., Krashenin- Nikov, V., Pflaumann, U., Rankin, J. G., Trabant, P. and Bukry, D., Washington
 1044 (U.S. Government Printing Office).

- 1045 Le Maitre RW, Streckeisen A, Zanettin B, Le Bas MJ, Bonin B, Bate-
 1046 man P, Bellieni G, Dudek A, Efremova A,
 1047 Keller J, Woolley AR (2002) Igneous rocks. A classification and glossary of terms, Recommendations of the IUGS
 subcommission on the systematics of igneous rocks
- 1048 Le Pichon, X.L., and Fox, P.J., (1971). Marginal offsets, fracture zones and the early opening of the North Atlantic.
 1049 *Journal of Geophysical Research* **75**: 6294-6307.
- 1050 Leva, C., Rümpler, G., Link, F. and Wölbern, I., (2019). Seismological evidence for subcrustal magmatic injection
 1051 beneath Fogo volcano, Cape Verde hotspot. EarthArXiv 10.31223/osf.io/f6zdp
- 1052 Liu, C., Lay, T., & Xiong, X. (2018). Rupture in the 4 May 2018 MW 6.9 earthquake seaward of the Kilauea east
 1053 rift zone fissure eruption in Hawaii. *Geophysical Research Letters*, *45*(18), 9508-9515.
- 1054 Lodge, A. and Helffrich, G., (2006). Depleted swell root beneath the Cape Verde Islands. *Geology*, *34*(6): 449-452.
- 1055 Longpré, M. A., Klügel, A., Diehl, A., & Stix, J. (2014). Mixing in mantle magma reservoirs prior to and during the
 1056 2011–2012 eruption at El Hierro, Canary Islands. *Geology*, *42*(4), 315-318.
- 1057 Longpré, M. A., Troll, V. R., & Hansteen, T. H. (2008). Upper mantle magma storage and transport under a
 1058 Canarian shield- volcano, Teno, Tenerife (Spain). *Journal of Geophysical Research: Solid Earth*, *113*(B8).
- 1059 Machado F, Azeredo Leme J, Monjardino J, Seita MF (1968) Carta geológica de Cabo Verde, notícia explicativa da
 1060 Ilha Brava e dos Ilhéus Secos. Garcia de Orta 16:123–130
- 1061 Madeira, J., Ramalho, R. S., Hoffmann, D. L., Mata, J., & Moreira, M. (2019) A geological record of multiple
 1062 Pleistocene tsunami inundations in an oceanic island: The case of Maio, Cape Verde. *Sedimentology*.
 1063 <https://doi.org/10.1111/sed.12612>
- 1064 Madeira J, Mata J, Mourão C, da Silveira AB, Martins S, Ramalho R, Hoffmn DL (2010) Volcano-stratigraphy and
 1065 structural evolution of Brava Island (Cape Verde) based on 40Ar/39Ar, U-Th and field constraints. *J Volcanol*
 1066 *Geotherm Res* 196:219–235
- 1067 Madeira, J., Brum da Silveira, A., Mata, J., Mourão, C., & Martins, S. (2008). The role of mass movements on the
 1068 geomorphologic evolution of island volcanoes: examples from Fogo and Brava in the Cape Verde archipelago.
 1069 *Comun. Geol*, *95*, 93-106.
 1070
- 1071 Madureira, P., Mata, J., Mattielli, N., Queiroz, G., and Silva, P. (2011) Mantle source heterogeneity, magma
 1072 generation and magmatic evolution at Terceira Island (Azores archipelago): Constraints from elemental and isotopic
 1073 (Sr, Nd, Hf, and Pb) data. *Lithos*, *126*, 402–418.
- 1074 Madureira, P., Mata, J., & Moreira, M. (2008). The Ne isotopic signature of Terceira lavas (Azores): evidence for
 1075 Ne recycling?. *e-Terra*, *5*(11).
- 1076 Magee, C., Stevenson, C. T., Ebmeier, S. K., Keir, D., Hammond, J. O., Gottsmann, J. H., O’Driscoll, B. (2018).
 1077 Magma plumbing systems: a geophysical perspective. *Journal of Petrology*, *59*(6), 1217-1251.
- 1078 Magnusson, E., (2016). Temporal evolution of historic mafic lavas from Fogo, Cape Verde. Examensarbete vid
 1079 Institutionen för geovetenskap, ISSN 1650-6553 ; 365. urn:nbn:se:uu:diva-296417
- 1080 Marianelli, P., Metrich, N., Sbrana, A. (1999) Shallow and deep reservoirs involved in magma supply of the 1944
 1081 eruption of Vesuvius. *Bulletin of Volcanology*, *61*, 48-63

- 1082 Martínez-Moreno, F. J., Santos, F. M., Madeira, J., Pous, J., Bernardo, I., Soares, A., Esteves, M., Adão, F., Ribeiro,
1083 J., Mata, J., & da Silveira, A. B. (2018). Investigating collapse structures in oceanic islands using magnetotelluric
1084 surveys: The case of Fogo Island in Cape Verde. *Journal of Volcanology and Geothermal Research*, 357, 152-162.
- 1085 Masotta, M.; Mollo, S.; Freda, C.; Gaeta, M.; Moore, G. (2013) Clinopyroxene–liquid thermometers and barometers
1086 specific to alkaline differentiated magmas. *Contributions to Mineralogy and Petrology*, 166(6), 1545-1561.
- 1087 Massin, F., Ferrazzini, V., Bachèlery, P., Nercessian, A., Duputel, Z., & Staudacher, T. (2011). Structures and
1088 evolution of the plumbing system of Piton de la Fournaise volcano inferred from clustering of 2007 eruptive cycle
1089 seismicity. *Journal of Volcanology and Geothermal Research*, 202(1-2), 96-106.
- 1090 Masson, D.G., Le Bas, T.P., Grevemeyer, I. & Weinrebe, W., (2008). Flank collapse and large-scale landsliding in
1091 the Cape Verde Islands, off West Africa, *Geochem. Geophys. Geosyst.*, 9, Q07015, doi:10.1029/2008GC001983.
- 1092 Mata, J., Martins, S., Mattielli, N., Madeira, J., Faria, B., Ramalho, R. S., Silva, P., Moreira, M., Caldeira, R.,
1093 Moreira, M., Rodrigues, J., & Martins, L. (2017). The 2014–15 eruption and the short-term geochemical evolution
1094 of the Fogo volcano (Cape Verde): Evidence for small-scale mantle heterogeneity. *Lithos*, 288, 91-107.
- 1095 Mata, J., Moreira, M., Doucelance, R., Ader, M. and Silva, L. C., (2010). Noble gas and carbon isotopic signatures
1096 of Cape Verde oceanic carbonatites: implications for carbon provenance. *Earth and Planetary Science Letters*,
1097 291(1), 70-83.
- 1098 McBride, J. H., White, R. S., Henstock, T. J., & Hobbs, R. W. (1994). Complex structure along a Mesozoic sea-floor
1099 spreading ridge: BIRPS deep seismic reflection, Cape Verde abyssal plain. *Geophysical Journal International*,
1100 119(2), 453-478.
- 1101 McNutt, M. K., (1988) Thermal and mechanical properties of the Cape Verde Rise, *J. Geophys. Res.*, 93, 2784–
1102 2794.
- 1103 Mitchell, J. G., M. J. LeBas, J. Zielonka, and H. Furnes (1983), On dating the magmatism of Maio, Cape Verde
1104 Islands, *Earth Planet. Sci. Lett.*, 64, 61–76.
- 1105 Mollo, S., Blundy, J., Scarlato, P., De Cristofaro, S. P., Tecchiato, V., Di Stefano, F., Vetere, F., Holtz, F., &
1106 Bachmann, O. (2018). An integrated PT-H₂O-lattice strain model to quantify the role of clinopyroxene fractionation
1107 on REE+ Y and HFSE patterns of mafic alkaline magmas: Application to eruptions at Mt. Etna. *Earth-Science*
1108 *Reviews*, 185, 32-56.
- 1109 Mollo, S., Putirka, K., Misiti, V., Soligo, M., & Scarlato, P. (2013). A new test for equilibrium based on
1110 clinopyroxene–melt pairs: clues on the solidification temperatures of Etnean alkaline melts at post-eruptive
1111 conditions. *Chemical Geology*, 352, 92-100.
- 1112 Morgan, D. J., Blake, S., Rogers, N. W., DeVivo, B., Rolandi, G., Macdonald, R., & Hawkesworth, C. J. (2004).
1113 Timescales of crystal residence and magma chamber volume from modelling of diffusin profiles in phenocrysts:
1114 Vesuvius 1944. *Earth and Planetary Science Letters* 222, 933-946, doi:10.1016/j.epsl.2004.03.030
- 1115 Mourão, C., Mata, J., Doucelance, J., Madeira, J., Brum da Silveira, A., Silva, L. & Moreira, M. (2010). Quaternary
1116 extrusive calciocarbonatite volcanism on Brava Island (Cape Verde). *Journal of African Earth Sciences*, 55, 59–74.
- 1117 Müller, R., Sdrolias, M., & Roest, W., (2008). Age, spreading rates and spreading symmetry of the world’s ocean
1118 crust, *Geochemistry Geophysics Geosystems*, 9(Q04006).
- 1119 Nascimento A. (2015) Post disaster needs assessment: Fogo volcanic eruption 2014-2015.
1120 <https://www.gfdrr.org/en/cape-verde-post-disaster-needs-assessment-volcano-eruption-2014-2015>

- 1121 Neave, D. A., & Putirka, K. D. (2017). A new clinopyroxene-liquid barometer, and implications for magma storage
1122 pressures under Icelandic rift zones. *American Mineralogist*, 102(4), 777-794.
- 1123 Nikogosian IK, Elliott T, Touret JLR (2002) Melt evolution beneath thick lithosphere: a magmatic inclusion study
1124 of La Palma, Canary Islands. *Chemical Geology* 183: 169-193.
- 1125 Nimis, P. (1995). A clinopyroxene geobarometer for basaltic systems based on crystal-structure modelling.
1126 *Contributions to Mineralogy and Petrology* **121**: 115-125.
- 1127 O'Mongain, A., Ottemoller, L., Baptie, B., Galloway, D., & Booth, D. (2007). Seismic activity associated with a
1128 probable submarine eruption near Tristan da Cunha, July 2004–July 2006. *Seismological Research Letters*, 78(3),
1129 375-382.
- 1130 Ogg, J.G., (1995). Magnetic polarity time scale of the Phanerozoic, in *Global Earth Physics: A handbook of physical*
1131 *constants. AGU Ref. Shelf, vol. 1*, edited by T.J. Ahrens, p 240-270. Washington D.C.
- 1132 Paris, R., Giachetti, T., Chevalier, J., Guillou, H. and Frank, N., (2011). Tsunami deposits in Santiago Island (Cape
1133 Verde archipelago) as possible evidence of a massive flank failure of Fogos volcano. *Sedimentary Geology*, 239(3-
1134 4), pp.129-145.
- 1135 Paris, R., Ramalho, R. S., Madeira, J., Ávila, S., May, S. M., Rixhon, G., Engel, M., Brückner, H., Herzog, M.,
1136 Schukraft, G., Pérez-Torrado, F. J., Rodrigues-González, A., Carracedo, J.C. & Giachetti, T. (2018). Mega-tsunami
1137 conglomerates and flank collapses of ocean island volcanoes. *Marine Geology*, 395, 168-187.
- 1138 Peltier, A., Bachèlery, P. and Staudacher, T., (2009). Magma transport and storage at Piton de La Fournaise (La
1139 Réunion) between 1972 and 2007: A review of geophysical and geochemical data. *Journal of Volcanology and*
1140 *Geothermal Research*, 184(1-2), pp.93-108.
- 1141 Pérez, M., Dionis, S., Fernandes, P., Barrancos, J., Rodríguez, F., Bandomo, Z., Hernández, P., Melián, G., Silva,
1142 S., Padilla, G., Padrón, E., Cabral, J., Calvo, D., Asensio-Ramos, M., Pereira, J., Gonçalves, A., Barros, I., &
1143 Semedo, H., (2015). Precursory signals of the 2014-15 Fogo eruption (Cape Verde) detected by surface CO₂
1144 emission and heat flow observations. *Geophysical Research Abstracts* Vol. 17, 2015, EGU General Assembly 2015.
- 1145 Pim, J., Peirce, C., Watts, A. B., Grevemeyer, I. and Krabbenhöft, A., (2008). Crustal structure and origin of the
1146 Cape Verde Rise. *Earth and Planetary Science Letters*, 272(1), 422-428.
- 1147 Plesner, S., Holm, P. M., & Wilson, J. R. (2003). 40Ar–39Ar geochronology of Santo Antão, Cape Verde Islands.
1148 *Journal of Volcanology and Geothermal Research*, 120(1-2), 103-121.
- 1149 Poland, M.P., Miklius, A. and Montgomery-Brown, E.K., (2015). Magma supply, storage, and transport at shield-
1150 stage. *Charact. Hawaii. Volcanoes*, 179(1801), pp.179-234.
- 1151 Putirka, K. D. (2017). Down the crater: where magmas are stored and why they erupt. *Elements*, 13(1), 11-16.
- 1152 Putirka, K. (2008) Thermometers and barometers for volcanic systems. *Reviews in Mineralogy and Geochemistry*,
1153 69, 61-120.
- 1154 Putirka K, Mikaelian H, Ryerson FJ, Shaw H (2003) New clinopyroxene-liquid thermobarometers for mafic,
1155 evolved and volatile-bearing lava compositions, with applications to lavas from Tibet and the Snake River Plain, ID.
1156 *Am Mineral* 88:1542–1554
- 1157 Putirka K (1999) Clinopyroxene + liquid equilibria to 100 kbar and 2450 K. *Contrib Mineral Petrol* 135: 151-163

- 1158 Putirka K (1997) Magma transport at Hawaii: Inferences based on igneous thermobarometry. *Geology* 25: 69-72
- 1159 Putirka K, Johnson M, Kinzler R, Longhi J, Walker D (1996) Thermobarometry of mafic igneous rocks based on
1160 clinopyroxene-liquid equilibria, 0-30 kbar. *Contrib Mineral Petrol* 123: 92-108
- 1161 Putirka K, Condit C (2003) A cross section of a magma conduit system at the margins of the Colorado Plateau.
1162 *Geology* 31:701-704
- 1163 Quilty, P. G., & Wheller, G. E. (2000). Heard Island and the McDonald Islands: a window into the Kerguelen
1164 Plateau. In *Papers and Proceedings of the Royal Society of Tasmania* (Vol. 133, No. 2, pp. 1-12).
- 1165 Ranero CR, Torne M, Banda E (1995) Gravity and multichannel seismic reflection constraints on the lithospheric
1166 structure of the Canary Swell. *Mar Geophys Res* 17:519–534
- 1167 Ramalho, R. S., Winckler, G., Madeira, J., Helffrich, G. R., Hipólito, A., Quartau, R., Adena, K. & Schaefer, J. M.
1168 (2015). Hazard potential of volcanic flank collapses raised by new megatsunami evidence. *Science advances*, 1(9),
1169 e1500456.
- 1170 Ramalho, R. A. dos Santos (2011). Vertical Movements of Ocean Island Volcanoes: Insights from a Stationary
1171 Plate. In *Building the Cape Verde Islands* (pp. 177-197). Springer, Berlin, Heidelberg.
- 1172 Ramalho, R. S., Helffrich, G., Cosca, M., Vance, D., Hoffmann, D., & Schmidt, D. N. (2010c). Vertical movements
1173 of ocean island volcanoes: insights from a stationary plate environment. *Marine Geology*, 275(1-4), 84-95.
- 1174 Ramalho, R., Helffrich, G., Schmidt, D. & Vance, D. (2010b). Tracers of uplift and subsidence in the Cape Verde
1175 Archipelago. *J. Geol. Soc. Lond.* 167, pp. 519-538.
- 1176 Ramalho, R., Helffrich, G., Cosca, M., Vance, D., Hoffmann, D. & Schmidt, D. (2010a). Episodic swell growth
1177 inferred from variable uplift of the Cape Verde hotspot islands. *Nature Geoscience*, Vol. 3, pp. 774-777.
- 1178 Renzulli, A. and Santi, P., (2000). Two-stage fractionation history of the alkali basalt-trachyte series of Sete Cidades
1179 volcano (São Miguel Island, Azores). *European Journal of Mineralogy*, 12(2), pp.469-494.
- 1180 Ribeiro, O. (1960). A ilha do Fogo e as suas Erupções. Memórias Série Geográfica I. Lisboa: Junta de Investigações
1181 do Ultramar.
- 1182 Richter, N., Favalli, M., de Zeeuw-van Dalssen, E., Fornaciai, A., Fernandes, R. M. D. S., Pérez, N. M., Levy, J.,
1183 Silva, S.V. & Walter, T. R. (2016). Lava flow hazard at Fogo Volcano, Cabo Verde, before and after the 2014-2015
1184 eruption. *Natural Hazards & Earth System Sciences*, 16(8).
- 1185 Risby, O. & Sandback, B. (2014) Mapping report Fogo, Cape Verde. Uppsala University.
- 1186 Roest, W. R., Danobeitia, J. J., Verhoef, J., & Collette, B. J. (1992). Magnetic anomalies in the Canary Basin and the
1187 Mesozoic evolution of the central North Atlantic. *Marine Geophysical Researches*, 14(1), 1-24.
- 1188 Rona, P. A. (1971). Bathymetry off central northwest Africa. In *Deep Sea Research and Oceanographic Abstracts*
1189 Vol. 18, No. 3, pp. 321-327. Elsevier.
- 1190 Ryabchikov, J. D.; Ntaflos, T.; Kurat, G.; Kogarko, L. N. (1995) Glass-bearing xenoliths from Cape Verde:
1191 evidence for a hot rising mantle jet. *Mineralogy and Petrology*, 55(4), 217-237.

- 1192 Ryan, W.B.; Carbotte, S.M.; Coplan, J.O.; O'Hara, S.; Melkonian, A.; Arko, R.; Weissel, R.A.; Ferrini, V.;
 1193 Goodwillie, A.; Nitsche, F.; Bonczkowski, J. (2009) Global multi- resolution topography synthesis. *Geochemistry,*
 1194 *Geophysics, Geosystems, 10, 3.*
- 1195 Rydeblad, E. (2018). Mineral Constraints on the Source Lithologies at Fogo, Cape Verde. Unpublished MSc thesis,
 1196 Uppsala University. ISSN 1650-6553 ; 433. [urn:nbn:se:uu:diva-354077](https://nbn-resolving.org/urn:nbn:se:uu:diva-354077)
- 1197 Sakai H, Des Marias DJ, Ueda A, Moore JG (1984) Concentrations and isotope ratios of carbon, nitrogen and sulfur
 1198 in ocean-floor basalts. *Geochim Cosmochim Acta* 48:2433–2441
- 1199 Samrock L.K., Wartho, J.-A., Hansteen, T.H. (2019). ^{40}Ar - ^{39}Ar dating of the active phonolitic Cadamosto Seamount
 1200 (Cape Verde): Indications for periodic volcanic activity and a possible relationship to global sea level changes.
 1201 *Lithos*
- 1202 Sandwell, D. T., & Smith, W. H. (1997). Marine gravity anomaly from Geosat and ERS 1 satellite altimetry. *Journal*
 1203 *of Geophysical Research: Solid Earth, 102*(B5), 10039-10054.
- 1204 Schwarz, S. & Klügel, A. (2004). Melt extraction pathways and stagnation depths beneath the Maderia and Desertas
 1205 rift zones (NE Atlantic) inferred from barometric studies. *Contributions to Mineralogy and Petrology* **147**: 228-240.
- 1206 Serralheiro, A. (1976). A geologia da Iha de Santiago (Cabo Verde). *Boletim do museu e laboratório mineralógico*
 1207 *e geológico da Faculdade de Ciências* 14: 157-369.
- 1208 Serralheiro, A., (1970). Geologia da Ilha de Maio (Cabo Verde). Junta de Investigações do Ultramar.
- 1209 Seifert, R., Malfait, W. J., Petitgirard, S., & Sanchez-Valle, C. (2013). Density of phonolitic magmas and time scales
 1210 of crystal fractionation in magma chambers. *Earth and Planetary Science Letters, 381*, 12-20.
- 1211 Silva, L., Le Bas, M. & Robertson, A. (1981). An oceanic carbonatite volcano on Santiago, Cape Verde Islands.
 1212 *Nature, 294, 644–645.*
- 1213 Silva, R., Havskov, J., Bean, C. and Wallenstein, N., (2012). Seismic swarms, fault plane solutions, and stress
 1214 tensors for São Miguel Island central region (Azores). *Journal of Seismology, 16*(3), pp.389-407.
- 1215 Silva, S.; Calvari, S.; Hernandez, P.; Pérez, N.; Ganci, G.; Alfama, V.; Barrancos, J.; Cabral, J.; Cardoso, N.; Dionis,
 1216 S.; Fernandes, P.; Melian, G.; Pereira, J.; Semedo, H.; Padilla, G. & Rodriguez, F., (2017). Tracking the hidden
 1217 growth of a lava flow field: the 2014-15 eruption of Fogo volcano (Cape Verde). *Geophysical Research Abstracts*
 1218 Vol. 19, EGU 2017-14514, 201. EGU General Assembly 2017.
- 1219 Silva, S., Cardoso, N., Alfama, A., Cabral, J., Semedo, H., Pérez, N., Dionis, S., Hernández, P., Barrancos, J.,
 1220 Melián, G., Pereira, J. & Rodríguez, R., (2015). Chronology of the 2014 volcanic eruption on the island of Fogo,
 1221 Cape Verde. *Geophysical Research Abstracts* Vol. 17, 2015 EGU General Assembly 2015.
- 1222 Skolotnev, S. G., Turko, N. N., Sokolov, S. Y., Peyve, A. A., Tsukanov, N. V., Kolodyazhnyi, S. Y., Eskin, A. E.
 1223 (2007). New data on the geological structure of the junction of the Cape Verde rise, Cape Verde abyssal basin, and
 1224 bathymetric seamounts (Central atlantic ocean). In *Doklady Earth Sciences* (Vol. 416, No. 1, pp. 1037-1041).
 1225 MAIK Nauka/Interperiodica.
- 1226 Skolotnev, S. G., Kolodyazhny, S. Y., Tsukanov, N. V., Chamov, N. P., & Sokolov, S. Y. (2009). Neotectonic
 1227 morphotstructures in the junction zone of the Cape Verde Rise and Cape Verde Abyssal Plain, Central Atlantic.
 1228 *Geotectonics, 43*(1), 51-66.

- 1229 Sparks, R. S. J., & Cashman, K. V. (2017). Dynamic magma systems: Implications for forecasting volcanic activity.
1230 *Elements*, 13(1), 35-40.
- 1231 Stephenson, J., Budd, G. M., Manning, J., & Hansbro, P. (2005). Major eruption-induced changes to the McDonald
1232 Islands, southern Indian Ocean. *Antarctic Science*, 17(2), 259-266.
- 1233 Stillman, C., Furnes, H., Le Bas, M., Robertson, A. & Zielonka, J. (1982). The geological history of Maio, Cape
1234 Verde Islands. *Journal of the Geological Society*, Vol. 139, n°3, pp. 347-361. Londres.
- 1235 Stock, M. J., Bagnardi, M., Neave, D. A., Maclennan, J., Bernard, B., Buisman, I., Gleeson, L.M. & Geist, D.
1236 (2018). Integrated petrological and geophysical constraints on magma system architecture in the western Galápagos
1237 Archipelago: insights from Wolf volcano. *Geochemistry, Geophysics, Geosystems*, 19(12), 4722-4743.
- 1238 Streck, M. J. (2008). Mineral textures and zoning as evidence for open system processes. *Reviews in Mineralogy
1239 and Geochemistry*, 69(1), 595-622.
- 1240 Tenzer, R., Bagherbandi, M., & Vajda, P. (2013). Global model of the upper mantle lateral density structure based
1241 on combining seismic and isostatic models. *Geosciences Journal*, 17(1), 65-73.
- 1242 Texier-Teixeira, P., Chouraqui, F., Perrillat-Collomb, A., Lavigne, F., Cadag, J. R., & Grancher, D. (2014).
1243 Reducing volcanic risk on Fogo Volcano, Cape Verde, through a participatory approach: which outcome?. *Natural
1244 Hazards and Earth System Sciences*, 14(9), 2347-2358.
- 1245 Till, C. B. (2017). A review and update of mantle thermobarometry for primitive arc magmas. *American
1246 Mineralogist*, 102(5), 931-947.
- 1247 Torres, P. C., Madeira, J., Silva, L. C., Brum da Silveira, A., Serralheiro, A. and Mota Gomes, A., (1997). Carta
1248 geológica das erupções históricas da Ilha do Fogo: revisão e actualização. In “A erupção vulcânica de 1995 na ilha
1249 do Fogo, Cabo Verde”; Edição do Instituto de Investigação Científica Tropical e Ministério da Ciência e
1250 Tecnologia: 119-132.
- 1251 Torres, P. C., Madeira, J., Silva, L. C., da Silveira, A. B., Serralheiro, A., & Gomes, A. M. (1998). Carta Geológica
1252 das Erupções Históricas da Ilha do Fogo (Cabo Verde): revisão e actualização. *Comunicações do Instituto
1253 Geológico e Mineiro*, 84, A193-196.
- 1254 Torres, P., Silva, L., Serralheiro, A., Tassinari, C., & Munhá, J., (2002). Enquadramento geocronológico pelo
1255 método K/Ar das principais sequências vulcano-estratigráficas da Ilha do Sal - Cabo Verde, Garcia de Orta, Serviços
1256 Geológicos, 18(1-2), 9–13.
- 1257 Turbeville, B. N., Wolff, J. A., & Le Bas, M. J. (1987). An oceanic nephelinite–phonolite–carbonatite association,
1258 Brava, Cape Verde Islands. *Eos*, 68, 1522.
- 1259 Vales, D., Dias, N.A., Rio, I., Matias, L., Silveira, G., Madeira, J., Weber, M., Carrilho, F. and Haberland, C.,
1260 (2014). Intraplate seismicity across the Cape Verde swell: A contribution from a temporary seismic
1261 network. *Tectonophysics*, 636, pp.325-337.
- 1262 Verhoef, J., Collette, B.J., Dañoibeitia, J.J., Roeser, H.A., Roest, W.R., (1991). Magnetic anomalies off West-Africa
1263 (20–38° N). *Marine Geophysical Research* 13 (2), 81–103.
- 1264 Weidendorfer, D., Schmidt, M. W., & Mattsson, H. B. (2016). Fractional crystallization of Si-undersaturated
1265 alkaline magmas leading to unmixing of carbonatites on Brava Island (Cape Verde) and a general model of
1266 carbonatite genesis in alkaline magma suites. *Contributions to Mineralogy and Petrology*, 171(5), 43.

- 1267 Weit, A., Trumbull, R.B., Keiding, J.K., Geissler, W.H., Gibson, S.A. and Veksler, I.V., (2017). The magmatic
1268 system beneath the Tristan da Cunha Island: Insights from thermobarometry, melting models and
1269 geophysics. *Tectonophysics*, 716, pp.64-76.
- 1270 Welsch, B., Hammer, J., Baronnet, A., Jacob, S., Hellebrand, E., & Sinton, J. (2016). Clinopyroxene in postshield
1271 Haleakala ankaramite: 2. Texture, compositional zoning and supersaturation in the magma. *Contributions to*
1272 *Mineralogy and Petrology*, 171(1), 6.
- 1273 White, R. S. (1984). Atlantic oceanic crust: seismic structure of a slow-spreading ridge. *Geological Society, London,*
1274 *Special Publications*, 13(1), 101-111.
- 1275 Williams, C., Hill, I., Young, R. & White, R. (1990). Fracture zones across the Cape Verde Rise, NE Atlantic.
1276 *Journal of Geological Society of London*, 1
- 1277 Wilson, D., Peirce, C., Watts, A., Grevemeyer, I., Krabbenhoft, A., (2010). Uplift at litho- spheric swells-I: seismic
1278 and gravity constraints on the crust and uppermost mantle structure of the Cape Verde mid-plate swell. *Geophysical*
1279 *Journal International* 182, 531–550.
- 1280 Wilson, D., Peirce, C., Watts, A., Grevemeyer, I., (2013). Uplift at lithospheric swells-II: is the Cape Verde mid-
1281 plate swell supported by a lithosphere of varying mechanical strength? *Geophysical Journal International* 193, 798–
1282 819.
- 1283 Worsley, P. (2015). Physical geology of the Fogo volcano (Cape Verde Islands) and its 2014–2015 eruption.
1284 *Geology Today*, 31(4), 153-159.
- 1285 Wunderman, R. (2003). Summary of recent volcanic activity. *Bulletin of Volcanology*, 65(6), 458-459.
1286
- 1287 Zanon, V., Kueppers, U., Pacheco, J.M. and Cruz, I., (2013). Volcanism from fissure zones and the Caldeira central
1288 volcano of Faial Island, Azores archipelago: geochemical processes in multiple feeding systems. *Geological*
1289 *Magazine*, 150(3), pp.536-555.
1290
- 1291 Zanon, V. and Pimentel, A., (2015). Spatio-temporal constraints on magma storage and ascent conditions in a
1292 transtensional tectonic setting: the case of the Terceira Island (Azores). *American Mineralogist*, 100(4), pp.795-805.
1293
- 1294 Zhao Z-F, Zheng Y-F (2003) Calculation of oxygen isotope fractionation in magmatic rocks. *Chem Geol* 193:59–80

1295 **Figure captions:**

1296 *Figure 1. Bathymetric and topographic map of the Cape Verde Archipelago as well as the Cadamosto*
1297 *Seamount, and islands of Brava, Fogo and Santiago. Note the existence of a “northern chain” composed*
1298 *of the islands of Santo Antão, São Vicente, Santa Luzia and islets, and São Nicolau, and a “southern*
1299 *chain” composed of the islands Santiago, Fogo and Brava and the Cadamosto Seamount. Relatively deep*
1300 *water separates most islands. Sources: [Ryan et al., 2009](#); www.geomapapp.org; [Hansteen et al., 2014](#).*

1301
1302 *Figure 2. Compiled stratigraphy of DSDP Site 368, the Cape Verde Rise and the Cape Verde islands.*
1303 *Several kilometer thick sequences of sediment are found above the ocean crust throughout the region*
1304 *([Dash et al. 1976](#); [Lancelot et al., 1978](#); [Pim et al., 2008](#)). The Moho is thickened beneath the islands and*
1305 *occurs at depths of 12 to 18 km, becoming deeper towards the East ([Dash et al. 1976](#); [Lancelot et al.,](#)*
1306 *[1978](#); [Ali & Watts, 2003](#); [Lodge & Helffrich, 2006](#); [Pim et al., 2008](#)).*

1307
1308 *Figure 3 (a) Map showing fractures zones, magnetic lineations, gravity and magnetism of the Cape Verde*
1309 *Rise. Black lines show fracture zones as mapped by [Williams et al. \(1990\)](#). Magnetic lineations of M4–*
1310 *M25 are plotted after [Klitgord and Schouten \(1986\)](#). The satellite-derived free-air gravity anomalies are*
1311 *shown ([Sandwell and Smith, 1997](#)). DSDP Site 368 is labeled. Magnetic quiet zone boundary from [Hayes](#)*
1312 *and [Rabinowitz \(1975\)](#). (b) Schematic cross-section NNW to SSE across the Cape Verde Rise following*
1313 *the yellow line ([Stillman et al., 1982](#); [Ryan et al., 2009](#); www.geomapapp.org).*

1314
1315 *Figure 4. Age distribution of exposed volcanic and intrusive products across the Cape Verde*
1316 *Archipelago. Black bars mark $^{40}\text{Ar}/^{39}\text{Ar}$ geochronology and He exposure dating whereas grey bars show*
1317 *K/Ar geochronology and other geological inferences. Modified from [Holm et al. \(2008\)](#) and based on the*
1318 *geochronological data of [Bernard-Griffiths et al. \(1975\)](#); [Mitchell et al. \(1983\)](#); [Torres et al. \(2002\)](#);*
1319 *[Plesner et al. \(2003\)](#); [Jørgensen and Holm \(2002\)](#); [Duprat et al., \(2007\)](#); [Holm et al. \(2008\)](#); [Foeken et](#)*
1320 *[al. \(2009\)](#); [Dyhr and Holm \(2010\)](#); [Madeira et al. \(2010\)](#); [Ramalho et al. \(2010c\)](#); [Samrock et al. \(2019\)](#).*
1321 *Note the tentative age progression of the oldest exposed rocks in East to the youngest in the West.*

1322
1323 *Figure 5. Photographs from the islands of Santiago, Fogo and Brava and the Cadamosto Seamount. a)*
1324 *Hyaloclastite from the submarine Flamengos Formation overlain by subaerial lavas of the Pico de*
1325 *Antónia Formation, Santiago. b) The Assomada Formation, Santiago, c) Pillow lavas in hyaloclastite*
1326 *from the Flamengos Formation overlain by a beach conglomerate followed by lavas of the Pico de*
1327 *Antónia Formation, Santiago, d) the iconic Pico do Fogo standing on the Chã das Caldeiras plateau,*

1328 Fogo, e) Bordeira cliffs that surround the western part of the Chã das Caldeiras, Fogo, f) the volcanic
1329 eruption at Fogo in November 2014, g) pillow lavas and hyaloclastites intruded by dike swarms, Brava h)
1330 sequence of ignimbrites, Brava, i) phonolitic lava near the summit of the Cadamosto Seamount (M80/3-
1331 033ROV), and j) steep cliffs of a crater at the Cadamosto Seamount (M80/3-033ROV).

1332
1333 Figure 6. Geological and topographic map of Santiago after [Serralheiro, 1976](#); [Ryan et al., 2009](#);
1334 www.geomapapp.org. The Flamengos Formation is exposed along river valleys and in highly eroded
1335 areas. The Pico da Antonía Formation is wide spread and represents the shield building stage of
1336 volcanism. An erosional phase was followed by lavas of the Assomada Formation that flowed into valleys
1337 and the Monte das Vacas scoria cones.

1338
1339 Figure 7. Geological and topographic map of Fogo after [Torres et al., 1998](#); [Ryan et al., 2009](#);
1340 www.geomapapp.org; [Carracedo et al., 2015](#). The shield volcano is composed of the Monte Amarelo
1341 Group volcanism and a large landslide created the Bordeira cliffs delineating the Cha das Caldeiras
1342 plateau that hosts the Pico do Fogo and recent volcanic eruptions.

1343
1344 Figure 8. Geological and topographic map of Brava after [Madeira et al., 2010](#); [Ryan et al., 2009](#);
1345 www.geomapapp.org. The island core complex is composed of alkaline and carbonatite intrusive rocks,
1346 whereas the volcanic rocks are mostly nephelinite to phonolite.

1347
1348 Figure 9. Compositional classification of the volcanic rocks from Santiago, Fogo, Brava and the
1349 Cadamosto Seamount after [LeMaitre et al. 2002](#). Santiago and Fogo host (mela)nephelinite, basanite and
1350 tephrite to basalt and even tephriphonolite at Fogo. In contrast Brava and the Cadamosto Seamount host
1351 dominantly phonolite and syenite. Data are unnormalized. Data sources: [Kokfelt, 1998](#); [Barker et al.,](#)
1352 [2009, 2012](#); [Hildner et al., 2011, 2012](#); [Magnusson, 2016](#); [Weidendorfer et al., 2016](#).

1353 Figure 10. Clinopyroxene Mg# histograms for Santiago, Fogo, Brava and the Cadamosto Seamount. All
1354 locations host diopside-augite, whereas Brava and the Cadamosto Seamount display highest abundances
1355 of aegirine-augite. Data sources: [Barker et al., 2009, 2012](#); [Hildner et al., 2011, 2012](#); [Weidendorfer et](#)
1356 [al., 2016](#); [Rydeblad, 2018](#).

1357 Figure 11. Clinopyroxene mineral chemistry for Santiago, Fogo, Brava and the Cadamosto Seamount.
1358 The clinopyroxene crystals from Santiago and Fogo display a distinct trend from the clinopyroxene found

1359 *at Brava and the Cadamosto Seamount. Data sources: [Barker et al., 2009, 2012](#); [Hildner et al., 2011,](#)*
1360 *[2012](#); [Weidendorfer et al., 2016](#); [Rydeblad, 2018](#).*

1361 *Figure 12. Zonation in clinopyroxene from Santiago, Fogo and the Cadamosto Seamount, shown by Mg#*
1362 *(mol%), TiO₂ and MnO content. Santiago Coastal group of the Flamengos Formation (121-306; [Barker](#)*
1363 *[et al., 2009](#)); Fogo eruption 1847 (CVF07 pyroxene 11; [Rydeblad, 2018](#)); Cadamosto Seamount (D885*
1364 *J1; [Barker et al., 2012](#)). Data sources: [Barker et al., 2009, 2012](#); [Hildner et al., 2011, 2012](#);*
1365 *[Weidendorfer et al., 2016](#); [Rydeblad, 2018](#).*

1366 *Figure 13. Multicomponent equilibrium Δ DiHd versus temperature for diopside-augite from Santiago,*
1367 *Fogo, Brava and the Cadamosto Seamount calculated after [Mollo et al. \(2013\)](#).*

1368 *Figure 14. Thermobarometry for Santiago, Fogo, Brava and the Cadamosto Seamount. Data sources:*
1369 *[Barker et al., 2009, 2012](#); [Hildner et al., 2011, 2012](#); [Rydeblad, 2018](#). The Moho is from [Lodge &](#)*
1370 *[Helffrich 2006](#) and [Pim et al. 2008](#).*

1371

1372 *Figure 15 Crystallization conditions; temperature and pressure, with composition for zoned*
1373 *clinopyroxene from Fogo; a) Prehistoric eruption CVF05 pyroxene 8, b) Eruption in 1785 CVF08*
1374 *pyroxene 15, c) Eruption in 1799 CVF09 pyroxene 5 and d) Eruption in 1847 CVF06 pyroxene 7.*

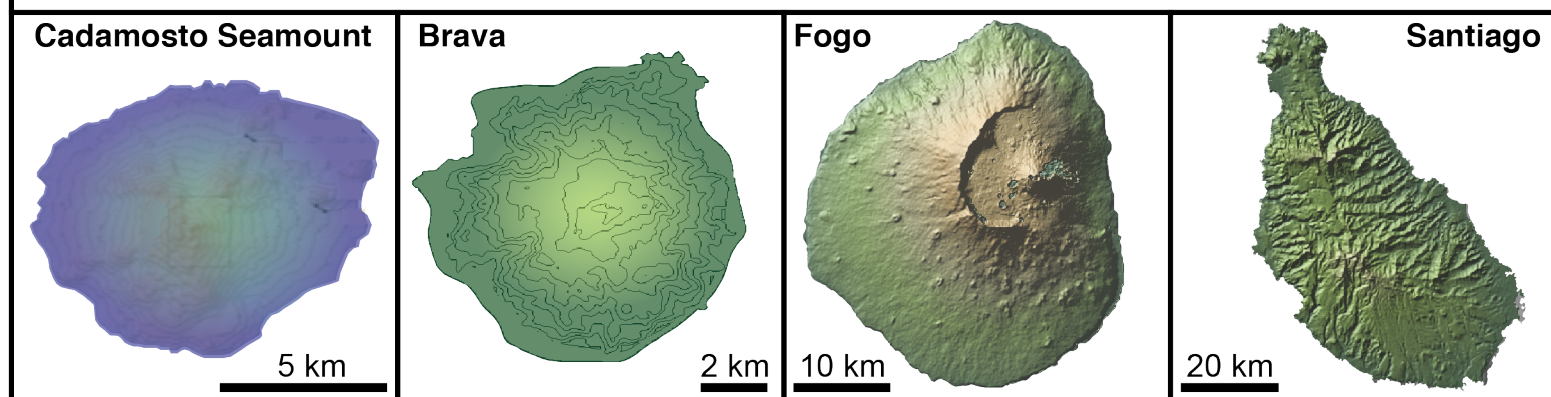
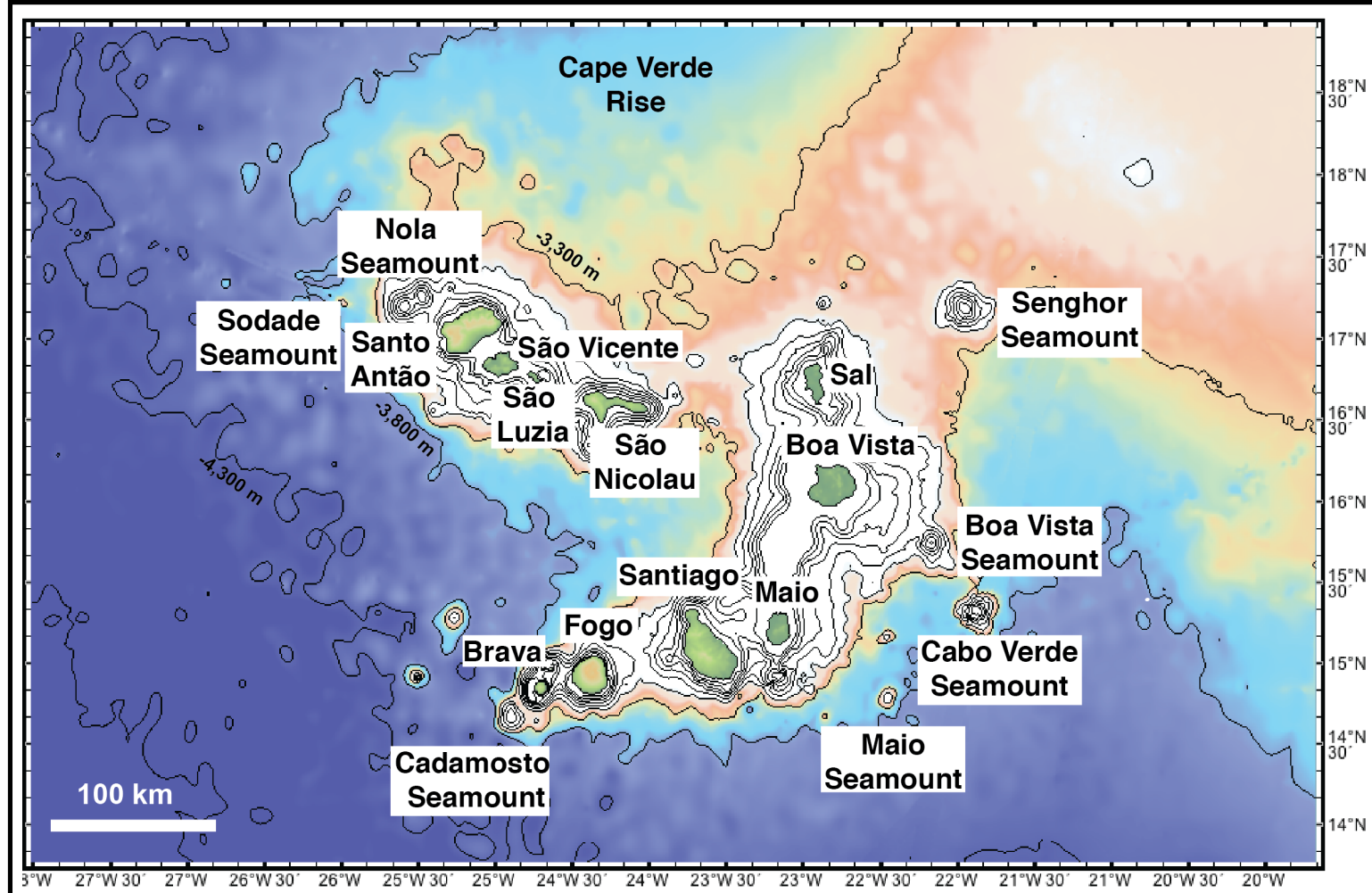
1375

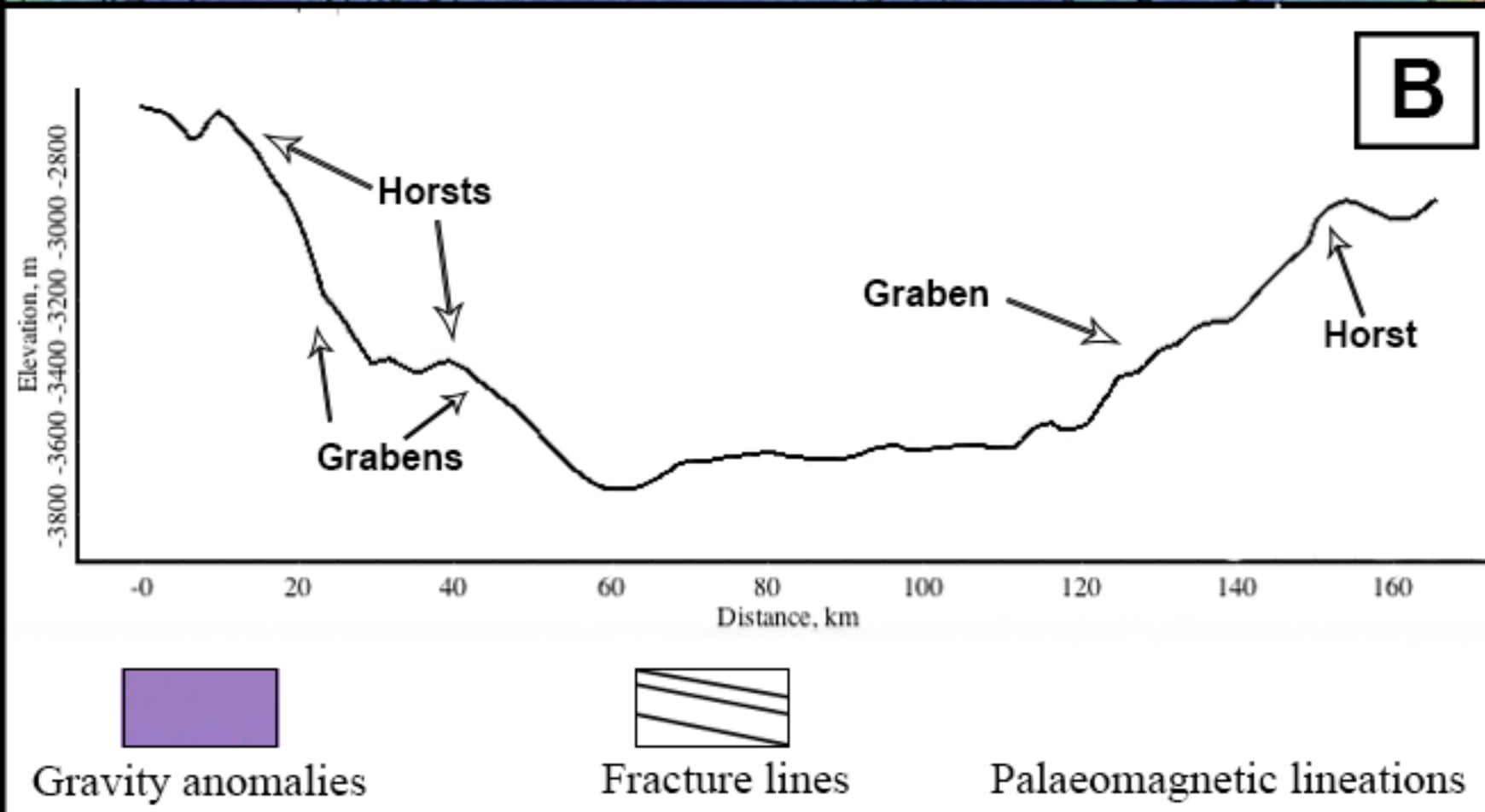
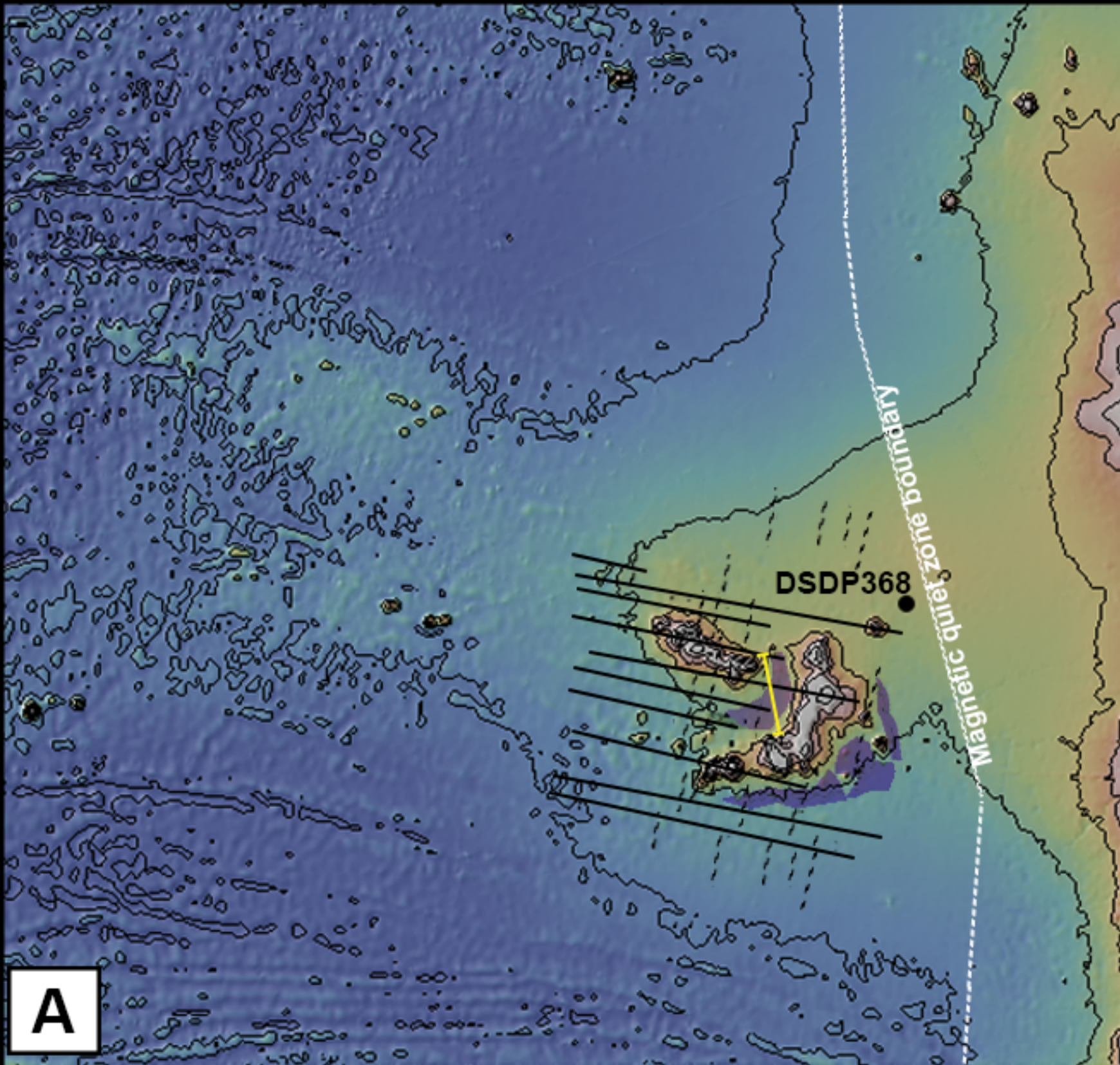
1376 *Figure 16. Crystallisation depth and model for the magma plumbing system beneath Santiago, Fogo,*
1377 *Brava and the Cadamosto Seamount. The shallow magma storage system is illustrated by fluid inclusion*
1378 *barometry as well as seismicity, deformation and the active hydrothermal systems. Data sources: [Da](#)*
1379 *[Silva et al., 1999](#); [Amelung & Day, 2002](#); [Barker et al., 2009, 2012](#); [Ryan et al., 2009](#);*
1380 *www.geomapapp.org; [Heleno et al., 2006](#); [Grevemeyer et al., 2010](#); [Hildner et al., 2011, 2012](#); [Faria &](#)*
1381 *[Fonseca, 2014](#); [Rydeblad, 2018](#). The Moho is from [Lodge & Helffrich 2006](#) and [Pim et al. 2008](#).*

1382

1383 *Figure 17. Schematic of the magma storage systems for Ocean Islands globally including results from*
1384 *clinopyroxene-melt thermobarometry, fluid inclusions, melt inclusions, experimental petrology*
1385 *deformation and seismicity. Cape Verde; [Da Silva et al 1999](#); [Amelung & Day 2002](#); [Lodge & Helffrich,](#)*
1386 *[2006](#); [Pim et al., 2008](#); [Barker et al., 2009, 2012](#); [Grevemeyer et al., 2010](#); [Hildner et al., 2011, 2012](#);*
1387 *[Faria & Fonseca 2014](#); [Fernandes & Faria, 2015](#); [Vales et al., 2015](#); [Jenkins et al., 2017](#); [Leva et al.,](#)*

1388 2019; Mata et al., 2017; this study. Canary Islands; Klügel et al., 2000; 2005; Galipp et al., 2006;
1389 Longpré et al., 2008, 2014; Aulinas et al., 2010; Barker et al., 2015; González et al., 2013. Madeira;
1390 Schwarz & Klügel 2004; Klügel & Klein, 2006. The Azores; Renzulli & Santi 2000; Beier et al., 2006;
1391 Dias et al., 2007; Silva et al 2012; Jeffery et al., 2016; Madureira et al., 2008; Zanon et al., 2013; Zanon
1392 & Pimentel 2015. Tristan da Cunha; Geissler et al., 2016; Weit et al., 2017. Ascension; Klinghofer et al.,
1393 2001; Hanson et al., 1996; Chamberlain et al., 2016. Hawaii; Putirka et al. 1996, Putirka 1997;
1394 Chatterjee et al., 2005; Poland et al 2015; Hammer et al., 2016. Galapagos; Stock et al., 2018. Reunion;
1395 Bureau et al., 1998; Famin et al., 2009; Peltier et al. 2009; Di Muro et al., 2014; Fontaine et al., 2014.
1396 Kerguelen; Freise et al., 2003.

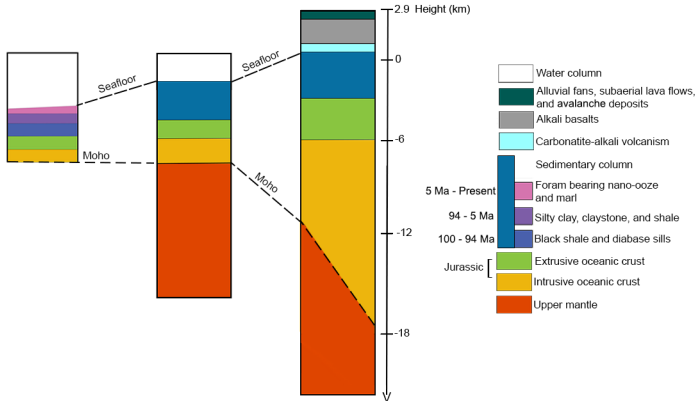


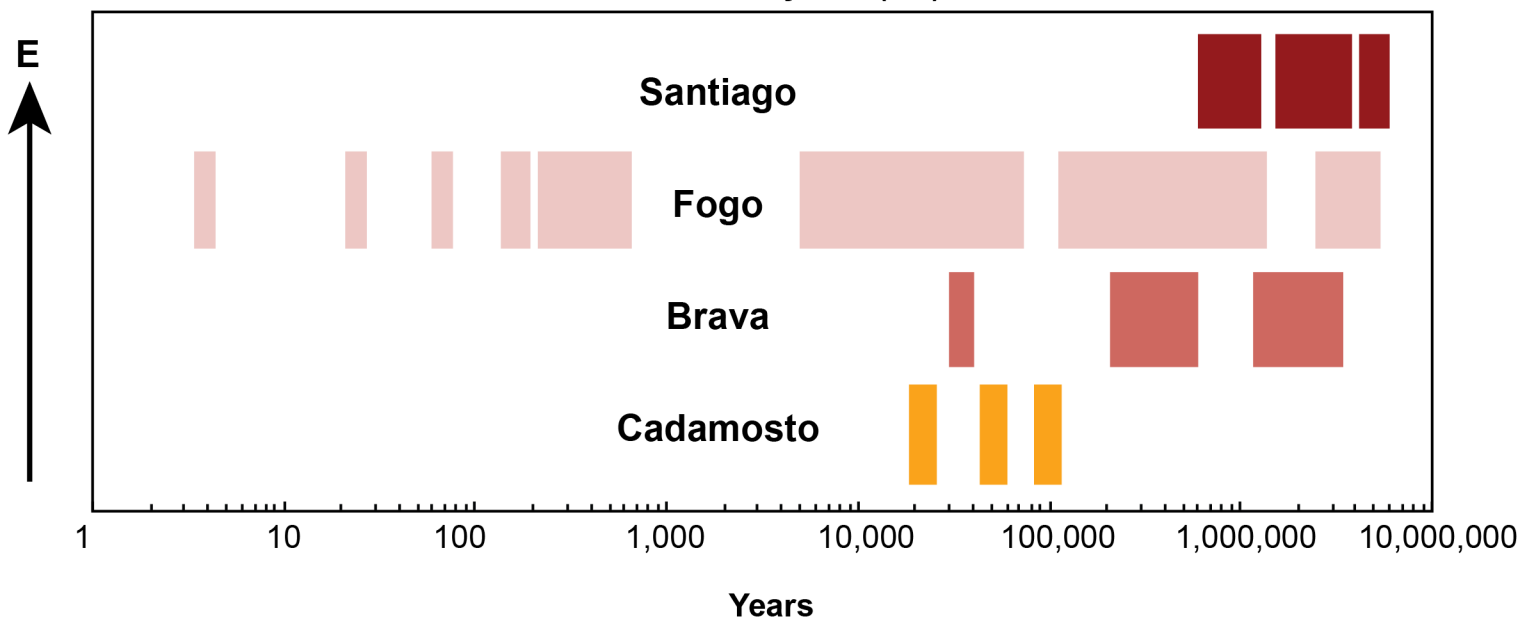
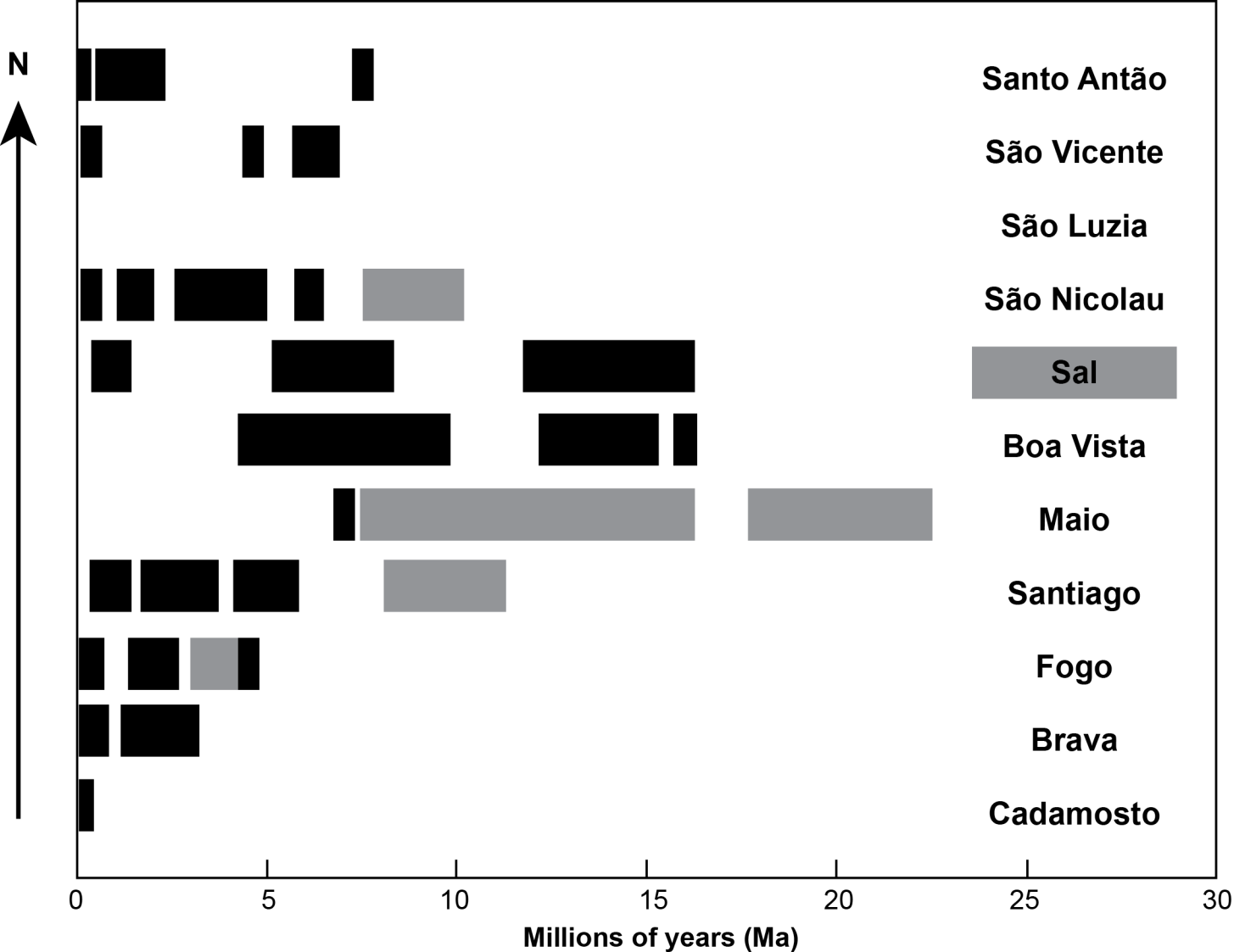


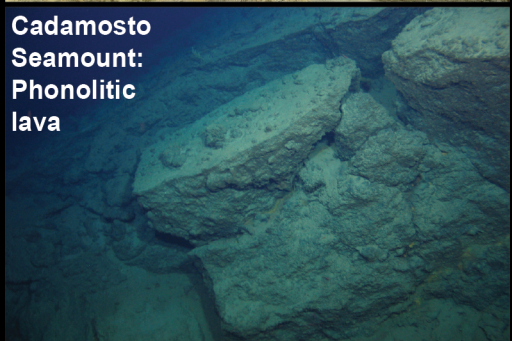
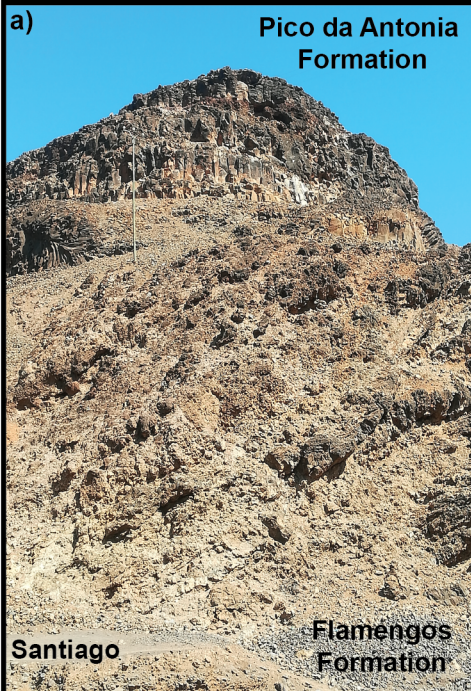
DSDP site 368

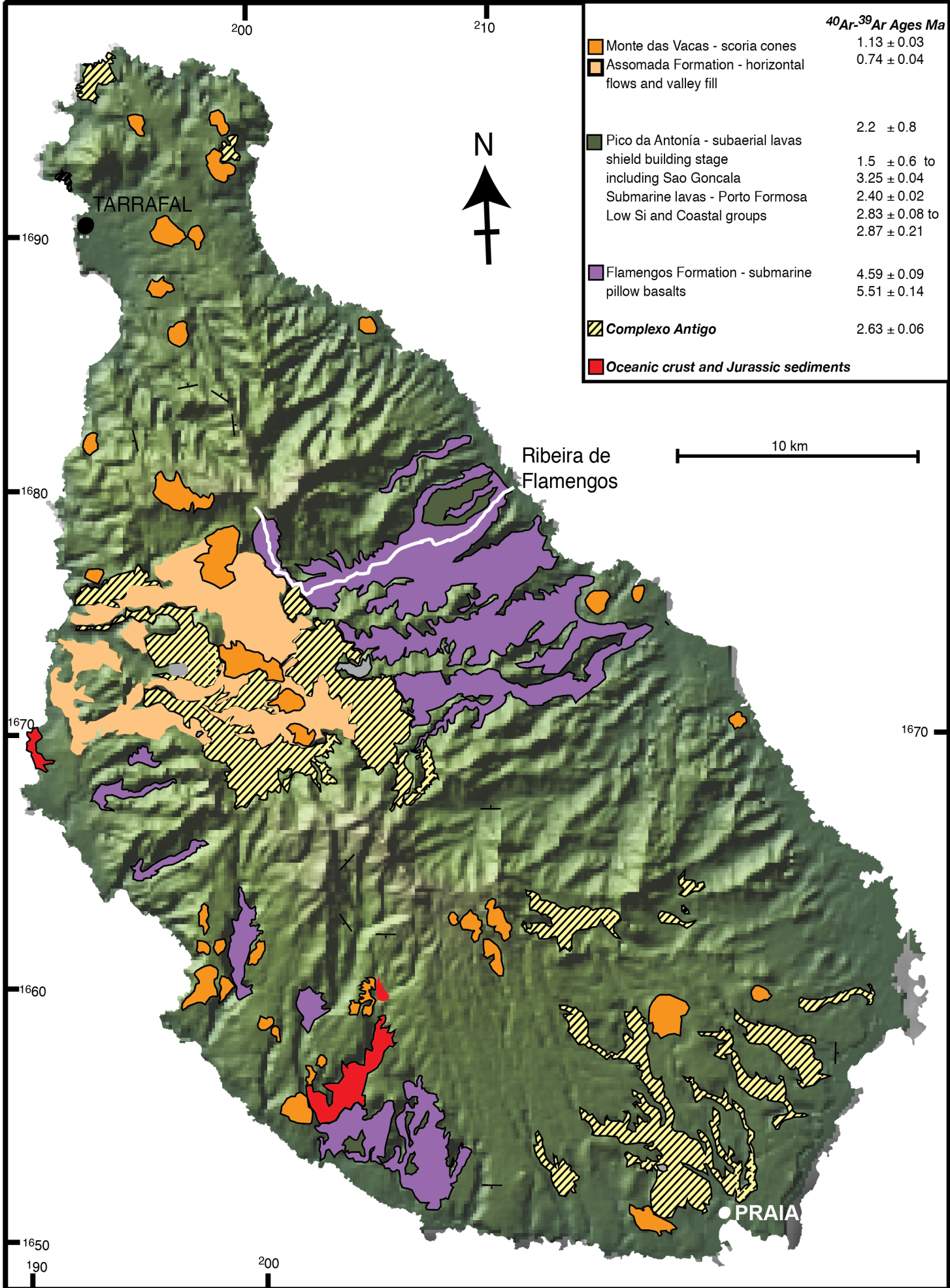
Cape Verde Rise

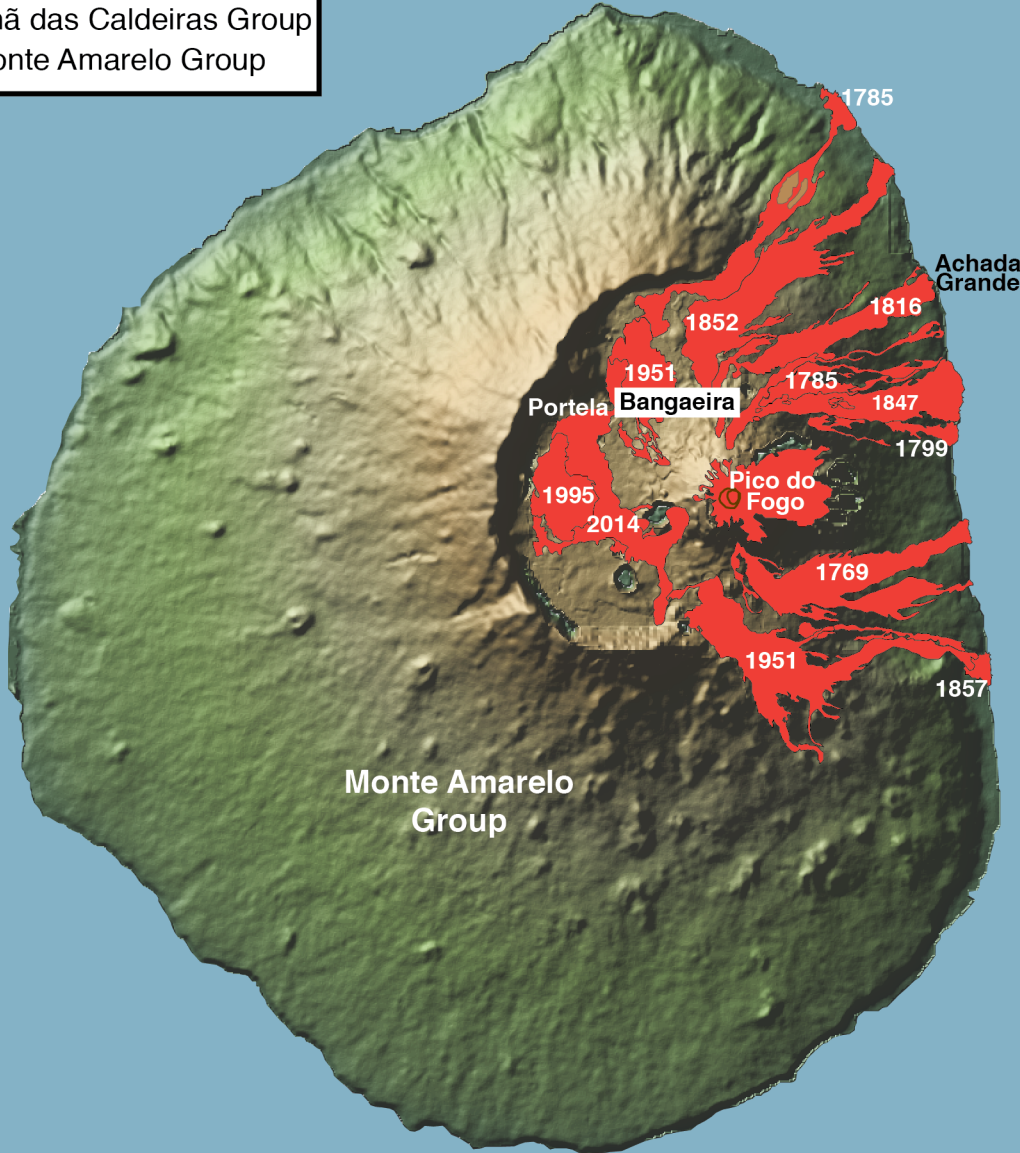
Cape Verde Islands







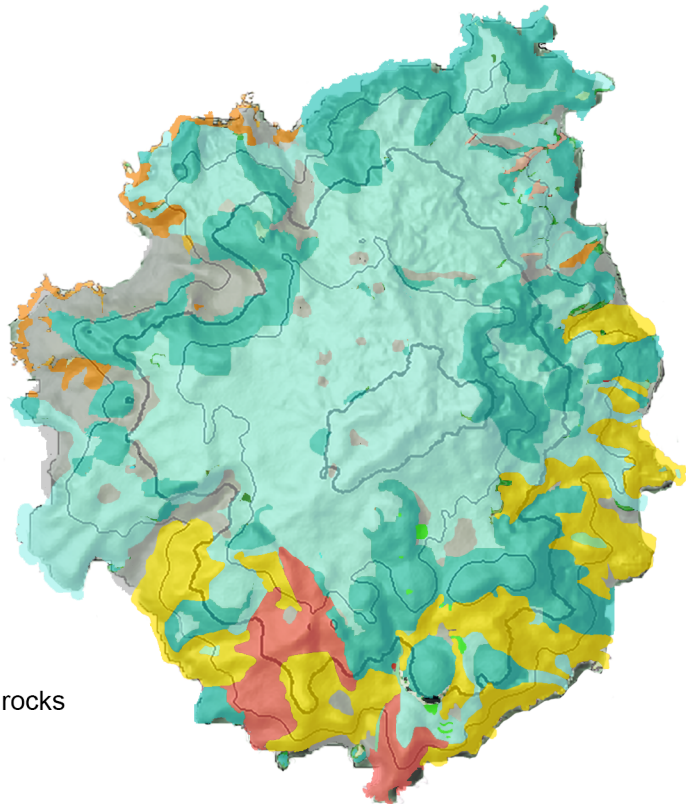


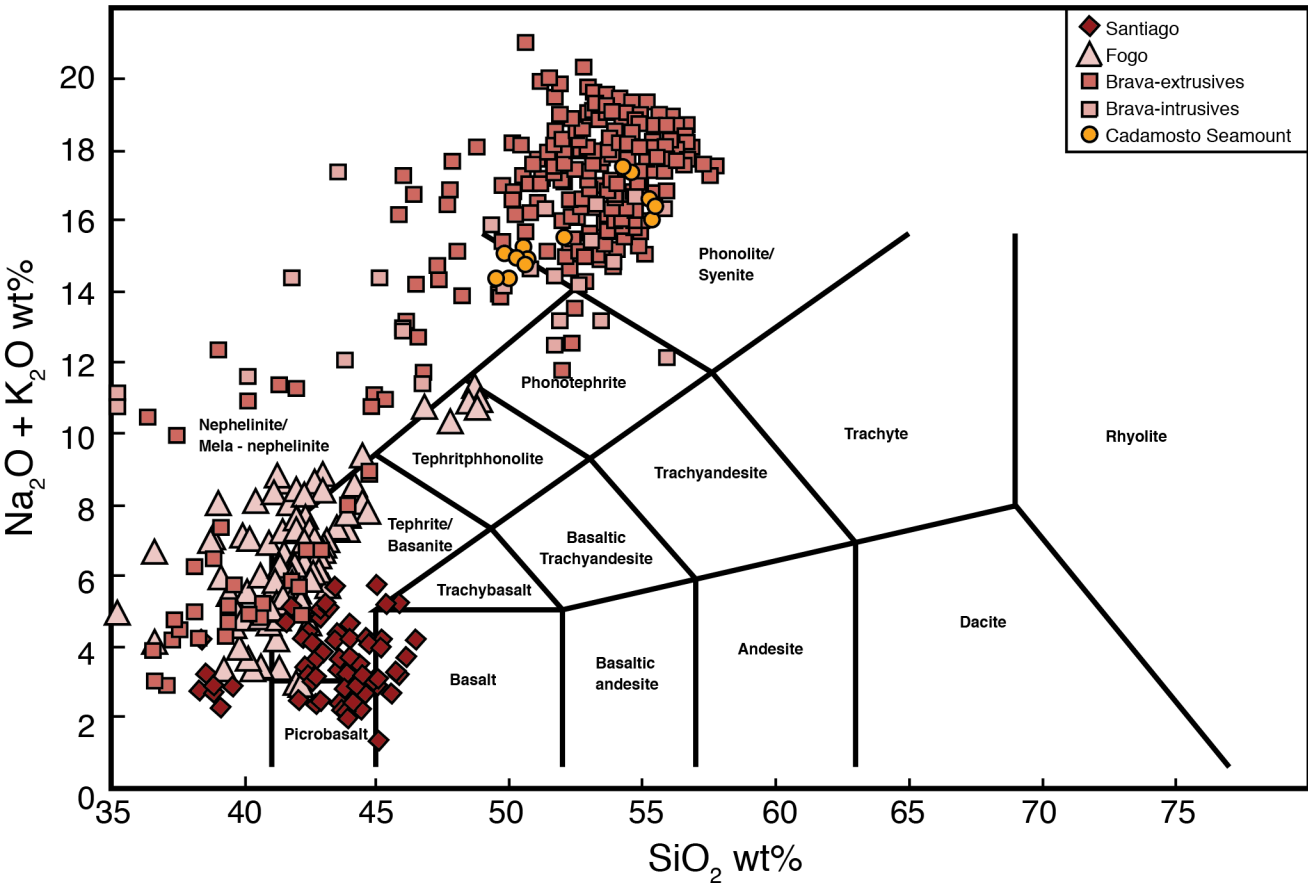


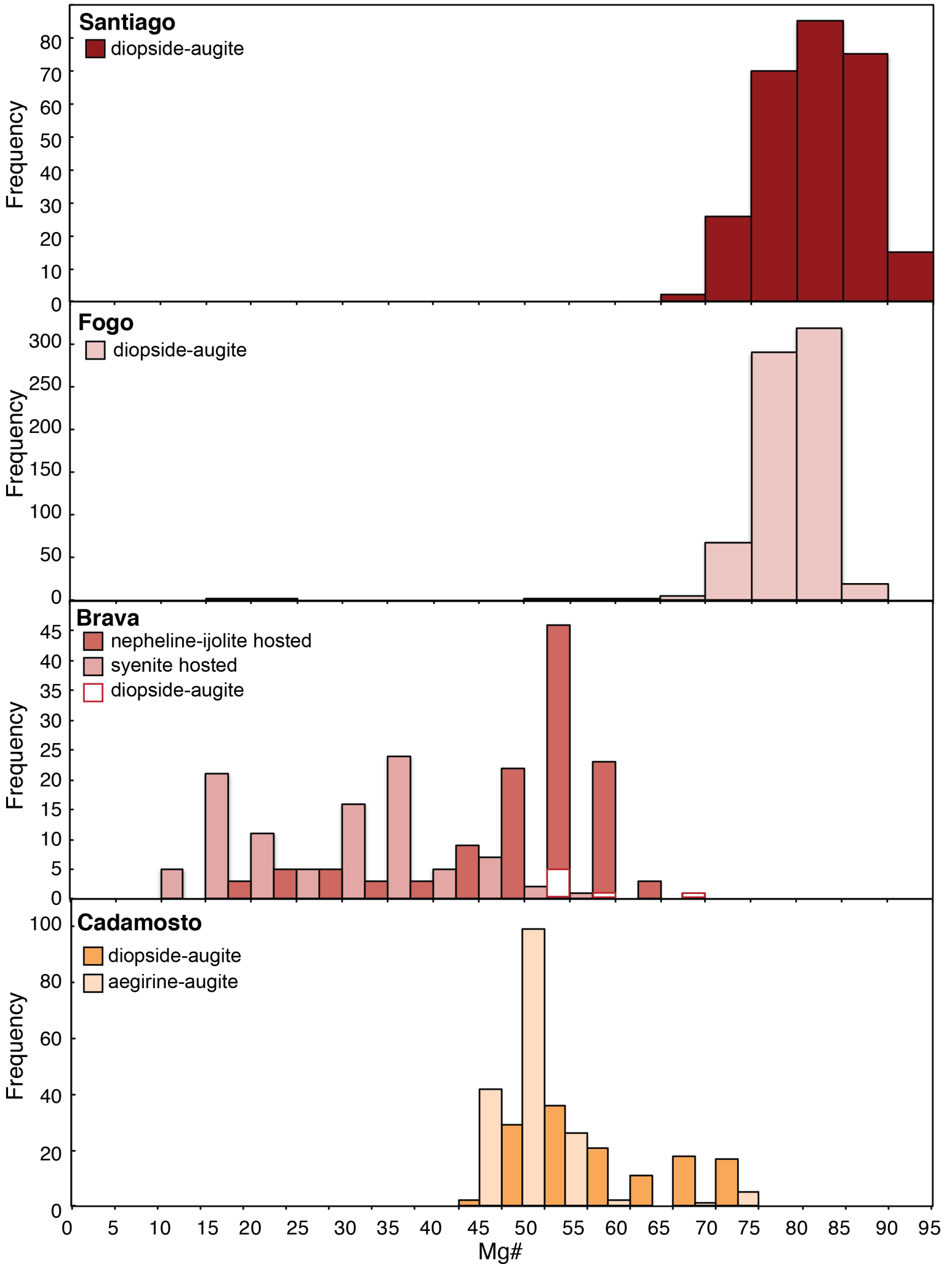


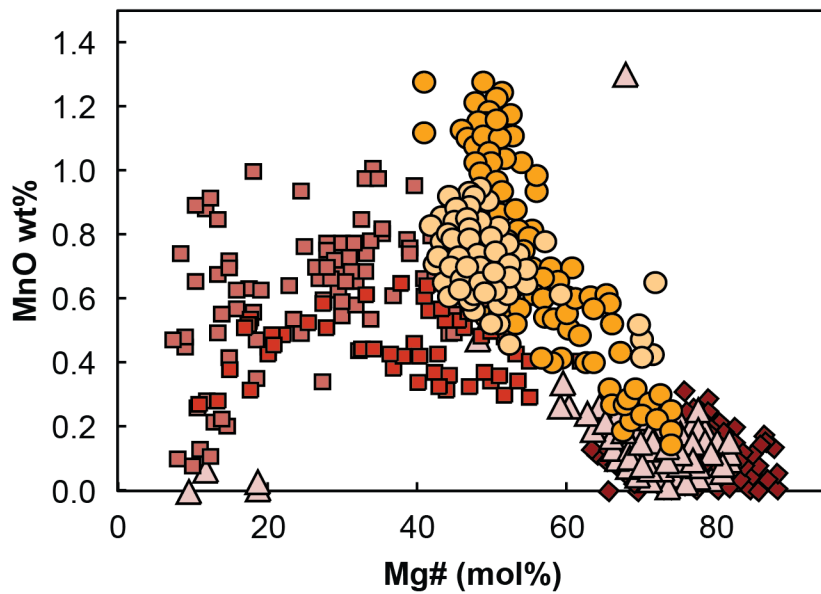
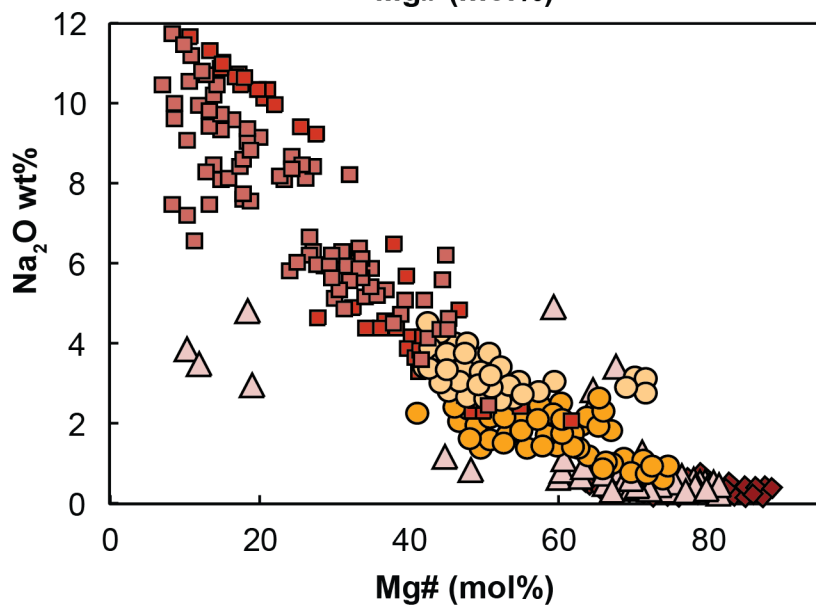
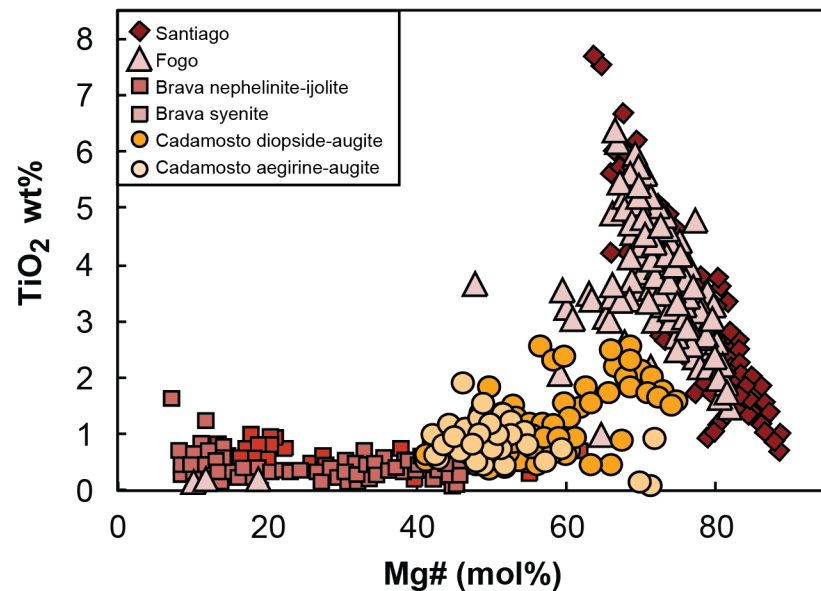
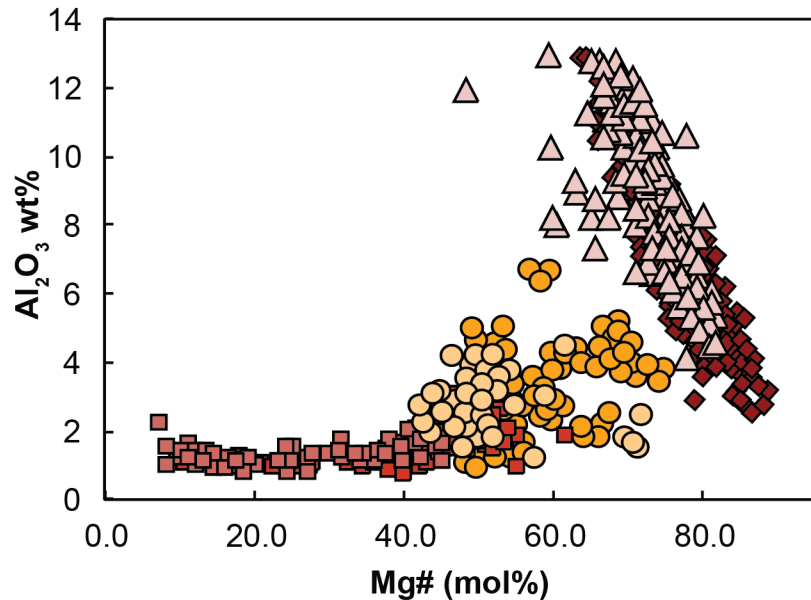
Legend

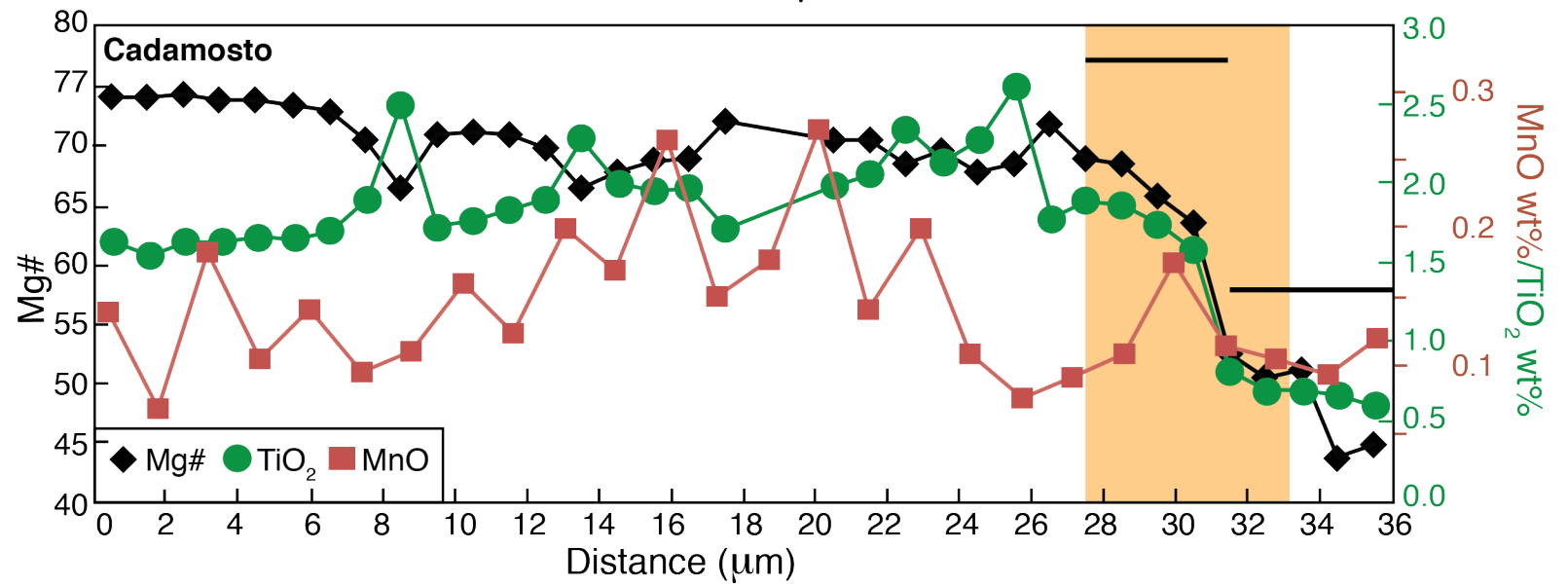
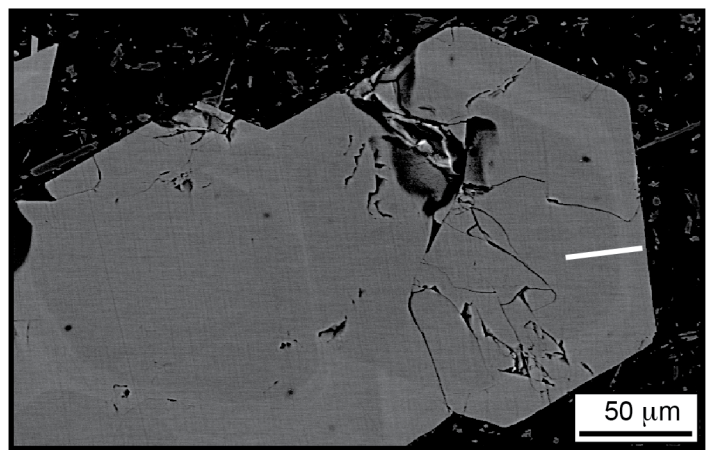
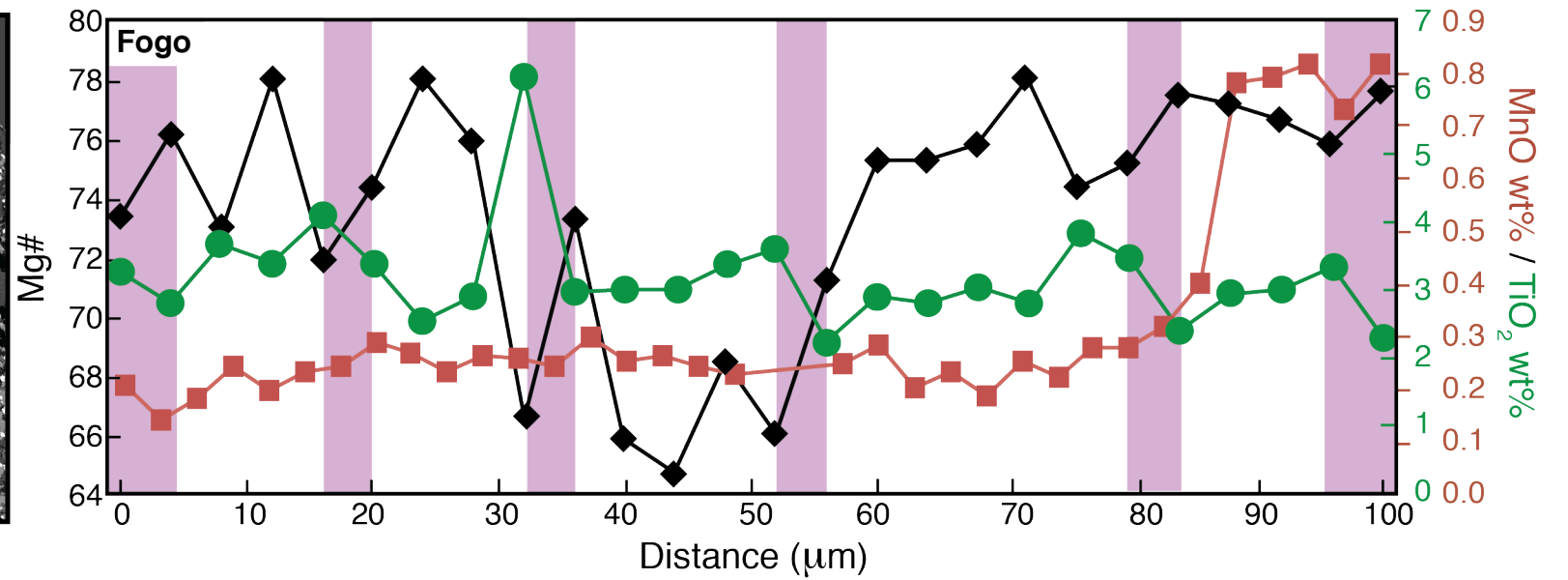
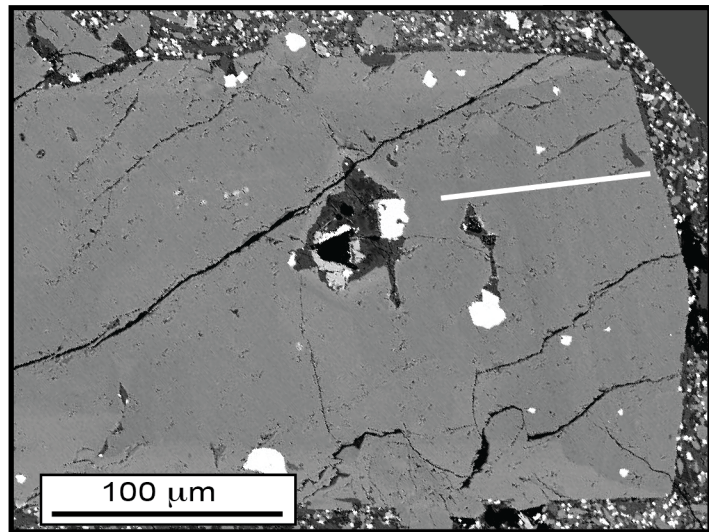
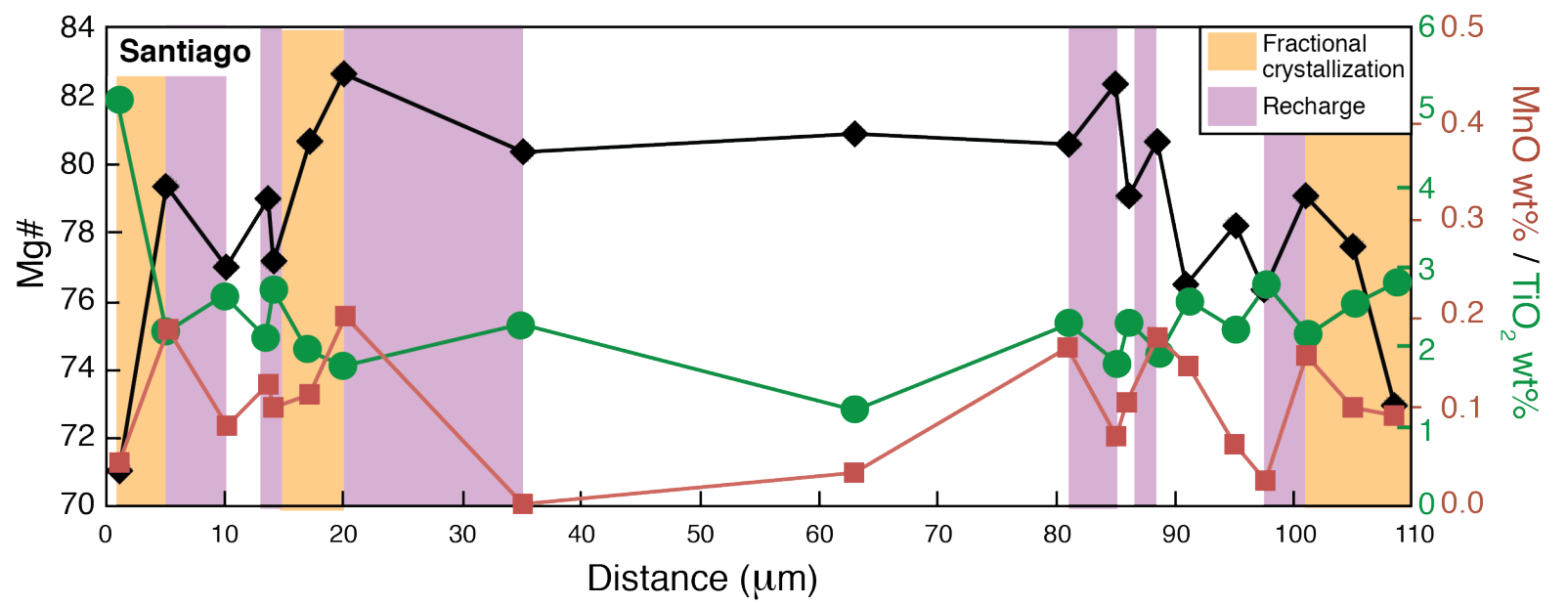
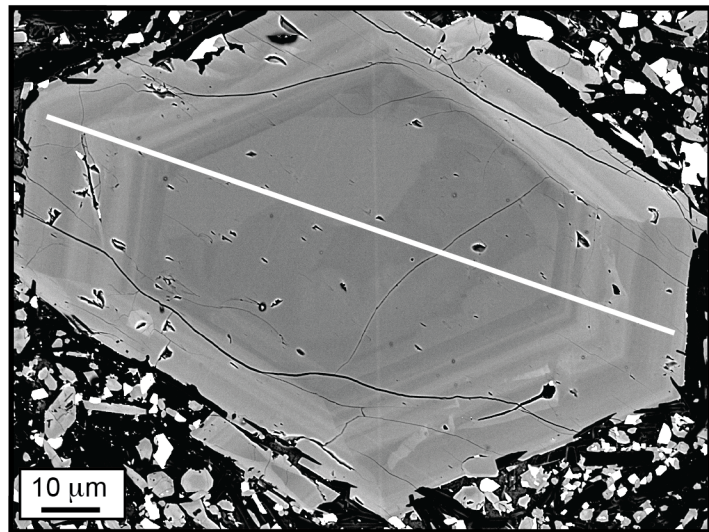
- ~0.5 Ma - Present  Sediments
-  < 0.5 Ma
-  Carbonatites
-  Mafic pyroclastic rocks
-  Mafic lava flows
-  Phonolitic lavas and breccias
-  Phonolitic pyroclastic rocks
- ~1.3 - 0.5 Ma  Unconformity
- 1.95 - 1.4 Ma  Alkaline-carbonatite intrusive rocks
- ~2.9 - 2 Ma  Submarine volcanic rocks

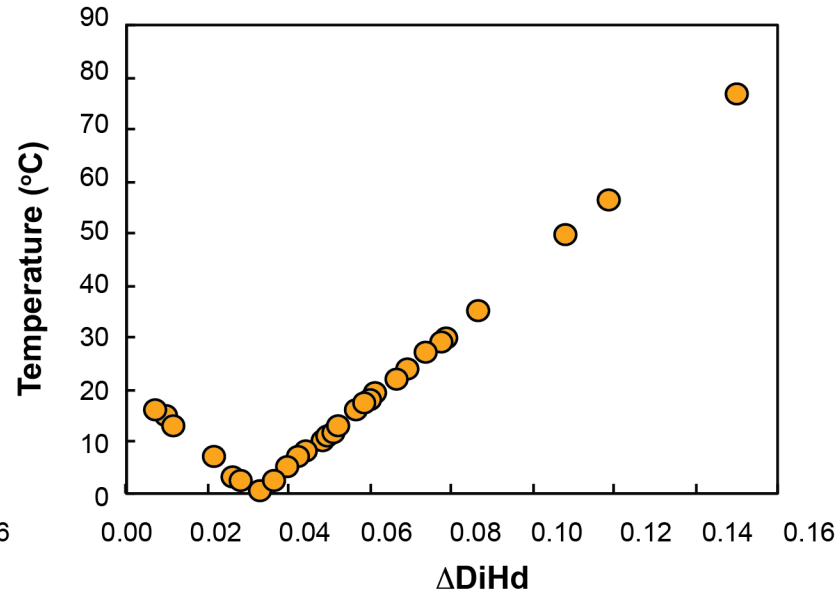
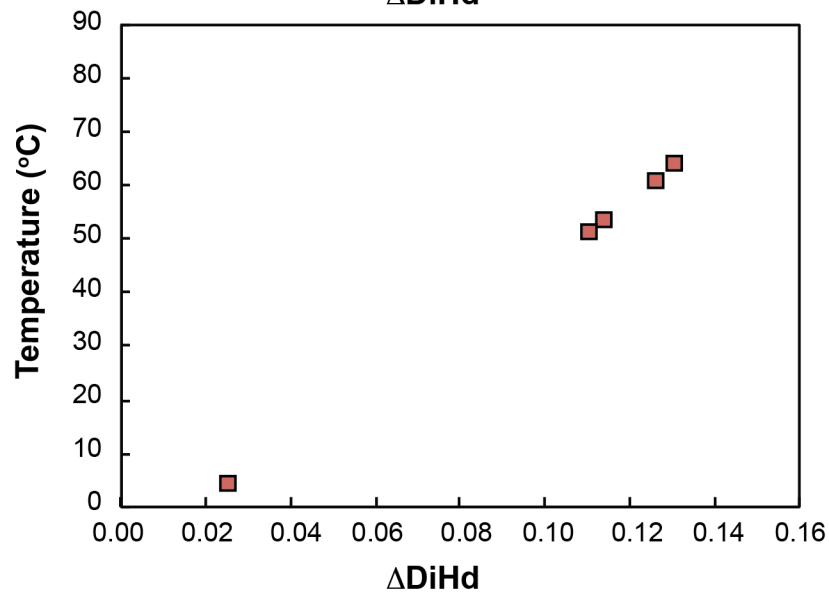
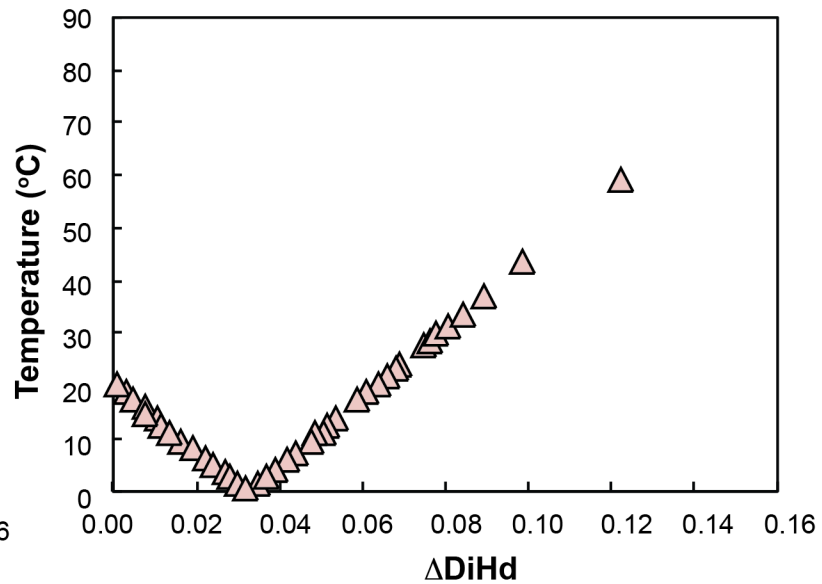
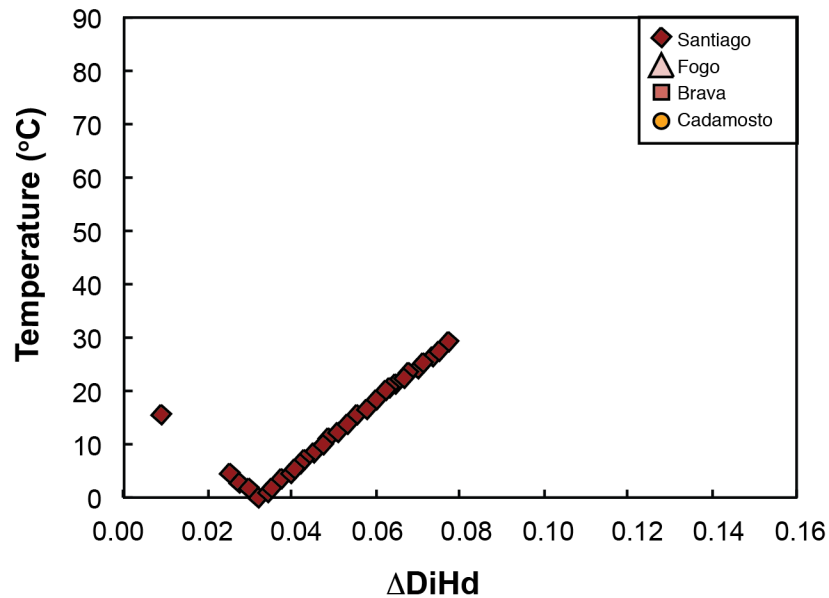


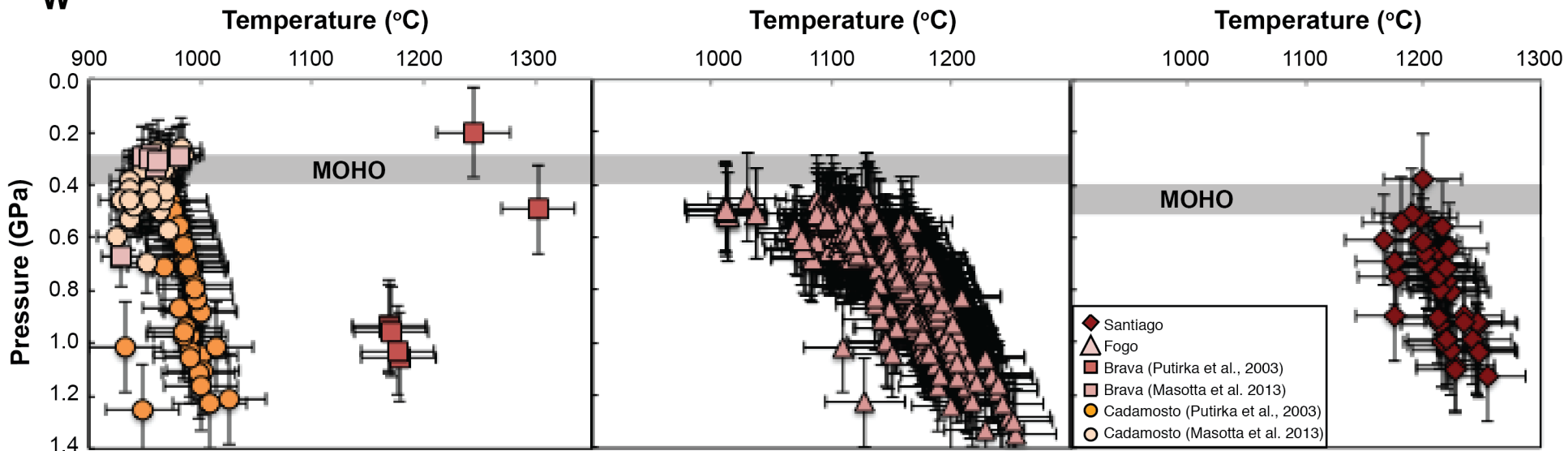




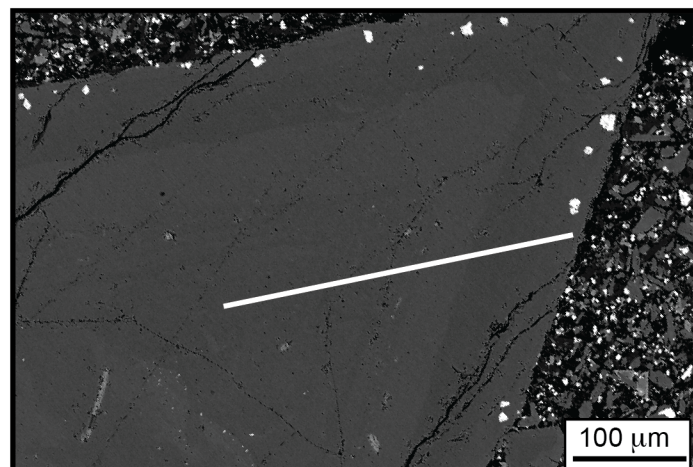




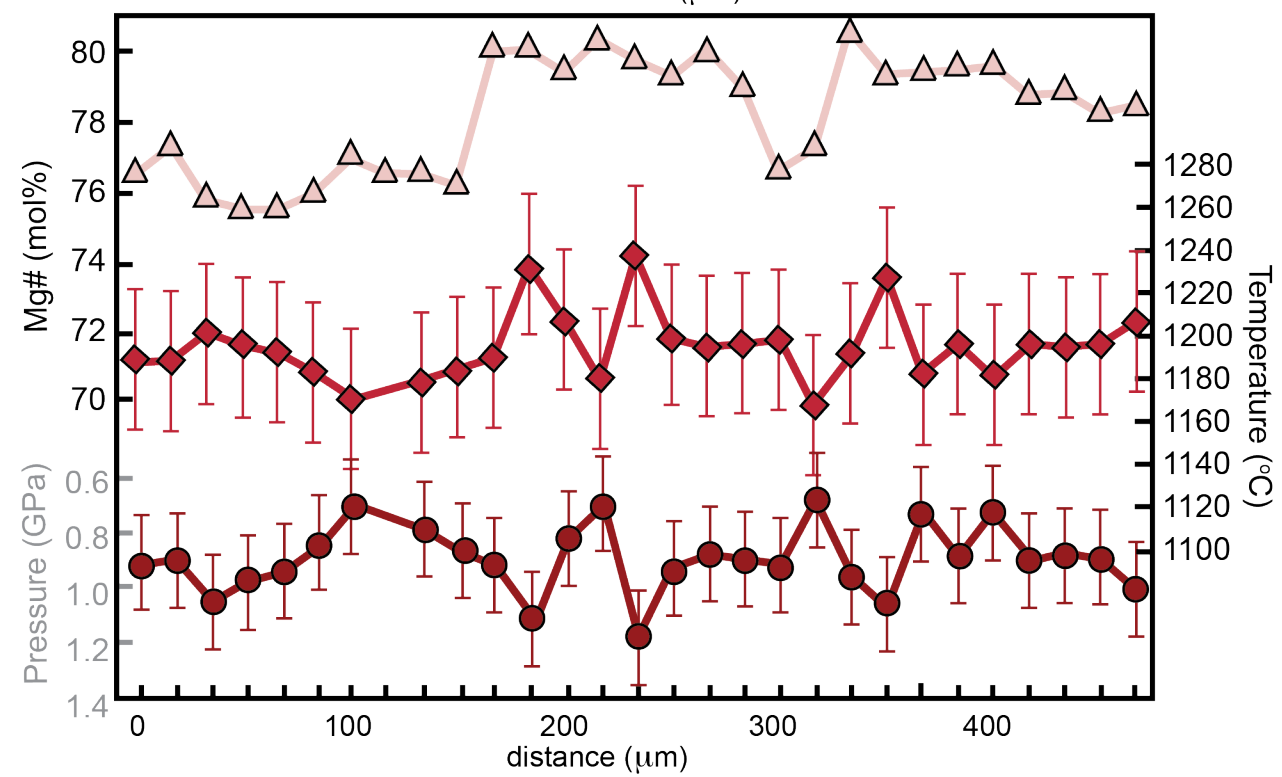
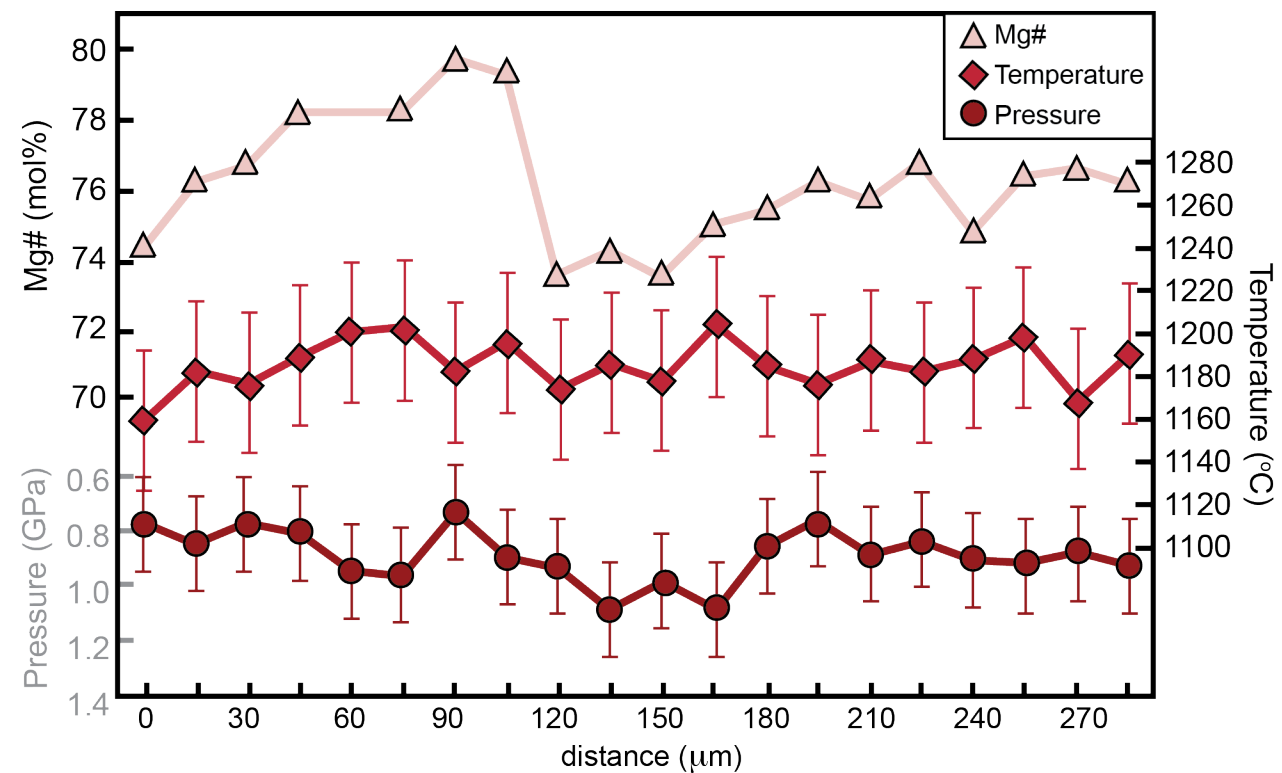
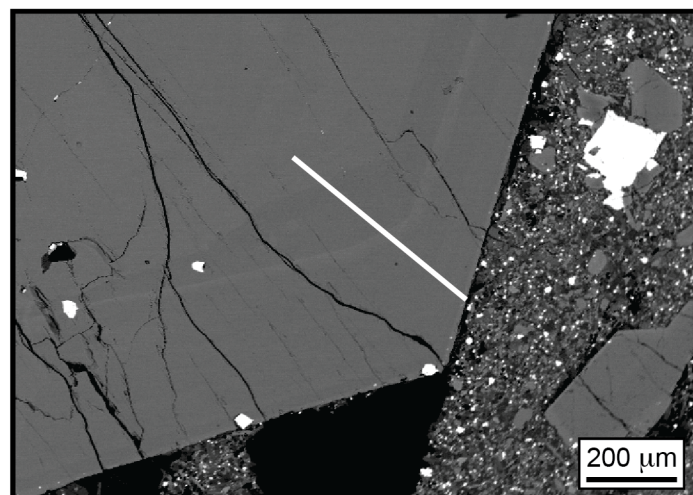


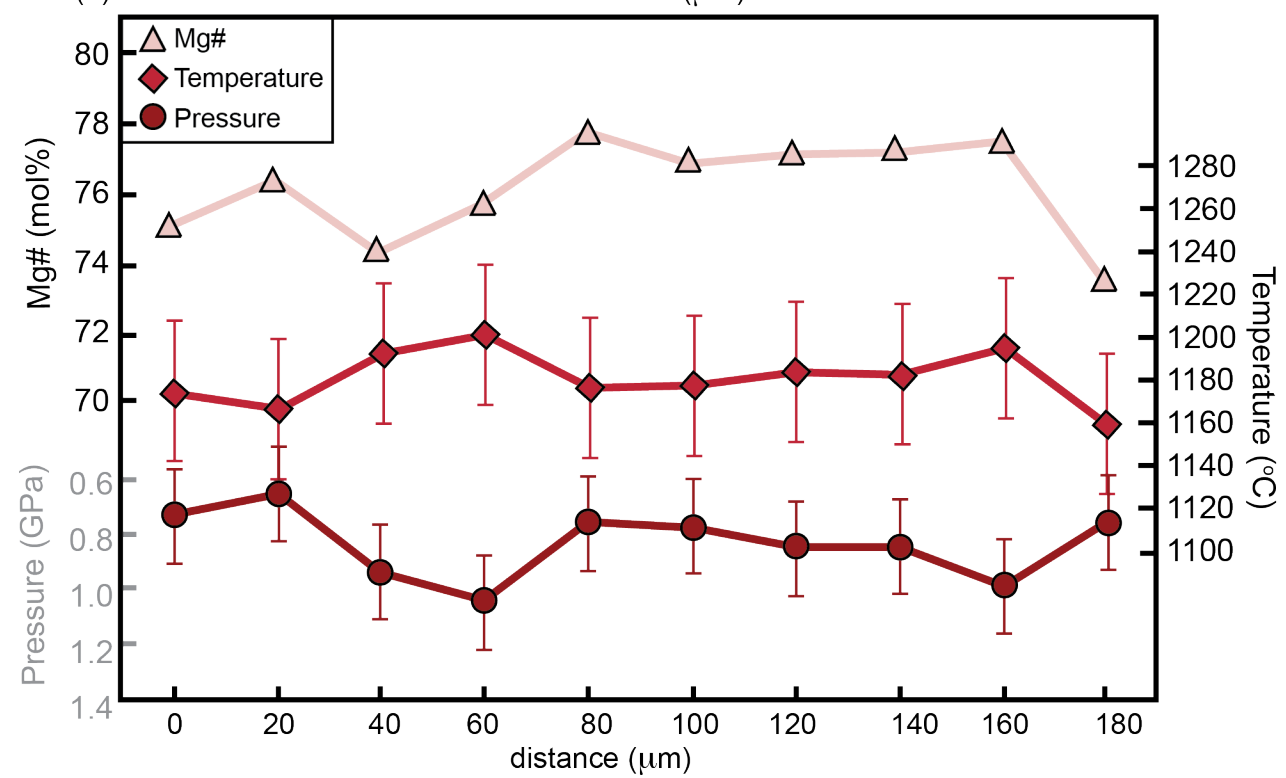
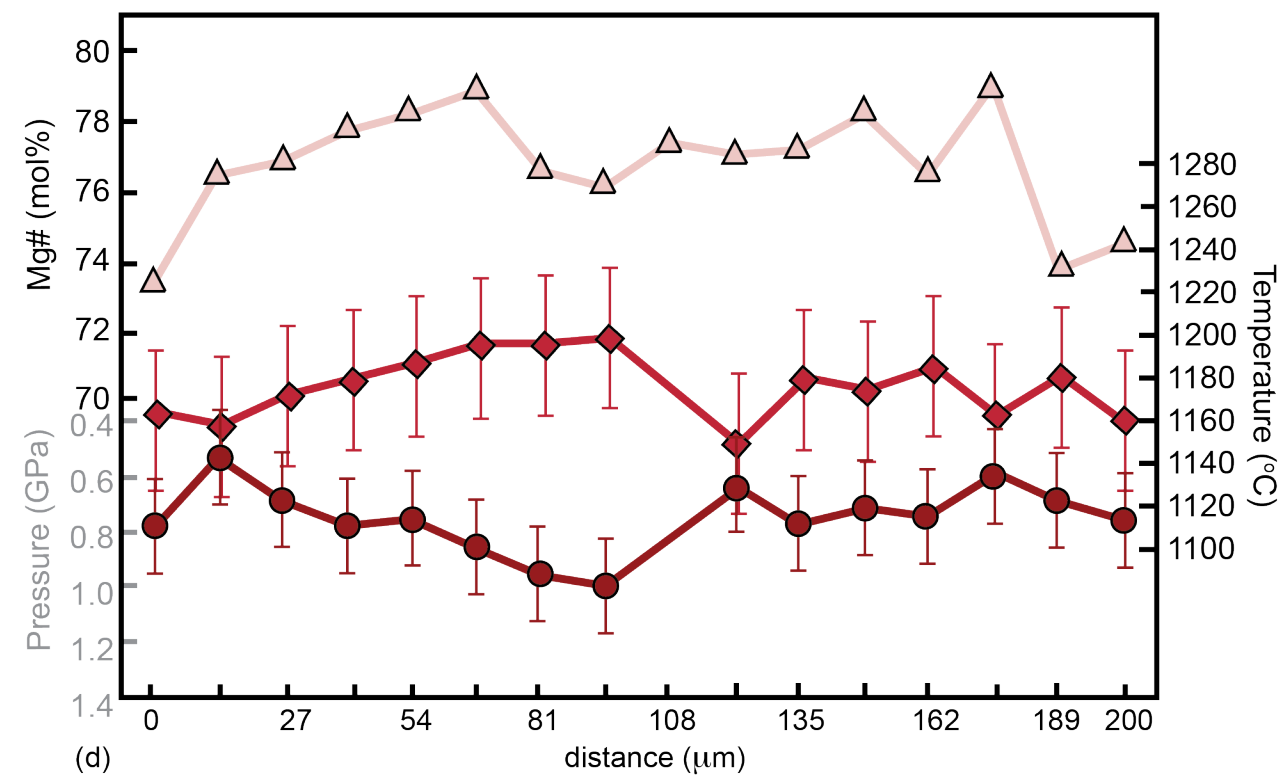
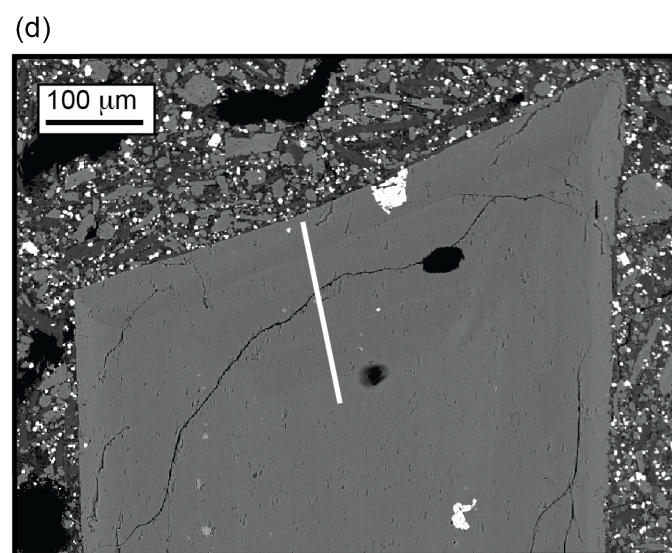
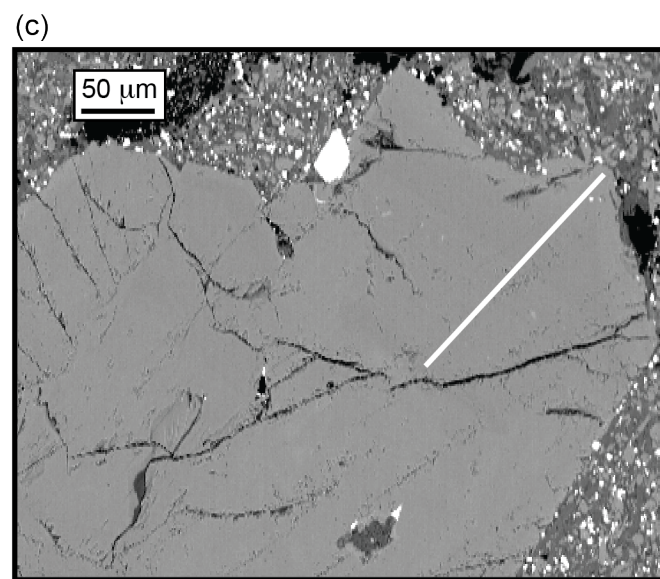
W**E**

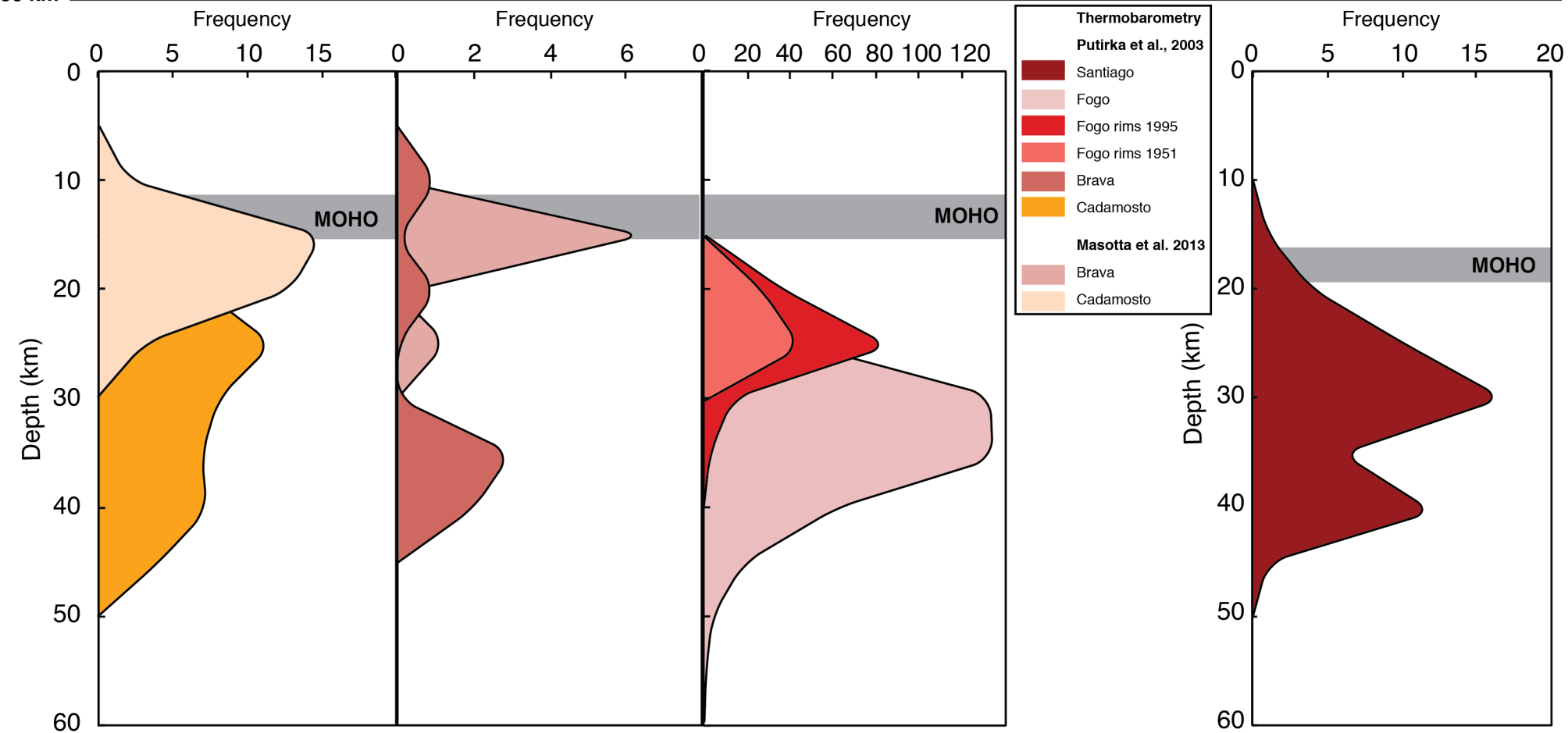
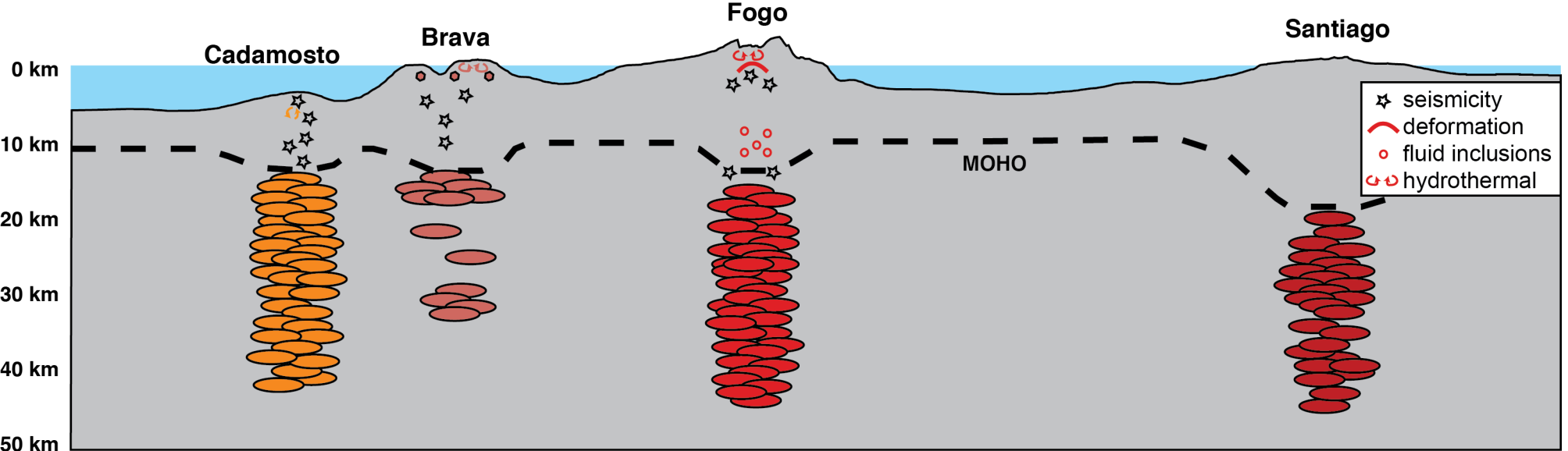
(a)



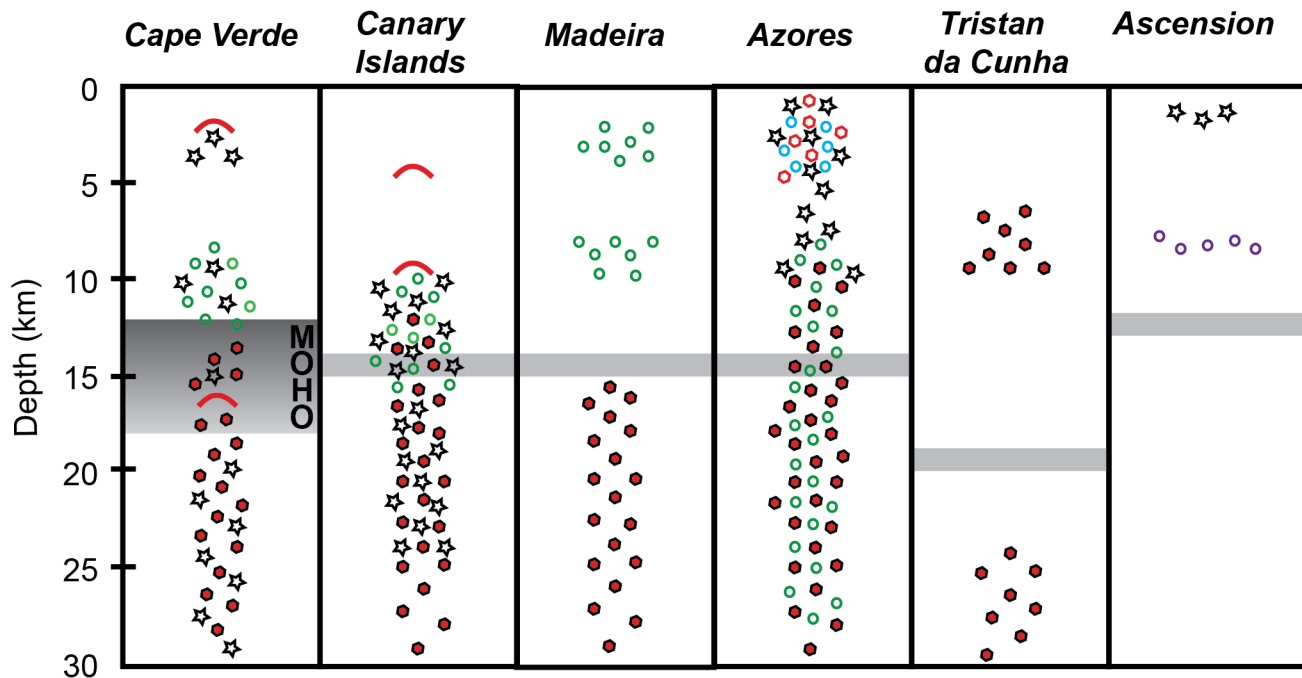
(b)





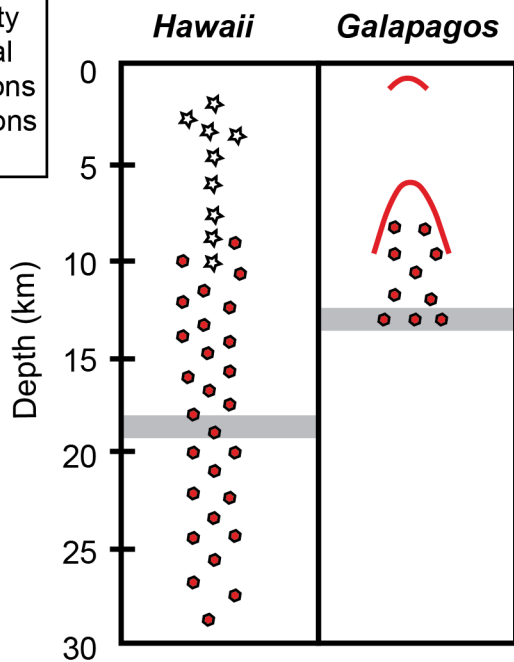


Atlantic Ocean

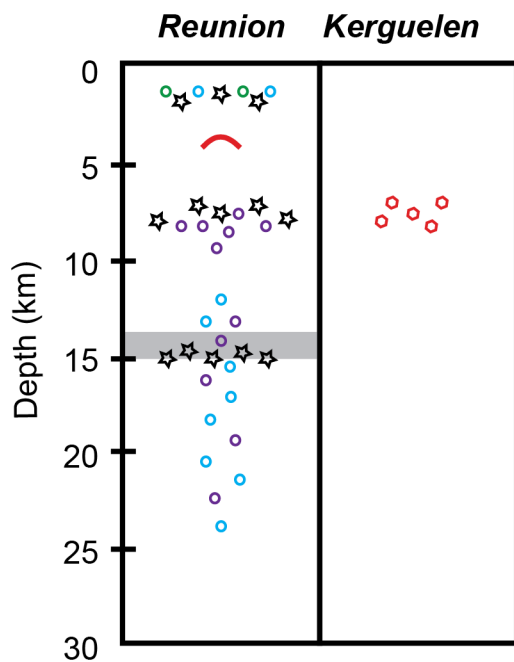


- ☆ seismicity
- ⤿ deformation
- H₂O solubility
- experimental
- fluid inclusions
- melt inclusions
- cpx-melt

Pacific Ocean



Indian Ocean



Atlantic Ocean

Cape Verde	Canary Islands	Madeira	Azores	Tristan da Cunha	Ascension
1 to 5 km seismicity, deformation	4.5 km deformation	2 to 4 km fluid inclusions	2 to 4 km water solubility, fractionation, seismicity	earthquakes prior to eruptions	1.5 to 2 km seismicity
8 to 13 km fluid inclusions, seismicity	10 to 16 km fluid inclusions, deformation	8 to 10 km fluid inclusions	>8 km fluid inclusions, cpx-melt, seismicity	6 to 10 km cpx-melt	8.5 km melt inclusions
12 to 18 km Moho	14 km Moho	14 to 15 km Moho	14 km Moho	19 km Moho	12 to 13 km Moho
13 to 46 km cpx-melt, seismicity, deformation	12 to 45 km cpx-melt, seismicity	15 to 35 km melt	<30 km cpx-melt, melt, fluid inclusions	24 to 36 km cpx-melt	
da Silva et al 1999; Amelung & Day 2002; Lodge & Helffrich, 2006; Pim et al., 2008; Barker et al., 2009, 2012; Grevemeyer et al., 2010; Hildner et al., 2011, 2012; Faria & Fonseca 2014; Fernandez & Faria, 2015; Vales et al., 2015; Jenkins et al., 2017; Leva et al., 2019; Mata et al., 2017; this study.	Klügel et al., 2000; 2005; Galipp et al., 2006; Longpre et al., 2008, 2014; Aulinas et al., 2010; Barker et al., 2015; Gonzalez et al., 2013.	Schwarz et al., 2004; Klügel & Klein, 2006	Renzulli & Santi 2000; Beier et al., 2006; Dias et al., 2007; Silva et al 2012; Jeffery et al., 2016; Madureira et al., 2008; Zanon et al., 2013; Zanon & Pimentel 2015	Geissler et al., 2016; Weit et al., 2017	Klinghofer et al., 2001; Hanson et al., 1996; Chamberlin et al., 2016

<u>Pacific Ocean</u>		<u>Indian Ocean</u>	
Hawaii	Galapagos	Reunion	Kerguelen
2 to 4 km (<10 km) seismicity	1 km deformation	0.5 to 2.5 km water solubility, melt inclusions, seismicity	
9 to 18 km cpx-melt	8 to 13 km cpx-melt, deformation	7 to 14 km water solubility, melt inclusions, seismicity	6 to 8 km experimental
18 to 19 km Moho	13 km Moho	14 to 15 km Moho	
19 to 46 km cpx-melt		15 to 24 km water solubility, melt inclusions, seismicity	
Putirka 1996, 1997; Chatterjee et al., 2005; Poland et al 2015; Hammer et al., 2016	Stock et al., 2018	Bureau et al., 1998; Famin et al., 2009; Peltier et al. 2009; Di Muro et al., 2014; Fontaine et al., 2014	Freise et al., 2003